

Strong interactions in alkaline-earth Rydberg ensembles

DISSERTATION

zur Erlangung des akademischen Grades

Doctor rerum naturalium
(Dr. rer. nat.)

vorgelegt

der Fakultät Mathematik und Naturwissenschaften
der Technischen Universität Dresden

von

Dipl.-Phys. Rick Mukherjee

geboren am 23.10.1984 in Jammu city

Eingereicht am 08.10.2013

Die Dissertation wurde am Max-Planck-Institut für Physik komplexer Systeme
angefertigt.

Eingereicht am 08.10.2013

1. Gutachter: Prof. Dr. Jan-Michael Rost

2. Gutachter: Prof. Dr. Walter Strunz

Contents

1	Introduction	1
1.1	Motivation	1
1.2	Outline	2
2	Alkali Rydberg atoms	5
2.1	Single electron model for alkali Rydberg atoms	5
2.2	Structure and properties	7
2.2.1	Rydberg energies and wave functions	7
2.2.2	Dipole matrix element	8
2.2.3	Spontaneous decay	8
2.2.4	Response to electric fields	9
2.2.5	Atom-atom interactions	10
2.3	Summary	12
3	Alkaline-earth Rydberg atoms: Strontium	17
3.1	Effective two electron model for strontium	17
3.1.1	Singly ionized strontium atom	17
3.1.2	Singlet and triplet states	18
3.2	Theory of two electron Rydberg atoms	19
3.2.1	Multi-channel quantum defect theory	19
3.2.2	Hartree-Fock equations	22
3.2.3	Perturbation theory	23
3.3	Structure and properties	24
3.3.1	Rydberg energies and wave functions	25
3.3.2	Rydberg interactions	26
3.4	Summary	27
4	Magic lattice for strontium	33
4.1	Laser trapping of atoms: Optical lattice	34
4.1.1	Variable lattice spacing	35
4.1.2	Harmonic approximation	35
4.1.3	Types of optical lattice	37
4.2	Dynamic polarizability of an atom	37
4.2.1	Core polarizability	37
4.2.2	Rydberg polarizability	40
4.3	Magic trapping for ground and Rydberg atoms	41
4.4	Decay processes in magic lattice	42
4.4.1	Spontaneous decay	43
4.4.2	Autoionization	44
4.4.3	Photoionization	44

4.4.4	Intensity dependent suppression of decay rates	46
4.5	Summary	47
5	Multi-particle entanglement in strontium Rydberg lattice	53
5.1	Rydberg atoms in optical lattice	53
5.2	Atomic motion in optical lattice	54
5.3	Many body energy spectrum	56
5.4	Generating entanglement: Double sweep protocol	57
5.5	Geometry effects of the lattice	59
5.6	Quantum Ising model	60
5.7	Summary	63
6	Coherent charge transport in optical lattice	67
6.1	Setup for ion transport	67
6.2	Rydberg states of molecular ion	67
6.2.1	Perturbative treatment	69
6.2.2	Non-perturbative treatment	69
6.3	Optical coupling of electronic states	73
6.3.1	Dressed state	76
6.3.2	Adiabatic optical coupling	77
6.4	Ion transport in a double well	80
6.4.1	Population of the excited states	81
6.4.2	Lifetime of the system	82
6.4.3	Condition for coherent dynamics	82
6.5	Analytical expressions for dynamical parameters	83
6.5.1	Constant laser field	84
6.5.2	Spatially varying laser field	86
6.6	Ion transport in an optical lattice	90
6.6.1	Many-body Hamiltonian	91
6.6.2	Numerical simulation	93
6.7	Summary	94
7	Conclusion and Outlook	109
A	Properties of spherical harmonics	115
B	van der Waals coefficient for ns states	117
C	Mean field potentials and energy corrections	119
D	Non-adiabatic couplings	123
E	Spatially varying laser field for N sites	127
F	Spin degree of Freedom	129

Contents	iii
Bibliography	131
Acknowledgements	147

Introduction

1.1 Motivation

Constant observation of nature has been a fundamental part and parcel of the process of human inquiry. The very act of observation involves light bouncing off from matter and reaching us with packets of information. With the advent of lasers, the process of using light to "see" objects extended to the process of being able to "control" objects. In the remarkable papers of [9, 46, 38]; it was suggested that lasers can be used to exert force on atoms that can not only cool them but also trap them. Since then, it has become a routine procedure to cool [208] and trap neutral atoms/ions in magnetic optical traps (MOTS) [165], Paul traps [155], dipole traps [36] and optical lattices [175]. This gave rise to a new field of research in physics namely 'ultra-cold physics'. This field has made such rapid progress that at least six Nobel prizes were given in this area in the last twenty years.

Some of the important milestones were the creation of the first Bose-Einstein condensate (BEC) in 1995 [5], the realization of a superfluid state in BEC's [88] and its transition to the Mott insulator state [86]. Fermi condensates were created in 2004 [87]. Atom-atom interactions were enhanced at such low temperatures in a controlled manner using the technique of Feshbach resonance [40]. BEC in optical lattices lead to observations of theoretical predictions such as the Kosterlitz-Thouless crossover [93]. Ultra-cold atomic gases in optical lattices had further applications such as the implementation of the Bose-Hubbard model [98, 122, 27, 47], study of disordered systems and Anderson localization [181], realization of frustrated models [56, 48], spinor models [53] and creation of artificial magnetic fields [153]. In all of the above examples, the interaction between the ground state atoms are mediated by the short range s-wave scattering. As the interest in using ultra-cold systems to simulate quantum processes for condensed matter grew [122], the need to implement long range interactions became obvious. It turns out that Rydberg atoms are ideal for implementing these long range interactions.

A Rydberg atom is an atom whose valence electron is excited to a state with a very large principal quantum number ($n = 10, 40, 80\dots$). As a result of such an excitation, these atoms are known to have very large size and thereby increased sensitivity to surrounding fields [154]. Advances in laser technology has permitted the efficient production [97, 33] and manipulation of Rydberg atoms [8, 126]. Gases of Rydberg atoms are prepared at densities higher than 10^{10} cm^{-3} and at temperatures in the micro-Kelvin regime giving rise to what is known as the 'frozen Rydberg gas limit' [146]. In this regime, the thermal motions are suppressed allowing to explore the interactions of the Rydberg atoms. Effects of Rydberg interactions such as density dependent broadening

of resonances [166, 186], modification to collision processes [52] and molecular resonances due to avoided crossings [64] have been observed. Rydberg atoms have also been useful in the study of inter-stellar gases [77] and plasma physics [161, 201, 14]. An interesting effect of the Rydberg-Rydberg interaction is the “dipole blockade” effect where the excitation of more than one Rydberg atom is suppressed within the blockade radius determined by the density of particles and the intensity of the laser [172]. The effect was first used to theoretically construct fast quantum gates [99, 131]. It was also used to improve the resolution of atomic clocks [29] and to create single atom and single photon sources [170]. The dipole blockade was experimentally verified in [195, 196]. Recently it has also been observed for an ensemble of Cs Rydberg atoms [203, 202]. This effect have been used to study the crystalline phase of Rydberg excitations [205, 160]. More applications of Rydberg atoms involve the simulation of strongly correlated physics such as the Kiteav model [206] and in nonlinear quantum optics [81, 157, 164]. Most of these applications are implemented using alkali Rydberg atoms and has driven the theoretical field of study of mainly alkali Rydberg atoms.

Historically moving from single electron atom (H atom) to the study of two electron atoms (He, H^-) lead to novel physics starting with revolutionizing the old quantum theory [24], testing of chaos theory analogous to the the Keplerian three body problem [22, 92] and the study of rich doubly excited autoionizing spectrum [132]. One might then ask the question, what interesting physics can occur if one makes a transition from alkali atoms to alkaline-earth atoms in ultra-cold physics? Recently laser cooled alkaline-earth atoms have had applications to optical metrology [191, 66, 15, 130], quantum sensors [194] and for the study of quantum degenerate gases [189, 51]. The first strontium BEC was realized in 2009 [190, 50]. There have been proposals that involve using of alkaline-earth atoms in quantum computation to construct few qubit quantum registers [79, 44], study of many-body phenomena governed by spin-orbital interactions [80] and Mott insulator phase with alkaline-earth atoms in optical lattice [72]. However all of these applications were done using ground state alkaline-earth atoms. In this thesis, the question we would like to address is **what are the implications of a Rydberg alkaline-earth atom in ultra-cold systems?** One of the main purpose of this thesis is to investigate many-body physics using Rydberg alkaline-earth atoms in optical lattices.

1.2 Outline

Chapter 2 is an introduction to Rydberg atoms explained in the context of alkali atoms. Apart from historical origin, the purpose of studying Rydberg atoms in terms of alkali atoms is two fold. Firstly the different properties of a Rydberg atom that scale with the principal quantum number are universal and can be understood for the simpler case of single electron atom. Secondly, it provides a background for comparison with the next chapter where we calculate Rydberg atoms for two electron atoms. Rydberg states for alkaline-earth atoms are calculated for the particular case of strontium using a mean field theory approach in chapter 3. The second valence electron of the alkaline earth Rydberg atoms provides this unique opportunity to trap both the Rydberg and the ground state

atom in the same optical lattice as explored in chapter 4 where “magic wavelengths” have been identified for the trapping laser [148]. This is not possible with alkali atoms where either one of the internal state can be trapped in an optical lattice but not both. The study of different decay processes involved in such a lattice is included in chapter 4. Using the magic lattice for Rydberg atoms, we implement a strongly interacting spin system in chapter 5. The dynamics of the spin system is similar to the one seen in an effective Ising model where the fields are controlled by the laser parameters. We present a scheme involving the variation of the laser intensity in a specific manner resulting in the creation of a maximally entangled state, more well known as the GHZ (Greenberger, Horne and Zeilinger) state for a large number of particles [148]. The magical wavelengths identified earlier applies as much to ions as to Rydberg atoms. So in chapter 6, we investigate the process of ion transport in one dimensional lattice system. We first study a simpler system of a Rydberg molecular ion where the hopping of the Rydberg electron is calculated exactly for very small inter-nuclear distances. We then couple the ground states to the excited spectrum of the molecular Rydberg ion and derive dynamical equations purely in terms of the ground states. We derive conditions for coherence and show that for a large range of detunings and lattice spacings, one avoids de-phasing in the dynamics. Finally we numerically simulate the ion transport over 19 sites using the dynamical parameters obtained numerically as well as analytically [147]. In the concluding chapter, all the essential results of the thesis are summarized followed up with an outlook on the future scope of this research.

Alkali Rydberg atoms

Contents

2.1	Single electron model for alkali Rydberg atoms	5
2.2	Structure and properties	7
2.2.1	Rydberg energies and wave functions	7
2.2.2	Dipole matrix element	8
2.2.3	Spontaneous decay	8
2.2.4	Response to electric fields	9
2.2.5	Atom-atom interactions	10
2.3	Summary	12

This chapter provides a basic introduction to Rydberg atoms focusing on alkali atoms. Any atom that is excited to large principle quantum number ($n > 10$) is a Rydberg atom. From a theoretical perspective, the study of alkali Rydberg atoms is simplified by using the effective single electron approximation. The highly excited single valence electron is attracted to the compact ionic core (consisting of the nucleus and the inner electrons) with total positive charge of unity similar to hydrogen. We introduce the concept of quantum defects and discuss the different properties of a Rydberg atom such as size, energy, lifetime, polarization and atom-atom interaction. Particular emphasis is given on how these different properties scale with the principal quantum number as it provides a simple and elegant way to distinguish them from those of ground state atoms.

2.1 Single electron model for alkali Rydberg atoms

Rydberg series were identified in the hydrogen spectrum by Balmer [13] already in 1885. Bohr solved the hydrogen atom [28] and verified the $1/n^2$ scaling of the energy with the principal quantum number n . Solving a multi-electron atom such as the alkali atom is more involved since one has to solve the Schrödinger equation for many electrons and include the inter-electronic interactions. An alkali Rydberg atom has a finite size closed shell core and single valence electron which can be excited to any higher bound state. A highly excited valence electron is so far from the core that the atom effectively behaves like a hydrogen atom but with a modified core. This is often known as the single active electron approximation. Using this approximation, we write the Schrödinger equation for a Rydberg electron as given in [32],

$$\left[-\frac{\hbar^2}{2m} \nabla^2 + V_C(r) \right] \psi_{nlm_l}(\mathbf{r}) = E_{nl} \psi_{nlm_l}(\mathbf{r}) . \quad (2.1)$$

where \hbar is the reduced Planck constant and m is the reduced mass of the Rydberg electron. The Rydberg electron experiences the nuclear potential that is screened by the inner core electrons and is described by the effective core potential V_C . The Rydberg states are labeled with the principal quantum number $n > 0$, orbital quantum number $l \in \{0 \text{ (s state)}, 1 \text{ (p state)}, 2 \text{ (d state)} \dots n-1\}$ and the magnetic quantum number $m_l \in \{-l, -l+1, \dots, 0 \dots l-1, l\}$. The wave function $\psi_{nlm_l}(\mathbf{r})$ can be separated into a radial $\mathcal{R}_{nl}(r)$ and angular $\mathcal{Y}_{lm_l}(\vartheta, \varphi)$ components.

$$\psi_{nlm_l}(\mathbf{r}) = \mathcal{R}_{nl}(r) \mathcal{Y}_{lm_l}(\vartheta, \varphi) \equiv |nlm_l\rangle . \quad (2.2)$$

The radial eigenfunction satisfies the radial part of the Schrödinger equation given as

$$\left[-\frac{\hbar^2}{2m} \left\{ \frac{d^2}{dr^2} - \frac{l(l+1)}{r^2} \right\} + V_C(r) \right] r \mathcal{R}_{nl}(r) = E_{nl} r \mathcal{R}_{nl}(r) . \quad (2.3)$$

The larger the l , the more difficult it is for the Rydberg electron to penetrate the core owing to the repulsive centrifugal barrier $l(l+1)/2r^2$. Although the high l Rydberg states do not enter the core, they do polarize it to a certain extent [74]. In contrast, a Rydberg electron with small orbital angular momentum ($l < 3$) has significant overlap with the inner electrons leading to stronger penetration and polarization of the core. The effect of the core on the Rydberg electron is thus dependent on the angular momentum of the Rydberg electron and is accounted by the effective core potential. The most commonly used effective core potential taken from [133, 137] and is written as

$$V_C(r) = -\frac{q^2}{4\pi\epsilon_0 r} \left[1 + (Z-1)e^{-a_1(l)r} - r(a_3(l) + a_4(l)r)e^{-a_2(l)r} \right] - \frac{\alpha_c}{2r^4} \left(1 - e^{-(r/r_c)^6} \right) . \quad (2.4)$$

where q is the charge and ϵ_0 is the vacuum permittivity. $a_{1-4}(l)$ are parameters that depend on the orbital angular momentum. α_c is the core dipole polarizability and r_c is the cut off radius that prevents any divergence at the origin. The values for $a_{1-4}(l)$ for alkali atoms are determined by fitting the low lying energies using the effective core potential against experimentally measured energies for various alkali atoms [143, 94]. Core polarizabilities α_c of alkali atoms are obtained by measuring the difference in the energies for different l states [39, 115]. It is clear that the success to obtain accurate Rydberg states from Eq.(2.1) depends on the accurate knowledge of the effective model potential, which relies on the accuracy and the abundance of empirical data available for a particular alkali element. From Eq.(2.4), we see that far from the core, the potential experienced by the Rydberg electron is similar to that due to a single proton like in hydrogen. At distances closer to the nucleus, the potential has significant deviations from the Coulomb potential (see Fig.2.1). The deviation in potential due to penetration of the Rydberg electron into the core are determined by the second and third terms in Eq.(2.4), while the deviation due to the polarization of the core is given by the last

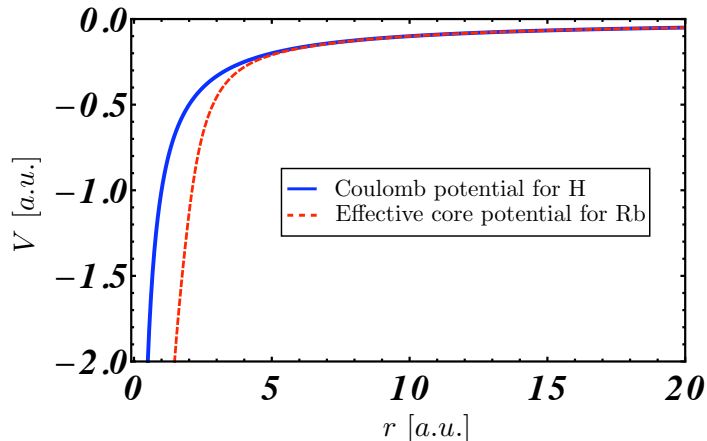


Figure 2.1: Comparison of Coulomb potential (blue) with effective core potential for Rb (red) with $l=0$ given by Eq.(2.4).

term in Eq.(2.4). The essential difference between a single electron Rydberg atom and a hydrogen atom is the behaviour of the Rydberg electron with low l 's ($l < 3$), where the energies are not degenerate due to the deviations from the Coulomb potential. This difference in behaviour is already captured by the low lying states of the alkali atom and so it is worthwhile to note that the model potential obtained by fitting low lying states can actually describe the high lying Rydberg states. The effect of broken degeneracy will have significance for the properties of the Rydberg atom as we shall see in the next section.

2.2 Structure and properties

In this section, the Rydberg states are calculated by solving the Schrödinger equation (2.1). Several of the key atomic properties along with the different scaling laws with respect to the principal quantum number n are discussed here.

2.2.1 Rydberg energies and wave functions

Various analytical [111] and numerical methods such as the Numerov algorithm [25] have been used to solve Eq.(2.1). For our purposes, the Rydberg states are calculated by discretizing the radial part of the Hamiltonian given in Eq.(2.3) in position space up to second order, generating a tri-diagonal matrix which is then diagonalized. The eigenfunctions obtained show an increase in the frequency of the radial oscillations pulling the nodes of the radial wave function closer to the origin compared to the hydrogen wave function (see Fig.2.2). This is because the effective model potential is deeper than the Coulomb potential at small distances from the core (see Fig.2.1). The oscillations of the Rydberg wave function extent up to 5000 a.u. for $n, l = 50, 0$ which is much larger than the size of the core (~ 5 a.u.). At large distances, the effective model potential is similar to the Coulomb potential. The deviation from the Coulomb potential near the core is

like a change in the boundary condition for a free particle reflected from the core. This gives a *phase shift* to the Rydberg radial wave function at large distances when compared to the hydrogen wave function as seen in Fig.2.2. Another interpretation of the radial phase shift is that it is the measure of the difference in momentum between the Rydberg electron of an alkali atom and that of a hydrogen atom [74]. This radial shift is directly proportional to a quantity known as the *quantum defect* $\delta_{n,l}$. The energies of Rydberg states are expressed in terms of an *effective principal quantum number* [183] defined as ,

$$n^* = n - \delta_{n,l} . \quad (2.5)$$

The corresponding Rydberg energy for a state in $|nl\rangle$ is

$$E_{nl} = - \left(\frac{mq^4}{8\epsilon_0^2 h^2} \right) \frac{1}{(n^*)^2} \sim (n^*)^{-2} . \quad (2.6)$$

The energy of a Rydberg state depends not only on the principal quantum number n but also on the orbital quantum number l in contrast to the hydrogen atom. The different angular momentum states ($l = 0, 1, \dots, n-1$) belonging to the same n of the hydrogen atom are degenerate. For a Rydberg atom, only the high l states are degenerate with essentially zero quantum defect. For low l Rydberg states, this degeneracy is broken by the non-zero quantum defects. Experimentally measured quantum defects for Rb taken from [125] in different $n(= 40 - 60)l$ states are $\delta_{ns} = 3.131$, $\delta_{np} = 2.654$, $\delta_{nd} = 1.348$ and $\delta_{n(l>3)} \simeq 0$. From Eq.(2.6), it is clear that the energy scales as n^{-2} and the energy difference for neighbouring Rydberg states scale as follows [74],

$$|E_{nl} - E_{n'l'}| \sim n^{-3} . \quad (2.7)$$

Most of these scaling laws for other atomic properties such as size, optical transition strengths, lifetime are derived by studying the behavior of the energy and the radial matrix element of the Rydberg state. For a low lying state $|n'l'\rangle$ far away from a Rydberg state $|nl\rangle$, the radial matrix element is determined the overlap of the low lying state wave function with the Rydberg wave function [32], which is given as

$$r_{nl,n'l'} = \langle n'l'|r|nl\rangle = \int_0^\infty \mathcal{R}_{nl}(r)\mathcal{R}_{n'l'}(r)r^3 dr \sim n^{-3/2} \quad \text{for } n' \ll n . \quad (2.8)$$

Since only the outer part of the Rydberg wave function contributes to the overlap, the above scaling law comes from the normalization constant which scales as $n^{-3/2}$. While for a neighbouring Rydberg state $|n'l'\rangle$ close to $|nl\rangle$, the scaling law is given as

$$r_{nl,n'l'} \sim n^2 \quad \text{for } n' \in \{n-1, n, n+1\} . \quad (2.9)$$

The size of the Rydberg atom is given by the expectation value $r_{nl,nl}$ and scales as n^2 . In case of Rb, the size of the Rydberg atom for the state $50s$ is 5000 times the size of the ground state hydrogen atom. Large size of the Rydberg atom means that it can exhibit long range interactions (refer section 2.2.5) and have larger sensitivity to external fields. Interaction with fields lead to optical transitions of the atom which are determined by dipole matrix element.

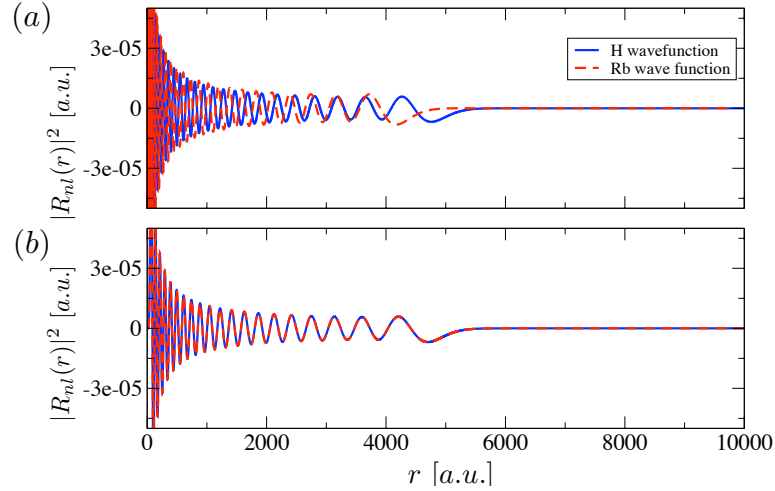


Figure 2.2: Comparison of hydrogen wave function (black) with Rb Rydberg wave function (red) for (a) $n, l = 50, 0$ (b) $n, l = 50, 10$. The radial wave functions for a Rydberg atom differ from the hydrogen wave function for $l < 3$.

2.2.2 Dipole matrix element

One of the first theoretical calculations of transition strengths for low l states for alkali atoms were done in [16]. The transition from an initial state $|nlm_l\rangle$ to a final state $|n'l'm'_l\rangle$ is determined by the dipole matrix element defined as

$$\mu_{nlm_l, n'l'm'_l} = \langle n'l'm'_l | \boldsymbol{\mu} | nlm_l \rangle \sim \begin{cases} n^{-3/2} & \text{for } n' \ll n, \\ n^2 & \text{for } n' \in \{n-1, n, n+1\}. \end{cases} \quad (2.10)$$

where $\boldsymbol{\mu} = q\mathbf{r}$ is the electric dipole moment for an electron with charge q . The angular part gives the well known dipole selection rules for optical transition between atomic states, $|l - l'| = \pm 1$ and $|m - m'| = 0, \pm 1$. The radial part of the dipole matrix element $\mu_{nl, n'l'} = \langle n'l' | \mu | nl \rangle = q r_{nl, n'l'}$ determines the scaling law which follows from Eq.(2.8) and (2.9). The n^2 scaling of the $\mu_{nl, n'l'}$ is responsible for the strong interaction between Rydberg atoms due to the strong dipole coupling. Whereas the $n^{-3/2}$ scaling plays a role in the spontaneous decay rates for Rydberg atoms as will be discussed in the following section.

2.2.3 Spontaneous decay

Rydberg lifetimes for alkali atoms like Li, Na, Rb have been measured using time resolved laser induced fluorescence techniques [75, 82] confirming larger lifetimes, for example 100 μs for Rb 80s. The rate with which a given state $|nlm_l\rangle$ decays to a particular dipole allowed state $|n'l'm'_l\rangle$ is given by

$$\Gamma_{nlm_l, n'l'm'_l} = \frac{\omega_{nl, n'l'}^3 \mu_{nlm_l, n'l'm'_l}^2}{3\pi\epsilon_0 \hbar c^3} \sim \begin{cases} n^{-3} & \text{for low } l (< 3), \\ n^{-5} & \text{for high } l (\simeq n-1). \end{cases} \quad (2.11)$$

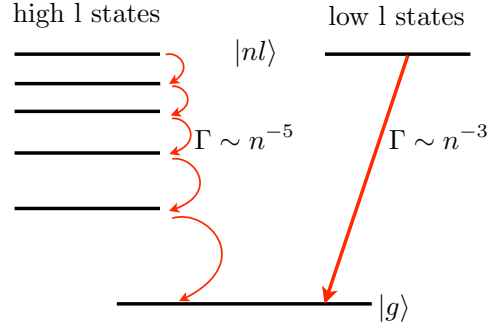


Figure 2.3: The figure shows that Rydberg states with high l decays to the ground state indirectly via multiple dipole allowed inter-mediate transitions. This accounts for higher life times compared to Rydberg states with low l where the dominant transition is to its ground state.

where $\omega_{nl,n'l'} = (E_{nl} - E_{n'l'})/\hbar > 0$ corresponds to transition frequency between the relevant states. The spontaneous decay rate can be understood by classifying the behaviour of the transition frequency and the dipole moment for different l 's. There are two different routes of decay for an initial Rydberg state depending on its l . For small l Rydberg state, the transition frequency $\omega_{nl,n'l'} \gg \mu_{nlm_l, n'l'm'_l}$ and thus the dominant dipole allowed transition is the transition to the ground state (typically the ground state is s or p). In this case, the transition frequency is independent of the initial Rydberg principal quantum number since it is so close to the threshold. The radial dipole matrix element scales as $n^{-3/2}$ from Eq.(2.10). Thus the over all decay rate for low l states scales as n^{-3} .

For Rydberg states with high l ($\simeq n - 1$), the decay process involves cascading down to a low lying states via the dipole allowed transitions to neighbouring Rydberg states $|n'l'\rangle$. The transition frequency for this case $\omega_{nl,(n'\simeq n)(l'=l\pm 1)}$ scales as n^{-3} (refer to Eq.(2.7)) and the radial dipole matrix element scales as n^2 as shown in Eq.(2.9). This gives an overall scaling of n^{-5} for the decay rate of high l Rydberg states. Often high l Rydberg states are accessed using microwave lasers for their longer lifetimes compared to the low l Rydberg states for atom manipulation using electric fields.

2.2.4 Response to electric fields

There have been many experiments measuring Stark effect in alkali Rydberg atoms [150, 199, 100, 106]. Rydberg atoms are susceptible to external fields due to its large size. The ground state of hydrogen exhibits a quadratic stark effect as it has zero permanent electric dipole moment. While the degenerate excited states of hydrogen exhibit linear Stark effect which follows from a pure Coulomb potential [24]. Any deviation from the Coulomb potential will destroy the linear Stark effect. The Rydberg electron with low orbital momentum ($l < 3$) will experience an effective potential that is different from

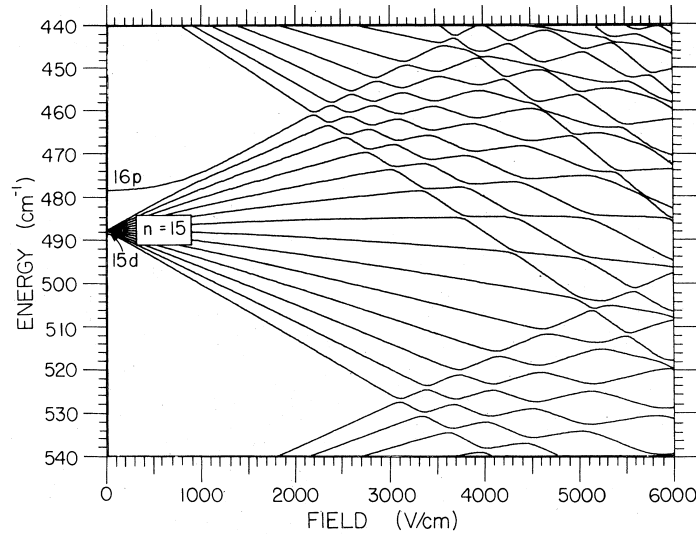


Figure 2.4: Stark effect for Na reproduced from [218]. The quadratic Stark effect is clearly visible for the p state. The presence of avoided crossings for large field intensities is a result of the non-zero quantum defects.

the Coulomb potential (see Fig.2.1). Even for extremely weak fields, the energies for different low l states are different for the same n resulting in a quadratic Stark shift (see Fig.2.4). Using non-degenerate perturbation theory in the weak field limit, one derives the shift in the energy for a Rydberg atom with $l < 3$ to be second order with respect to the electric field and is given by

$$E_{Stark} = \alpha \frac{\mathcal{E}^2}{2}, \quad (2.12)$$

Here α is the scalar, static polarizability defined as

$$\alpha = -2 \sum_{nlm_l \neq n'l'm'_l} \frac{|\langle n'l'm_l | \boldsymbol{\mu} | nlm_l \rangle|^2}{|\hbar\omega_{nl,n'l'}|} \sim \frac{n^4}{n^{-3}} \sim n^7. \quad (2.13)$$

For weak field, the states couple to the energetically close by states and hence the scaling of the polarizability is given by the combined scaling of the dipole moment and transition frequency for neighbouring Rydberg states.

For $l > 3$, the Rydberg states are degenerate and exhibit a linear Stark effect. The resulting shift is calculated using degenerate perturbation theory. When very strong electric fields are applied to Rydberg states then perturbation theory is not valid anymore. Nevertheless for strong fields, one can diagonalize the Hamiltonian for several n states as was done in [218]. The number of basis states depends on the required accuracy and strength of the field. Yet another difference in the Stark map between an excited hydrogen atom and a Rydberg atom is the presence of avoided crossings in the strong field regime (see Fig.2.2). One can solve the hydrogen atom in the external electric field in parabolic co-ordinates by exploiting the symmetry due to the $1/r$ potential. As a

result of this symmetry, there is no coupling between the degenerate excited states and thus no avoided crossings. The strong coupling between the n and $n - 1$ manifolds of the alkali Rydberg atom for low l states occurs for non-zero quantum defects where this degeneracy is broken. By changing the electric field along the avoided crossings in a controlled manner, one is able to selectively prepare high l states in a Rydberg atom which is not possible in hydrogen atom [154, 69].

2.2.5 Atom-atom interactions

Strong Rydberg interactions can be used to study short as well as long range interactions in many body physics. The very first direct measurement of van der Waals interaction between two Rydberg atoms was done very recently in [17]. Two Rydberg atoms placed next to each other at a distance R will experience an interaction due to the mutually induced electric dipole moments. The position of the electron relative to their respective nuclei is denoted by $\mathbf{r}_{i=1,2}$. The Hamiltonian for such a system is

$$H = H_A^{(1)} + H_A^{(2)} + V_{int}(\mathbf{r}_1, \mathbf{r}_2, \mathbf{R}) . \quad (2.14)$$

where $H_A^{(i)} \equiv H_A(r_i)$ is the atomic Hamiltonian defined in Eq.(2.1) and $V_{int}(\mathbf{r}_1, \mathbf{r}_2, \mathbf{R})$ is the interaction potential given as

$$V_{int}(\mathbf{r}_1, \mathbf{r}_2, \mathbf{R}) = \left[\frac{1}{|\mathbf{R}|} - \frac{1}{|\mathbf{R} - \mathbf{r}_1|} - \frac{1}{|\mathbf{R} + \mathbf{r}_1|} + \frac{1}{|\mathbf{R} - \mathbf{r}_1 + \mathbf{r}_2|} \right] . \quad (2.15)$$

If the inter-nuclear distance between the two Rydberg atoms is much larger compared to the size of the individual Rydberg electronic wave function ($R \gg r_i$), we can approximate $V_{int}(\mathbf{r}_1, \mathbf{r}_2, \mathbf{R})$ using the multipole expansion. Keeping the dipole terms in Eq.(2.15), we get

$$V_{int}(\mathbf{R}) \simeq \left[\frac{\boldsymbol{\mu}_1 \cdot \boldsymbol{\mu}_2}{R^3} - \frac{3(\mathbf{R} \cdot \boldsymbol{\mu}_1)(\mathbf{R} \cdot \boldsymbol{\mu}_2)}{R^5} \right] . \quad (2.16)$$

where $\boldsymbol{\mu}_{i=1,2}$ are the electric dipole moments corresponding to each atom. Consider that each of the two Rydberg atoms are in state $|ns0\rangle$. In the two atom basis, the state is given as $|ns0, ns0\rangle$ which are coupled to energetically close by states, $|n'p, m'_p, n''pm''_p\rangle$ due to the interaction defined by Eq.(2.16),

$$\begin{aligned} V(\mathbf{R}) &= \langle n'pm'_p, n''pm''_p | V_{int}(\mathbf{R}) | ns0, ns0 \rangle \\ &= \delta_{m'_p, 0} \delta_{m''_p, 0} \left[\frac{\boldsymbol{\mu}_{ns, n'p} \cdot \boldsymbol{\mu}_{ns, n''p}}{R^3} - \frac{3(\mathbf{R} \cdot \boldsymbol{\mu}_{ns, n'p})(\mathbf{R} \cdot \boldsymbol{\mu}_{ns, n''p})}{R^5} \right] . \end{aligned} \quad (2.17)$$

where $n', n'' = n \pm 1$. In general, all the m sub levels contribute to the van der Waals coefficient, but for simplicity, we assume that the quantization axis is along the inter-nuclear axis (which is the z-axis). The Hamiltonian expressed in the two atom basis $\{|ns0, ns0\rangle, |n'p0, n''p0\rangle\}$ is written as

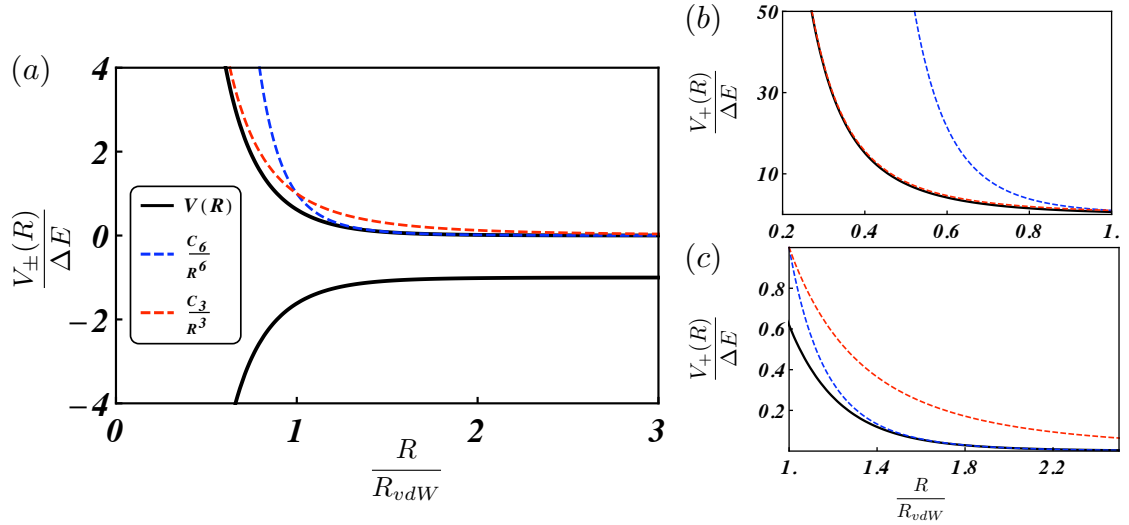


Figure 2.5: (a) Comparison of the full interaction potential (black) using Eq.(2.19) with the dipole interaction (dashed red) and van der Waals interaction (dashed blue) at small R shown in (b) and for large R as shown in (c).

$$\begin{pmatrix} \Delta E & V(R) \\ V(R) & 0 \end{pmatrix}, \quad (2.18)$$

where $\Delta E = 2E_{ns} - (E_{n''p} + E_{n'p})$. Upon diagonalization we get the eigenvalues,

$$V_{\pm}(R) = \frac{\Delta E \pm \sqrt{(\Delta E)^2 + 4V^2(R)}}{2}. \quad (2.19)$$

Depending on the strength of the interaction $V(R)$ and the energy difference ΔE , there are two different limiting cases.

(a) Dipole-Dipole interaction ($V(R) \gg \Delta E$): For small distances, the dipole-dipole interaction dominates (see Fig.2.5). This is derived by expanding Eq.(2.19) around $\Delta E = 0$ which gives,

$$V_{dip} = \pm V(R) = \frac{C_3}{R^3} \sim n^4. \quad (2.20)$$

The scaling law for n is determined by the square of the radial dipole matrix element for nearest neighbouring Rydberg states.

(b) van der Waals interaction ($\Delta E \gg V(R)$): The van der Waals interaction is dominant at large distances (see Fig.2.5) and is calculated perturbatively by expanding in terms of $V(R)/\Delta E$ in Eq.(2.19),

Property	n scaling
Size $\langle r \rangle$	n^2
Energy E_{nl}	n^{-2}
Energy difference $ E_{nl} - E_{n'=n\pm 1, l'=l\pm 1} $	n^{-3}
Geom. cross section σ	n^4
Dipole moment $\mu_{nl, n'=n\pm 1, l'=l\pm 1}$	n^2
Radiative lifetime τ	n^3
Polarizability α	n^7
van der Waals interaction C_6	n^{11}

Table 2.1: Properties of Rydberg atoms scaling with the principal quantum number.

$$V_{vdW} = \frac{V(R)^2}{\Delta E} = \frac{C_6}{R^6} \sim \frac{(n^4)^2}{n^{-3}} \sim n^{11}. \quad (2.21)$$

The strength of this long range interaction is determined by the van der Waal coefficient (dispersion coefficient) C_6 . The nature of the interaction (attractive/repulsive) is determined by the sign of ΔE which in turn depends on the quantum defects. The scaling law for n is determined by the square of the radial dipole matrix element and the energy difference in the denominator. This scaling indicates that for a highly excited state, the interactions are very strong. For example, the interaction between two Rb Rydberg atoms in 40s state can be 15 orders of magnitude larger compared to their ground state counterparts [186]. The transition from the short range interaction to the long range interaction occurs at the van der Waals radius defined as $R_{vdW} = \sqrt[6]{|C_6/\Delta E|}$ where the van der Waals interaction equals the dipole interaction. Although we have derived here for a reduced basis set involving only two Rydberg states, the interactions determined by the the full state (including all the magnetic sub levels) will have the same qualitative behaviour as discussed here (refer to Appendix B).

2.3 Summary

The multi-electron alkali Rydberg atom is studied as an effective single electron atom. An electron in the Rydberg state is far from the ionic core and the effective potential experienced by it is modified by the inner electrons. The deviation from the pure Coulomb potential is given by the quantum defects and is included in the effective principal quantum number. The quantum defects determine the extent of non-degeneracy for low l states of a Rydberg atom in contrast to hydrogen atom. A direct consequence of the non-degenerate low l states of a Rydberg atom, is the quadratic stark effect and avoided crossings for high electric field. Rydberg atoms are ideal for manipulation due to its high sensitivity to surrounding fields as a result of its large atomic size (three orders of magnitude larger than the ground state hydrogen atom). Since the Rydberg electron is isolated from the core, there is small overlap with its ground state resulting in long lifetimes (few hundred μs for 70s Rb) of the Rydberg atom. The interaction energy between two Rydberg atoms has a scaling law with respect to the principal quantum number as

n^{11} giving rise to very strong interactions between atoms. Table 2.1 summarizes the different scaling laws for the various properties of the Rydberg atom.

In the next chapter, we study alkaline-earth Rydberg atoms which have two valence electrons where one of the valence electron is in the Rydberg state. The extra valence electron provides an opportunity to have additional control on the Rydberg atom but in order to calculate the Rydberg states of any alkaline-earth atom, one needs to take into account the effect of the interaction between the two valence electrons.

Alkaline-earth Rydberg atoms: Strontium

Contents

3.1	Effective two electron model for strontium	17
3.1.1	Singly ionized strontium atom	17
3.1.2	Singlet and triplet states	18
3.2	Theory of two electron Rydberg atoms	19
3.2.1	Multi-channel quantum defect theory	19
3.2.2	Hartree-Fock equations	22
3.2.3	Perturbation theory	23
3.3	Structure and properties	24
3.3.1	Rydberg energies and wave functions	25
3.3.2	Rydberg interactions	26
3.4	Summary	27

Alkaline-earth Rydberg atoms will have additional control due to the presence of two valence electrons. One of the valence electron is free for manipulation while the other is excited to the Rydberg state. One direct application is the optical detection of Rydberg states using the second non-excited electron [185]. Similar to alkali Rydberg atoms, alkaline-earth Rydberg atoms are treated effectively as two electron atoms [176, 85]. The crucial difference with alkali Rydberg atoms is the effect of the interaction between the two valence electrons present in alkaline-earth Rydberg atoms. Focusing on strontium (Sr), the Rydberg states are calculated using single configuration mean field theory. The calculated states are compared with available experimental data. The van der Waals interaction for ns states of strontium are evaluated and compared with alkali Rydberg atoms.

3.1 Effective two electron model for strontium

The full Hamiltonian for the strontium Rydberg atom consists of the singly ionized strontium Hamiltonian and the electron-electron repulsion between the two valence electrons located at positions \mathbf{r}_1 and \mathbf{r}_2 relative to the nucleus respectively,

$$\hat{H}\psi(\mathbf{r}_1, \mathbf{r}_2) = \left[\hat{H}_1^{Sr^+} + \hat{H}_2^{Sr^+} + \frac{1}{r_{12}} \right] \psi(\mathbf{r}_1, \mathbf{r}_2) . \quad (3.1)$$

where $\mathbf{r}_{12} = \mathbf{r}_2 - \mathbf{r}_1$ is the distance between the two valence electrons. Similar to alkali atoms, the singly ionized strontium atom has one valence electron. Using the single electron approximation (refer section 2.1), one defines an effective model potential. This simplifies the study of strontium Rydberg atom to effectively a two electron atom problem.

3.1.1 Singly ionized strontium atom

The Schrödinger equation for a singly ionized strontium atom (Sr^+) is

$$\hat{H}_{1,2}^{Sr^+} \psi_k^{Sr^+}(\mathbf{r}_{1,2}) = \left[-\frac{\hbar^2}{2m} \nabla^2 + V_{eff}^{Sr^+}(r) \right] \psi_k^{Sr^+}(\mathbf{r}_{1,2}) = E_k^{Sr^+} \psi_k^{Sr^+}(\mathbf{r}_{1,2}) . \quad (3.2)$$

where $k = nljm_j$, with $j \in \{l - 1/2, l + 1/2\}$ as the total angular momentum of the individual electron and $m_j \in \{-j, -j+1, \dots, j-1, j\}$ is the projection of the total angular momentum on the quantization axis. $V_{eff}^{Sr^+}(r)$ is the effective model potential for the singly ionized strontium atom [176] given as

$$V_{eff}^{Sr^+}(r) = V_C^{Sr^+}(r) + V_{SO}^{Sr^+}(r) . \quad (3.3)$$

It has two parts, the core potential and the spin-orbit coupling potential. The core potential $V_C^{Sr^+}(r)$ [176, 85] is similar to the potential used for alkali Rydberg atoms in Eq.(2.4) as seen below,

$$V_C^{Sr^+}(r) = -\frac{q^2}{4\pi\epsilon_0 r} \left[2 + (Z - 2)e^{-a_1(l)r} + a_2(l)re^{-a_3(l)r} \right] - \frac{\alpha_c}{2r^4} \left[1 - e^{-(r/r_l)^6} \right] . \quad (3.4)$$

The physical significance for each of the above terms has been discussed in great detail in section 2.1. The parameters of the model potential are determined from fits to experimental data for low and inter-mediate levels of Sr^+ energies [116, 89]. The fine structure interval is determined by the interaction of the valence electron with the polarized core and is defined in the spin-orbit coupling interaction term which is defined as

$$V_{SO}^{Sr^+}(r) = \frac{1}{4m^2c^2} \frac{1}{r} \frac{dV_C^{Sr^+}}{dr} (j(j+1) - l(l+1) - s(s+1)) . \quad (3.5)$$

This interaction depends on the inverse power of r and scales as n^{-3} [74]. Thus the spin-orbit coupling is negligible for highly excited states as compared to the low lying states of the atom [61]. This is also why we did not include it for the model potential in the alkali Rydberg atoms in Eq.(2.4). But for our purposes, we would often be dealing with low lying states and its coupling to the Rydberg states particularly in later chapters. Thus from here onwards we do not refer to the index j, m_j for the Rydberg states but only for the low lying states.

3.1.2 Singlet and triplet states

The total spin for a two electron atom can either be in a singlet or triplet state. Denoting χ_{\pm} as the total spin wave function for the two electron atom where

$$(S = 0) \quad \chi_{-} = \frac{1}{\sqrt{2}} [\uparrow\downarrow - \downarrow\uparrow] , \quad (3.6)$$

$$(S = 1) \quad \chi_{+} = \begin{cases} \frac{1}{\sqrt{2}} [\uparrow\downarrow + \downarrow\uparrow] \\ \uparrow\uparrow \\ \downarrow\downarrow . \end{cases}$$

\mathbf{S} is the total spin quantum number which takes value 0 (singlet state) or 1 (triplet state) depending on whether the spins of the two valence electrons are aligned or anti-aligned. Radiative transitions between the singlet and triplet states (intercombination lines) are dipole forbidden where the spin-orbit interactions are negligible as is the case in He atom [103]. In contrast to lighter atoms, for heavier atoms such as strontium, there can be weak intercombination lines. A shorthand notation to write the two electron state in LS coupling (Russel-Saunders coupling) is $^{2S+1}L_J$ where $\mathbf{L} = \mathbf{l}_1 + \mathbf{l}_2$ is the total orbital quantum number and $\mathbf{J} = \mathbf{L} + \mathbf{S}$ is the total angular momentum (orbital and spin). Forbidden low lying transition lines have applications, for example the 1S_0 - 3P_1 (689 nm) transition has been used to trap strontium in red detuned MOT's [105] of the inter-mediate state which has a lifetime of 21.32 μ s. While the transition 1S_0 - 3P_0 (698 nm) has been used for lattice clocks [191] exploiting the large lifetime (159 s) of the meta-stable state.

3.2 Theory of two electron Rydberg atoms

Already for the simplest two electron atom, helium, exact analytical solutions cannot be found even for the ground state and approximate solutions have been obtained using variational principle [109, 118] or perturbation theory [188]. In the central field theory, the total energy of the atom depends on the *electronic configuration* which determines the distribution of the electrons with respect to the quantum numbers n and l . For a closed shell, it is sufficient to describe the quantum states of the valence electrons which are referred as the optically active electrons. In general for alkaline-earth atoms, there are many possible configurations. For example for strontium, one can have $5sns$, $5snp$, $5pns$, $5pnp$... and so on. In order to take into account the electron-electron interaction in Eq.(3.1), one uses multi-configuration Hartree-Fock theory (MCHF). Such full scale configuration interaction calculations have been carried out for various alkaline-earth atoms [197]. MCHF equations are solved using a trial wave function given as a sum of single Slater determinant wave function ψ_i [74],

$$\Psi(\mathbf{r}_1, \mathbf{r}_2) = \sum_i C_i \psi_i(\mathbf{r}_1, \mathbf{r}_2) . \quad (3.7)$$

Consider a particular configuration $i \equiv 5sns$ then the corresponding single Slater determinant is given by

$$\psi_{5sns}(\mathbf{r}_1, \mathbf{r}_2) = \frac{1}{\sqrt{2}} \begin{vmatrix} u_{5s}(\mathbf{r}_1) & u_{ns}(\mathbf{r}_1) \\ u_{5s}(\mathbf{r}_2) & u_{ns}(\mathbf{r}_2) \end{vmatrix}. \quad (3.8)$$

where $u_k = \phi_k \chi_k$ are spin-orbital wave functions for a single particle. Here ϕ_k and χ_k correspond to the atomic orbital and spin wave function of the single particle respectively. The energy corresponding to the full wave function Ψ is variationally minimized with respect to the coefficients and the single Slater determinants. For sufficiently large number of configurations included in Eq.(3.7), the diagonalization of the two electron Hamiltonian in terms of the single Slater wave functions gives a reasonably accurate result. The difference in the energy obtained from single configuration Hartree-Fock method (E_{HF}) and MCHF (E_{MCHF}) is the measure of the correlation energy $E_{\text{corr}} = |E_{\text{HF}} - E_{\text{MCHF}}|$. This can be significant in certain cases, for example for ground state He, it is $E_{\text{corr}} = -0.042$. This implies that the interactions between the two or more configurations cannot be neglected. Interactions between configurations occur when there are accidental resonances or near resonances between states belonging to two different series. However, there are special cases where the states in question are described by a single channel and one can employ single configuration Hartree-Fock theory. The concept of channel mixing is best understood using multi-channel quantum defect theory (MQDT).

3.2.1 Multi-channel quantum defect theory

MQDT was first used by Seaton [183] and Fano [62, 63] to study interacting Rydberg series. Two different Rydberg series (channels) converge to two different ionic states with the continua above them (see Fig.3.1). For spherically symmetric ground state, one assumes that all the excited states of the ion are far away from the Rydberg states of the atom. This is usually justified if the inner core does not exchange energy or angular momentum with the Rydberg electron. A particular state of one series is a *perturbing state* if that particular state is resonant to another bound state or a continuum state belonging to another series. The latter corresponds to autoionization where one of the electron is lost to the continuum. For example for strontium, $5p^2$ is a perturber to the $5sns$ series as it is near resonant to $5s7s$ as shown in Fig.3.1. This phenomena of *resonance interference* is studied in great detail using MQDT [176, 74]. The effect of the perturbers in alkaline-earth atoms has been theoretically investigated to a great extent using MQDT [10, 11]. Experimentally it was shown that the only perturber that exists to the strontium $5sns$ series is $5p^2$. No perturbers were found for high lying states.

The basic principle of MQDT is borrowed from scattering theory which is to distinguish the effects of the long range and short range interaction between the core and the valence electron. In chapter 2, we know that an electron within the core radius experiences a deeper Coulomb potential which leads to a phase shift of $\pi\delta$ for the reflected outer part of the wave function since the incoming Coulomb wave scatters from the core

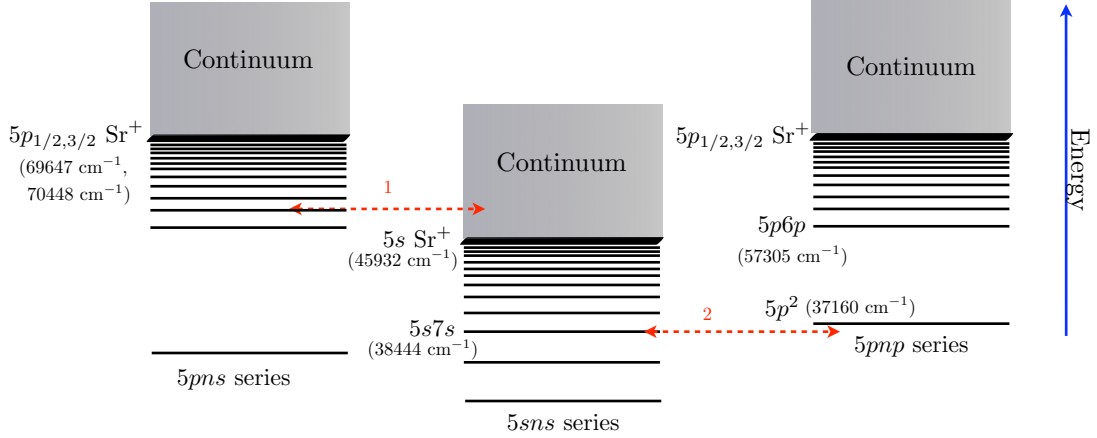


Figure 3.1: The figure shows different series of bound Rydberg states (thin lines) of strontium converging to respective ionic states (bold lines) with their corresponding continuum states (grey region). The electron-electron interaction causes coupling between different channels as depicted by the red dashed lines. The energies have been taken from various sources [158, 60, 83, 210]

and not a proton. Far away from the core, the open channel (also known as collision channels) wave function would be similar to a scattering wave function [74] given as

$$\psi_i^o = \frac{1}{r} [f(E_i, l, r) \cos \pi \nu_i + g(E_i, l, r) \sin \pi \nu_i] F_i . \quad (3.9)$$

where F_i is the product of the angular part of the Rydberg wave function, spin part and the ionic wave function. f is the regular Coulomb wave function while g is the irregular Coulomb wave function, both dependent on the Rydberg energy E_i and angular momentum l . For $r \rightarrow 0$, $f \propto r^{l+1}$ and $g \propto r^{-l}$. For $r \rightarrow \infty$, f and g are sine and cosine functions respectively. The open channel wave functions match the outer boundary condition of vanishing at $r \rightarrow \infty$ iff $E_i = -1/(2(n^*)_i^2)$ (in atomic units), where n^* is the effective principal quantum number defined in Eq.(2.5). For close to the ion core, the wave functions would correspond to normal modes scattered from the core which are given as standing waves [74] given as

$$\psi_\alpha^c = \frac{1}{r} \sum_i U_{i\alpha} [f(E_i, l, r) \cos \pi \mu_\alpha + g(E_i, l, r) \sin \pi \mu_\alpha] F_i . \quad (3.10)$$

The above is a linear combination of all the incoming hydrogen wave functions and the outgoing phase shifted wave functions with eigenchannel quantum defects μ_α . The above closed wave function satisfies the inner boundary condition for $r = r_c$ (core radius). For a Rydberg wave function at an arbitrary distance $r > r_c$, one can express it either in terms of the open or closed channel eigenfunctions.

$$\Psi(\mathbf{r}_1, \mathbf{r}_2) = \sum_i A_i^{(n)} \psi_i^o + \sum_\alpha B_\alpha^{(n)} \psi_\alpha^c . \quad (3.11)$$

One can define a unitary transformation $U_{i\alpha}$ that takes one basis to the other as follows,

$$A_i^{(n)} = \sum_{\alpha} U_{i\alpha} \cos[\pi(n_i^* + \mu_{\alpha})] B_{\alpha}^{(n)}. \quad (3.12)$$

It essentially describes the change in the coupling between the core and the electron as the distance varies. Using Eq.(3.9) and Eq.(3.10) into Eq.(3.11), one obtains the Fano formulation of QDT [62] with the following equations,

$$\frac{1}{2(n_i^*)^2} = \frac{1}{2(n_j^*)^2} = \dots, \quad (3.13)$$

$$\det|U_{i\alpha} \sin[\pi(n_i^* + \mu_{\alpha})]| = 0. \quad (3.14)$$

The above two sets of fundamental equations in MQDT need to be simultaneously satisfied. The full wave function is expressed as a linear combination of the normalized bound wave functions corresponding to each channel from Eq.(3.11),

$$\Psi(\mathbf{r}_1, \mathbf{r}_2) = \sum_i Z_i^{(n)} \psi_i^o = \sum_i \frac{(n_1^*)^{3/2}}{N_n} A_i^{(n)} \psi_i^o. \quad (3.15)$$

where $Z_i^{(n)}$ are the admixture coefficients corresponding to each channel and $N_n^2 = \sum_i (A_i^{(n)})^2 (n_i^*)^3$ is the normalization constant. As an exercise, we consider two channels for the 1S_0 series of strontium, namely $5sns$ denoted as channel 1 and the $5pnp$ series denoted as channel 2. Then we have,

$$\Psi(\mathbf{r}_1, \mathbf{r}_2) = Z_1^{(n)} \psi_1^o(\mathbf{r}_1, \mathbf{r}_2) + Z_2^{(n)} \psi_2^o(\mathbf{r}_1, \mathbf{r}_2). \quad (3.16)$$

The unitary matrix $U_{i\alpha}$ for two channels is determined using parameters β and $\mu_{1,2}$ given as

$$\begin{pmatrix} \cos \beta \sin[\pi(n_1^* + \mu_1)] & \cos \beta \sin[\pi(n_1^* + \mu_2)] \\ \cos \beta \sin[\pi(n_2^* + \mu_1)] & \cos \beta \sin[\pi(n_2^* + \mu_2)] \end{pmatrix}. \quad (3.17)$$

β is the interaction parameter between the two channels. Both these parameters (β and $\mu_{1,2}$) are determined either by using R-matrix theory [12] or by fitting the energies from experimental data as was done in [43]. Following [43], the admixture coefficients corresponding to each channel are

$$A_1^{(n)} = (-1)^{l_1+1} \left[\cos \beta \cos[\pi(n_1^* + \mu_1)] C_{1,1}^{(n)} + \sin \beta \cos[\pi(n_1^* + \mu_2)] C_{1,2}^{(n)} \right], \quad (3.18)$$

$$A_2^{(n)} = (-1)^{l_2+1} \left[-\sin \beta \cos[\pi(n_2^* + \mu_1)] C_{2,1}^{(n)} + \cos \beta \cos[\pi(n_2^* + \mu_2)] C_{2,2}^{(n)} \right]. \quad (3.19)$$

where $C_{i,\alpha}^{(n)}$ is defined as

$$C_{i,\alpha}^{(n)} = \frac{Cof[U_{i,\alpha}]}{\sqrt{Cof[U_{i,1}]^2 + Cof[U_{i,2}]^2}}. \quad (3.20)$$

where $Cof[U_{i,\alpha}]$ is the co-factor of the 2×2 matrix in Eq.(3.17). The admixture coefficients are calculated for low lying states. As shown in Table 3.1, there is considerable mixing of the series for the low lying states but it effectively reduces to a single channel theory for large n 's in $5sns$ series.

$5s(n)s$	$ Z_1^{(n)} ^2$	$ Z_2^{(n)} ^2$
6	0.86	0.14
7	0.72	0.28
8	0.98	0.02
9	0.9998	0.0002
10	0.998	0.002
11	0.99995	0.00005

Table 3.1: The admixture coefficients were calculated for MQDT parameters, $\mu_1 = 0.291$, $\mu_2 = 0.145$, $\beta = 0.359$ taken from [43].

This implies that for singly excited Rydberg state belonging to the $5sns$ series, a single configuration approximation can be used as they are no states from another series resonant to it. All the other states in other series are far away from the Rydberg states $5sns$ (some are shown in Fig.3.1). Having justified the single configuration approximation, we now proceed to solving the Hartree-Fock equations for the effective two electron model.

3.2.2 Hartree-Fock equations

We solve for the specific case of a singly excited Rydberg atom and thus considering only a single configuration. Thus the wave function for the effective two electron atom expressed in terms of the ground state $|5s\rangle$ and a Rydberg state $|nl\rangle$ (refer to the orbital part of u_k in Eq.(3.8)) is

$$\psi_{\pm}(\mathbf{r}_1, \mathbf{r}_2) = \frac{1}{\sqrt{2}} (\phi_{5s}(\mathbf{r}_1)\phi_{nl}(\mathbf{r}_2) \pm \phi_{5s}(\mathbf{r}_2)\phi_{nl}(\mathbf{r}_1)) . \quad (3.21)$$

It is assumed that the single particle orbitals are orthonormal. One applies variational principle where the energy of the full system $\delta E[\psi]$ remains stationary ($\delta E[\psi] = 0$) for small variation in the Slater determinant. To calculate the energy functional $E[\psi]$, we need to evaluate the matrix elements for the Hamiltonian in Eq.(3.1) in terms of the trial wave function ψ_{\pm} ,

$$\begin{aligned}
E[\psi_{\pm}] &= \langle \psi_{\pm}(\mathbf{r}_1, \mathbf{r}_2) | \hat{H} | \psi_{\pm}(\mathbf{r}_1, \mathbf{r}_2) \rangle \\
&= \left[\langle \phi_{5s}(\mathbf{r}_1) | \hat{H}_1^{Sr+} | \phi_{5s}(\mathbf{r}_1) \rangle + \langle \phi_{nl}(\mathbf{r}_2) | \hat{H}_2^{Sr+} | \phi_{nl}(\mathbf{r}_2) \rangle \right] + \\
&\quad \frac{1}{2} \left[\langle \phi_{5s}(\mathbf{r}_1) \phi_{nl}(\mathbf{r}_2) | \frac{1}{r_{12}} | \phi_{5s}(\mathbf{r}_1) \phi_{nl}(\mathbf{r}_2) \rangle + \langle \phi_{5s}(\mathbf{r}_2) \phi_{nl}(\mathbf{r}_1) | \frac{1}{r_{12}} | \phi_{5s}(\mathbf{r}_2) \phi_{nl}(\mathbf{r}_1) \rangle \right. \\
&\quad \left. \pm \langle \phi_{5s}(\mathbf{r}_1) \phi_{nl}(\mathbf{r}_2) | \frac{1}{r_{12}} | \phi_{5s}(\mathbf{r}_2) \phi_{nl}(\mathbf{r}_1) \rangle + \langle \phi_{5s}(\mathbf{r}_2) \phi_{nl}(\mathbf{r}_1) | \frac{1}{r_{12}} | \phi_{5s}(\mathbf{r}_1) \phi_{nl}(\mathbf{r}_2) \rangle \right] .
\end{aligned} \tag{3.22}$$

The second line consists of only single particle matrix elements while the last line contains two particle matrix elements. One can define a Fock operator that acts on the single particle state as follows,

$$\hat{F} \phi_{5s}(\mathbf{r}_1) = H_{Sr+}(r_1) \phi_{5s}(\mathbf{r}_1) + V_{nl}(r_1) \phi_{5s}(\mathbf{r}_1) \pm V_{5s,nl}(r_1) \phi_{nl}(\mathbf{r}_1) , \tag{3.23a}$$

$$\hat{F} \phi_{nl}(\mathbf{r}_2) = H_{Sr+}(r_2) \phi_{nl}(\mathbf{r}_2) + V_{5s}(r_2) \phi_{nl}(\mathbf{r}_2) \pm V_{nl,5s}(r_2) \phi_{5s}(\mathbf{r}_2) . \tag{3.23b}$$

$\phi_{5s,nl}$ solve Eqs.(3.23a,3.23b) and $(V_{nl}(r_1), V_{5s}(r_2))$ are the *direct Coulomb potentials* defined as

$$V_{nl}(r_1) = \int_0^{\infty} \frac{1}{\mathbf{r}_{12}} \phi_{nl}^*(\mathbf{r}_2) \phi_{nl}(\mathbf{r}_2) d\mathbf{r}_2 , \tag{3.24}$$

$$V_{5s}(r_2) = \int_0^{\infty} \frac{1}{\mathbf{r}_{12}} \phi_{5s}^*(\mathbf{r}_1) \phi_{5s}(\mathbf{r}_1) d\mathbf{r}_1 . \tag{3.25}$$

It is the local Coulomb field experienced by one electron due to other located at a distance r_{12} from it. Whereas $V_{5s,nl}(r_1)$, $V_{nl,5s}(r_2)$ are the non-local *exchange potentials* defined as follows,

$$V_{5s,nl}(r_1) = V_{nl,5s}(r_2) = \int_0^{\infty} \frac{1}{\mathbf{r}_{12}} \phi_{nl}^*(\mathbf{r}_2) \phi_{5s}(\mathbf{r}_2) d\mathbf{r}_2 = \int_0^{\infty} \frac{1}{\mathbf{r}_{12}} \phi_{5s}^*(\mathbf{r}_1) \phi_{nl}(\mathbf{r}_1) d\mathbf{r}_1 . \tag{3.26}$$

The above potential is based on the spatial exchange symmetry and distinguishes the singlet from the triplet state. A sufficient but not necessary condition ensuring that $\delta E[\psi] = 0$ is fulfilled if the Fock operators defined Eq.(3.23a)-(3.23b) are diagonal in the single particle basis states and thus giving

$$[H_{Sr+}(r_1) + V_{nl}(r_1)] \phi_{5s}(\mathbf{r}_1) \pm V_{5s,nl}(r_1) \phi_{nl}(\mathbf{r}_1) = \varepsilon_{5s} \phi_{5s}(\mathbf{r}_1) , \tag{3.27a}$$

$$[H_{Sr+}(r_2) + V_{5s}(r_2)] \phi_{nl}(\mathbf{r}_2) \pm V_{nl,5s}(r_2) \phi_{5s}(\mathbf{r}_2) = \varepsilon_{nl} \phi_{nl}(\mathbf{r}_2) . \tag{3.27b}$$

The above coupled set of equations are *not eigenvalue equations* since the potential terms depend on the single particle orbitals itself. Hartree-Fock method involves a self

consistency issue which is solved iteratively. The integro-differential equations (3.27a) and (3.27b) can be solved by starting with a trial function $\phi_1^{(0)}$ and then using them in (3.27a) and (3.27b) iteratively to obtain $\phi_1^{(0)}$, $\phi_0^{(1)}$, $\phi_1^{(1)}$ and so on until convergence is achieved. Quite often the trial functions used for the single particle orbitals ϕ_i 's are the eigenfunctions of the single particle Hamiltonian which in our case is the singly ionized strontium wave functions $\psi_k^{Sr^+}$ where $k = nl$ (suppressing the j, m_j).

3.2.3 Perturbation theory

Due to the very small overlap between the Rydberg electron and the ground state electron, we treat the Rydberg potential on the ground state ($V_{nl}(r_1)$) and the exchange terms ($V_{5s,nl}(r_1)$, $V_{nl,5s}(r_2)$) as perturbations to the ionic energies $E_{5s}^{Sr^+}$ and $E_{nl}^{Sr^+}$. The starting point is to take the ground state wave function for strontium ion as our initial trial function $\phi_{5s}^{(0)} = \psi_{5s}^{Sr^+}(\mathbf{r})$ with energy $\varepsilon_{5s}^{(0)} = E_{5s}^{Sr^+}$ satisfying Eq.(3.2). Using $\phi_{5s}^{(0)}$ in Eq.(3.25), the ground state potential for the Rydberg electron is calculated and inserted into the following equation,

$$[H_{Sr^+}(r_2) + V_{5s}(r_2)] \phi_{nl}^{(0)}(\mathbf{r}_2) = \varepsilon_{nl}^{(0)} \phi_{nl}^{(0)}(\mathbf{r}_2) , \quad (3.28)$$

$$\text{where } V_{5s}(r_2) = \int_0^\infty |\phi_{5s}(r_1)|^2 \frac{r_1^2 dr_1}{r_>} . \quad (3.29)$$

to obtain Rydberg wave functions $\phi_{nl}^{(0)}$ with energies $\varepsilon_{nl}^{(0)}$. Using the Rydberg wave functions, we calculate the first order corrections to the ground state energy and the Rydberg energy

$$\varepsilon_{5s} = E_{5s}^{Sr^+} + E_{nl,D}^{(1)} \pm E_{nl,Ex}^{(1)} , \quad (3.30)$$

$$\varepsilon_{nl} = \varepsilon_{nl}^{(0)} \pm E_{nl,Ex}^{(1)} . \quad (3.31)$$

where the energy corrections $E_D^{(1)}$ and $E_{Ex}^{(1)}$ are given by

$$\begin{aligned} E_{nl,D}^{(1)} &= \langle \phi_{5s}^{(0)}(\mathbf{r}_2) | V_{nl} | \phi_{5s}^{(0)}(\mathbf{r}_2) \rangle \\ &= \int_0^\infty |\phi_{5s}^{(0)}(r_1)|^2 |\phi_{nl}^{(0)}(r_2)|^2 \frac{1}{r_>} r_1^2 r_2^2 dr_1 dr_2 , \end{aligned} \quad (3.32)$$

$$\begin{aligned} E_{nl,Ex}^{(1)} &= \langle \phi_{nl}^{(0)}(\mathbf{r}_2) | V_{nl,5s}(r_2) | \phi_{5s}^{(0)}(\mathbf{r}_1) \rangle = \langle \phi_{5s}^{(0)}(\mathbf{r}_1) | V_{5s,nl}(r_1) | \phi_{nl}^{(0)}(\mathbf{r}_1) \rangle \\ &= \frac{1}{2l+1} \int_0^\infty \phi_{5s}^{(0)}(r_1) \phi_{5s}^{(0)}(r_2) \phi_{nl}^{(0)}(r_1) \phi_{nl}^{(0)}(r_2) \frac{r_<^l}{r_>^{l+1}} r_1^2 r_2^2 dr_1 dr_2 . \end{aligned} \quad (3.33)$$

The expressions for the potential V_{5s} in Eq.(3.29) and the energy corrections in Eqs.(3.32)-(3.33) are obtained by implementing multipole expansion for $\frac{1}{r_{12}}$. The properties of spherical harmonics are used to solve the angular part of the integrals (see Appendix C).

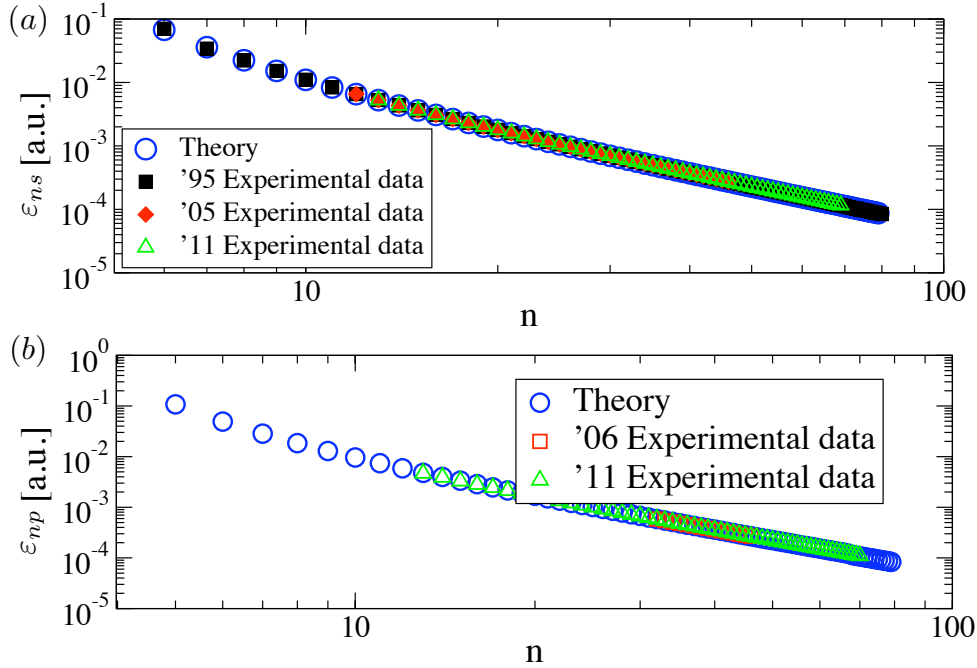


Figure 3.2: (a) Calculated energies for ns states of strontium and are compared to experimental data from [43](black square), [158](red rhombus) and [141](green triangle). (b) np energies of strontium and compared to experimental data from [158](red square) and [141](green triangle).

3.3 Structure and properties

Many of the strontium Rydberg atom properties such as the oscillator strength, lifetime, and Stark effect have been calculated theoretically and measured experimentally [174, 114, 139, 217, 140]. In this section, we show the results of our calculations such as the Rydberg energies and wave functions of strontium and the Rydberg-Rydberg interaction for ns states.

3.3.1 Rydberg energies and wave functions

Considering that a simplified (single configuration) mean field approach was used to calculate the Rydberg states, the energies obtained for (for $n > 10$) agree with available experimental data within an error of 0.1-0.2% as shown in Table 3.2 and Fig.3.2. The first order correction from the exchange energies are two to three orders of magnitude less than the ionic energies (see Fig.3.3). Negligible exchange energies for the Rydberg states imply that the Rydberg singlet and the triplet states are nearly degenerate.

In order to obtain reliable quantum defects, we however require a higher accuracy in energies than obtained in Table 3.2. Thus we fit the experimentally measured energies of ns and np from [141] with Langer's formula [74] to obtain more accurate quantum

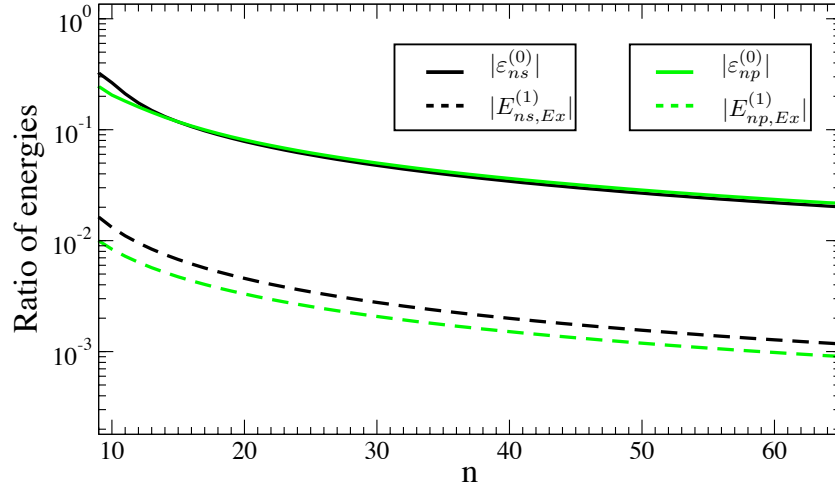


Figure 3.3: The plot compares the first order energy corrections of the exchange energy with the unperturbed energy (refer to Eq.(3.31)) for a Rydberg electron in s and p states.

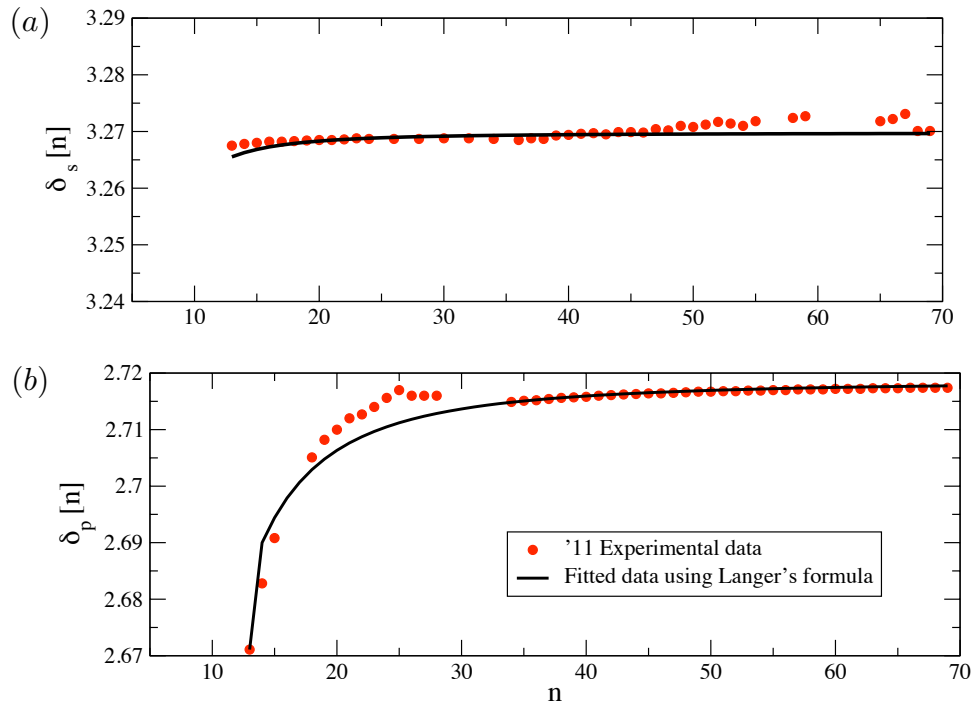


Figure 3.4: Fitted quantum defects for (a) s states (b) p states as a function of the principal quantum number given by Eqs.(3.34) and (3.35).

defects (see Fig.3.4).

Rydberg states	[78, 158, 60] [a.u.]	Theory [a.u.]	Error [%]
50s	-0.000228588	-0.000228704	0.05
65s	-0.000130771	-0.000131083	0.2
40p	-0.000361228	-0.000360699	0.14
45p	-0.000280687	-0.000280328	0.12

Table 3.2: Calculated values of ns and np Rydberg energies.

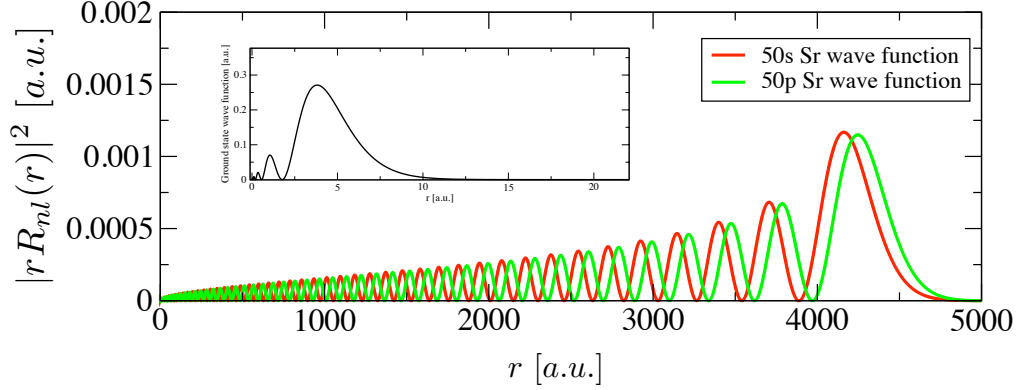


Figure 3.5: Sr wave functions for 50s and 50p states. The inpanel shows the ground state wave function.

$$\delta_s = 3.27 + \frac{1.34}{2n^2} - \left(\frac{0.016}{2n^2}\right)^2, \quad (3.34)$$

$$\delta_p = 2.715 + \frac{1.79}{2n^2} - \left(\frac{5.16 \times 10^{-9}}{2n^2}\right)^2, \quad (3.35)$$

where n is the principal quantum number. In the next section, we employ the strontium Rydberg wave functions and fitted energies to calculate the Rydberg interactions. The accuracy of the quantum defects play an important role in determining the nature of the Rydberg interactions (repulsive/attractive).

3.3.2 Rydberg interactions

In section 2.2.5, we discussed the shift in the Rydberg energies as a result of the induced interaction between two Rydberg atoms. Here we calculate the van der Waals interaction for the 1S_0 series for Sr. The dominant coupling considered here is the $ns + ns \rightarrow (n+1)p + (n-1)p$. The expression for the van der Waals interaction for this coupling (as shown in Appendix B) is given as

$$V_{vdW} = \frac{4\mu_{ns,n'p}^2 \mu_{ns,n''p}^2}{3\Delta E R^6} = -\frac{C_6}{R^6}, \quad (3.36)$$

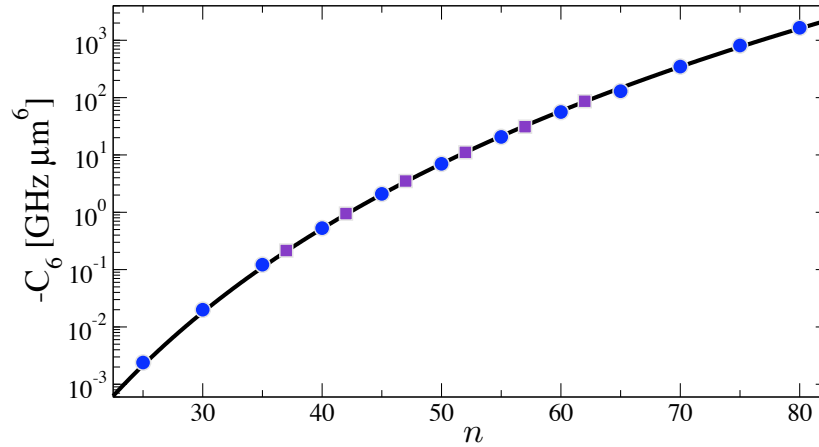


Figure 3.6: Scaling of the van der Waals coefficient with the principle quantum number as given in Eq.(3.37).

where $\Delta E = 2E_{ns} - (E_{n''p} + E_{n'p})$ and $\mu_{ns,n'(n'')p}$ are the induced dipole moments. In the above formula, Using the fitted energies and the calculated Rydberg wave functions, the scaling law for the C_6 coefficient for ns states of strontium obtained is as follows

$$C_6[a.u.] \simeq -(1.4 + 2.2 \times 10^{-1}n - 9.0 \times 10^{-4}n^2)n^{11}. \quad (3.37)$$

The van der Waals interaction for ns strontium is *attractive* (see Fig.3.6) in contrast to the alkali Rydberg atom particularly Rb [187]. Spin-orbit coupling can have significant effect on the interactions. For example, the calculation of C_6 coefficient, neglecting the spin-orbit coupling for Rb at $n=60$ has an error by a factor of 3-5 [187]. The exchange energy though argued to be small for ns strontium Rydberg states, is sufficient to contribute a flip in the sign of the interactions via the energy difference ΔE for the triplet ns states. The Rydberg interactions for the 1D_2 and 3S_0 series in strontium were shown to be repulsive [54, 142, 198]. Thus the accuracy of the quantum defects is crucial in determining the nature of the interactions.

3.4 Summary

Singly excited Rydberg states for strontium are calculated using three main approximations. Firstly, similar to alkali atoms discussed in chapter 2, we assume an effective model potential for the singly ionized alkaline-earth atom. This reduces the many electron problem to an effective two electron atom problem. We then solve the two electron Hamiltonian using mean field theory similar to Hartree-Fock theory but for a single configuration. This is our second approximation. Single configuration mean field theory is justified from experimental observations that show no high lying perturbers as discussed in section 3.2.1. Finally due to the asymmetry in the size of the Rydberg electron and the ground state electron, the exchange interaction between the two valence electrons is treated perturbatively while solving the mean field equations. The energies obtained

agrees with experimental data with a 99% accuracy. For more precise energies, we fitted the experimental data to obtain the quantum defects for strontium Rydberg atom. Using our wave functions and the fitted energies, the Rydberg interactions were calculated for ns strontium states and were found to be attractive unlike those of Rb. Attractive interactions in Rydberg gases have had interesting implications such as forming self-focusing nonlinear optical response [184] and Rydberg induced solitons in BEC's [136].

In this thesis, we will explore yet another application of attractive Rydberg interaction which is the generation of multi-particle entanglement (in Chapter 5). A direct example of involving the manipulation of the second valence electron is shown in the forthcoming chapter, where the possibility to trap Rydberg atoms along with the ground state atoms in the same optical lattice is explored.

Magic lattice for strontium

Contents

4.1	Laser trapping of atoms: Optical lattice	34
4.1.1	Variable lattice spacing	35
4.1.2	Harmonic approximation	35
4.1.3	Types of optical lattice	37
4.2	Dynamic polarizability of an atom	37
4.2.1	Core polarizability	37
4.2.2	Rydberg polarizability	40
4.3	Magic trapping for ground and Rydberg atoms	41
4.4	Decay processes in magic lattice	42
4.4.1	Spontaneous decay	43
4.4.2	Autoionization	44
4.4.3	Photoionization	44
4.4.4	Intensity dependent suppression of decay rates	46
4.5	Summary	47

If the trapping potential for the ground state atom is different from that of the Rydberg state atom, then the coupling between the two internal states will lead to excitation of higher motional states of the trapped atoms. Excited motional states are responsible for de-coherence and lead to lower fidelity in many of the theoretical proposals of quantum simulation [206] and quantum information [73, 172, 207] involving Rydberg atoms. A magic lattice is an optical lattice that is identical for two different internal states of the atom [104]. The challenge is to create traps for Rydberg atoms that are sufficiently as strong as the trap for ground state atoms. In this respect, divalent alkaline-earth atoms offer a promising approach due to the extra valence electron. The chapter begins with a general discussion on the basic principles of optical trapping. The trapping potential is derived in terms of the dynamic polarizability of the atom for a standing wave laser field. The trapping potential for the Rydberg electron known as the *ponderomotive potential* [58] is also discussed. The polarizabilities for the ground and Rydberg state for strontium are calculated and compared to identify magic wavelengths of the trapping laser. The feasibility of realizing such a lattice system with experimentally realistic values for different parameters is discussed by considering the relevant decay processes.

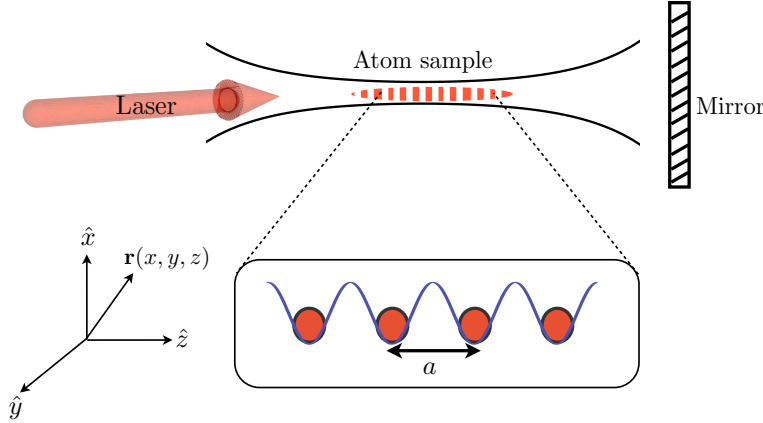


Figure 4.1: The figure shows the construction of a one dimensional optical lattice with lattice spacing a .

4.1 Laser trapping of atoms: Optical lattice

Trapping of atoms using dipole force was first suggested in [121]. Since then the far off resonance optical traps (FORTS) often referred as *optical tweezers* have been used to manipulate micrometer size particles, from colloids, bacteria to DNA [36]. In this section, we give a brief introduction to optical lattices and how the lattice spacings and depth are controlled by the laser parameters.

Here we treat the laser field classically where the electric field component of the laser at any given position $\mathbf{r}(x, y, z)$ is given as

$$\mathcal{E}(\mathbf{r}, t) = \hat{\boldsymbol{\epsilon}} \mathcal{E}_0 \cos(\mathbf{k} \cdot \mathbf{r} - \omega_L t) = \boldsymbol{\mathcal{E}}_0 \cos(\mathbf{k} \cdot \mathbf{r} - \omega_L t) . \quad (4.1)$$

where \mathcal{E}_0 is the electric field amplitude, $\hat{\boldsymbol{\epsilon}}$ is the polarization, $\mathbf{k}(k^x, k^y, k^z)$ is the wave number and ω_L is the off-resonant laser frequency. An atom subjected to a far detuned laser experiences a dipole force. The dipole moment \mathbf{d} experienced by such an atom is given as [138],

$$\mathbf{d}(\mathbf{r}, t) = \alpha \mathcal{E}(\mathbf{r}, t) , \quad (4.2)$$

where α is the dynamic polarizability. To trap atoms using light, one requires a potential gradient. The trapping potential due to a light field as given in [35] is

$$U(\mathbf{r}) = -\frac{1}{2} \langle \mathbf{d} \cdot \mathcal{E}(\mathbf{r}, t) \rangle_t = -\frac{1}{2} \alpha \langle \mathcal{E}^2(\mathbf{r}, t) \rangle_t . \quad (4.3)$$

The angular brackets with the subscript t indicates time averaging. The spatial dependence of the trapping potential is obtained from the spatial variation in the intensity of the electric field. One way to create a spatially varying potential is to construct a standing wave using two or more lasers. A one dimensional optical lattice is formed by superimposing two laser beams (with a retro-reflected laser) to form a standing wave

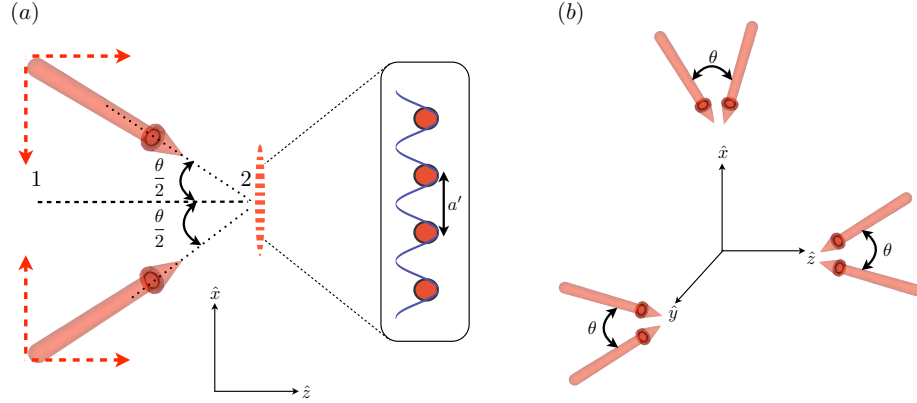


Figure 4.2: (a) A pair of lasers used to modify the lattice spacing as a function of the angle θ . (b) Variable lattice spacing for a 3D lattice.

[159] as shown in Fig.4.1. Assuming that the two counter-propagating laser beams have the same intensity, we then have

$$\mathcal{E}^2(\mathbf{r}, t) = \mathcal{E}_0^2 [\cos(\mathbf{k}_1 \cdot \mathbf{r} - \omega_L t) + \cos(\mathbf{k}_2 \cdot \mathbf{r} - \omega_L t)]^2 \quad (4.4)$$

$$= 4\mathcal{E}_0^2 \cos^2\left(\frac{(\mathbf{k}_1 + \mathbf{k}_2) \cdot \mathbf{r} - 2\omega_L t}{2}\right) \cos^2\left(\frac{(\mathbf{k}_1 - \mathbf{k}_2) \cdot \mathbf{r}}{2}\right). \quad (4.5)$$

Here we have neglected the laser profile in the direction perpendicular to the axes of propagation and have assumed linear, parallel polarization. If the two counter-propagating lasers travel along the z axis with the same wave number $k = 2\pi/\lambda_L$, then using $\mathbf{k}_1 = -\mathbf{k}_2 = k$ in Eq.(4.5), we get

$$\mathcal{E}^2(z, t) = 4\mathcal{E}_0^2 \cos^2(kz) \cos^2(\omega_L t). \quad (4.6)$$

Taking the time average of the above equation and defining $\mathcal{E}(z) = 2\mathcal{E}_0 \cos(kz)$ gives,

$$\langle \mathcal{E}^2(z, t) \rangle_t = 2\mathcal{E}_0^2 \cos^2(kz) = \frac{\mathcal{E}^2(z)}{2}. \quad (4.7)$$

The period of the lattice is given by the condition of $\cos^2(nka) = 1$ where n is the site number and a is the lattice spacing and is equal to $\lambda_L/2$ (refer to Fig.4.1). Thus using the above expression for time averaged intensity into Eq.(4.3), we get the trapping potential for a one dimensional optical lattice,

$$U(z) = 2U_0 \cos^2(kz). \quad (4.8)$$

where $U_0 = -\frac{1}{2}\alpha\mathcal{E}_0^2$ and the trap depth of the lattice is $2U_0$.

4.1.1 Variable lattice spacing

Often one requires lattice spacing larger than the $\lambda_L/2$ to balance the strong Rydberg interactions between the atoms. As demonstrated in [151, 123], one can have variable

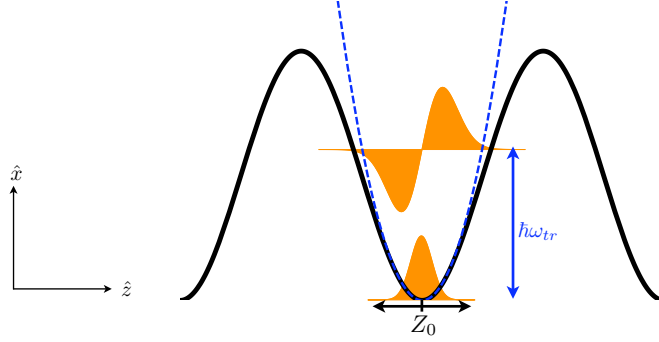


Figure 4.3: The figure shows that for a deep optical lattice, every site can be approximated by a parabola (blue) around the minima of the trap. The different motional states of the trapped particle are shown in orange.

lattice spacings in optical lattices by introducing an angle θ between the two laser beams as shown in Fig.4.2(a). In that case, the individual components of the wave numbers are $k_1^x = -k_2^x = 2k \sin \theta/2$ and $k_1^y = k_2^y = 2k \cos \theta/2$ respectively. Thus the lasers interfere to form a standing wave in the \hat{x} direction (see Fig.4.2(a)). Hence,

$$\begin{aligned} \langle \mathcal{E}^2(x, t) \rangle_t &= \langle \mathcal{E}_0^2 [\cos(kx \sin(\theta/2) - \omega_L t) + \cos(-kx \sin(\theta/2) - \omega_L t)]^2 \rangle_t \\ &= 2\mathcal{E}_0^2 \cos^2(kx \sin(\theta/2)) . \end{aligned} \quad (4.9)$$

Thus the condition for lattice spacing is $\cos^2(nka' \sin(\theta/2)) = 1$ which gives $a' = \frac{\lambda_L}{2 \sin(\theta/2)}$. Hence the lattice spacing can be varied by adjusting the angle θ between the two co-propagating lattice beams.

4.1.2 Harmonic approximation

For a deep enough lattice, which is when U_0 is larger than the thermal energy of the atoms given by $k_B T$, where k_B is the Boltzmann constant and T is the average temperature of the trapped atoms, one can make a harmonic approximation for the trap. Defining the relative displacement (along the axis) of the trapped particle at the minima of a site as $Z = z - Z_0$ as shown in Fig.4.3, we can expand $\cos^2(kZ - \frac{\pi}{2})$ giving,

$$\cos^2(kZ - \frac{\pi}{2}) = \sin^2(kZ) = \left(kZ - \frac{(kZ)^3}{3!} + \dots \right)^2 \simeq k^2 Z^2 . \quad (4.10)$$

Thus around the minima at every site of the lattice, one can approximate the trap to be parabolic as shown in Fig.4.3. This implies that the particle trapped at every site can be effectively treated as a harmonic oscillator problem. The Hamiltonian of a particle in a harmonic potential is

$$\hat{H}_{\text{CoM}} = \frac{-\hbar^2 \nabla_Z^2}{2M} + \frac{1}{2} M \omega_{\text{tr}}^2 Z^2 . \quad (4.11)$$

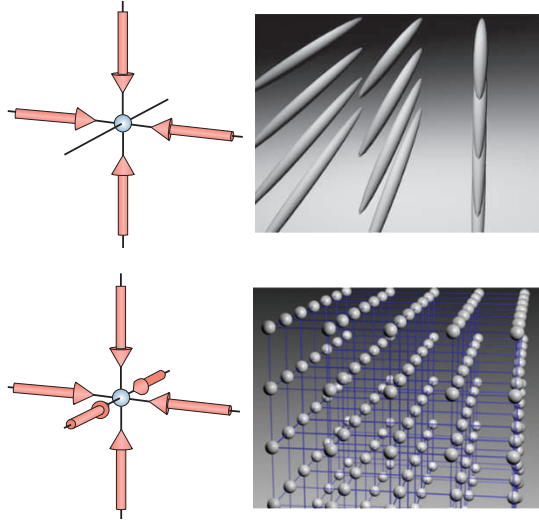


Figure 4.4: The figure shows optical lattices in higher dimensions reproduced from [26].

where ω_{tr} is the trapping frequency of the harmonic trap. The above Hamiltonian describes the motion of the trapped particle with nuclear mass M . The eigenstates also referred as the motional states of the trapped atom $|n\rangle$ are defined as follows,

$$\langle Z|n\rangle = \sqrt{\frac{1}{\sqrt{\pi}2^n n! \sigma_0}} e^{-1/2(\frac{Z}{\sigma_0})^2} H_n\left(\frac{Z}{\sigma_0}\right). \quad (4.12)$$

where H_n are the Hermite polynomials and $\sigma_0 = \sqrt{\frac{\hbar}{M\omega_{tr}}}$ is the size of the motional ground state $\phi_0(Z)$. For a trapping frequency of 500 KHz and the nuclear mass of strontium being $M = 87.2$ (in atomic mass units), the typical extension for motional ground state is few tens of nanometers. These motional eigenstates satisfy the following equation,

$$\hat{H}_{CoM}|n\rangle = \left[\left(n + \frac{1}{2} \right) \hbar\omega_{tr} \right] |n\rangle = \left[\left(\hat{a}^\dagger \hat{a} + \frac{1}{2} \right) \hbar\omega_{tr} \right] |n\rangle, \quad (4.13)$$

with the property $\langle n|m\rangle = \delta_{nm}$. \hat{a}^\dagger and \hat{a} are the creation and annihilation operators respectively for the motional states with its usual properties [32]. By comparing the potential energy energy of the trapped particle in a harmonic potential with Eq.(4.8) with the harmonic approximation, we obtain

$$U_0 k^2 Z^2 = \frac{1}{2} M \omega_{tr}^2 Z^2, \quad (4.14)$$

$$\implies \omega_{tr} = k \sqrt{\frac{2U_0}{M}}. \quad (4.15)$$

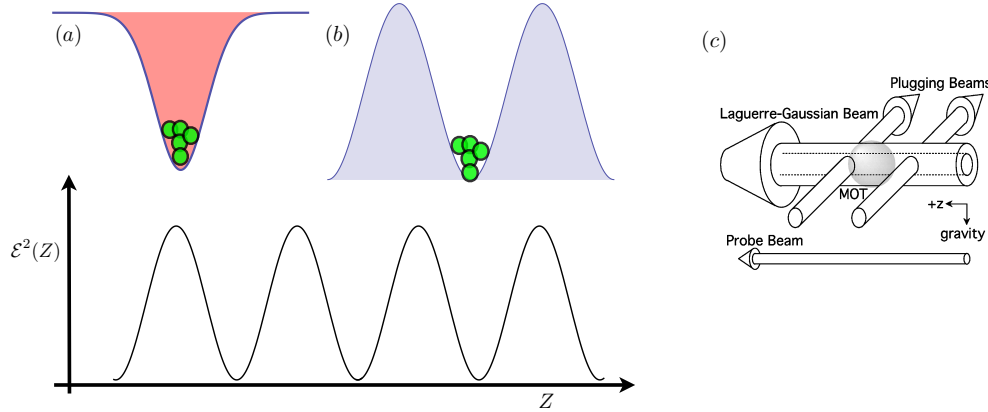


Figure 4.5: (a) The figure depicts atoms confined in optical traps for two different kinds of polarizabilities. Below is the intensity profile as a function of distance. (a) For $\alpha < 0$ (red) atoms are confined in the high intensity region. (b) For $\alpha > 0$ (blue) atoms are confined in the low intensity region. (c) Blue detuned trap with hollow beams reproduced from [113].

4.1.3 Types of optical lattice

Optical lattices can be easily generalized to higher dimensions using more pairs of laser beams [138]. For example, a 3 dimensional optical lattice is constructed with the help of three pairs of laser beams as shown in Fig.4.4. From equation Eq.(4.8), one sees that for $\alpha < 0$, the atoms are high field seeking while for $\alpha > 0$ are low field seeking (see Fig 4.5). It is easier to experimentally realize traps for the case $\alpha < 0$ case, since the focus of the laser beam with a Gaussian profile naturally forms a confining potential well. In case of $\alpha > 0$, since the atoms are pushed away from the high fields, the decay rates associated with photon scattering are low. But the construction of low field seeking optical traps are experimentally more involved. Hollow laser beams with radial confinement [113] (see Fig 4.5) and two dimensional trapping using optical walls with elliptical focusing of the laser [49] have been very successful. Yet another method is the use of evanescent waves formed by the total internal reflection on the surface of the dielectric medium [55].

4.2 Dynamic polarizability of an atom

To calculate the trapping potential from Eq.(4.8) for a given intensity, we need to evaluate the dynamical polarizability. In this section we calculate the polarizability for the core electron and the Rydberg electron separately.

4.2.1 Core polarizability

To derive the dynamic polarizability for the core electron is derived by solving the Schrödinger equation for an electron of an atom interacting with a standing laser field. Here the atom is treated quantum mechanically and the laser field classically. In the

framework of the dipole approximation and using Eq.(4.6), the Hamiltonian describing the optical coupling of the atom to the laser field is [38],

$$\hat{H}_O(t) = -\frac{\hbar\Omega}{2} [e^{i\omega_L t} + e^{-i\omega_L t}] . \quad (4.16)$$

where the identity $\cos\omega_L t = \frac{e^{i\omega_L t} + e^{-i\omega_L t}}{2}$ has been applied. The Rabi frequency of the coupled two level system is defined as

$$\Omega = (2\boldsymbol{\mu} \cdot \boldsymbol{\mathcal{E}})/\hbar , \quad (4.17)$$

where $\boldsymbol{\mu}$ denotes the electric dipole moment. For simplicity we first consider a two level atom which is later generalized to a multi-level system. The two levels of the the atom are denoted as $|a\rangle$ for the ground state and $|b\rangle$ for a low lying excited state with energies $\hbar\omega_a$ and $\hbar\omega_b$ respectively. The Hamiltonian for the atom is thus written as

$$\hat{H}_A = \hbar\omega_a |a\rangle\langle a| + \hbar\omega_b |b\rangle\langle b| . \quad (4.18)$$

The wave function $|\psi(r, t)\rangle$ is expressed as a linear combination of the two level electronic eigenfunctions,

$$|\psi(r, t)\rangle = c_a(t)e^{-i\omega_a t}|a\rangle + c_b(t)e^{-i\omega_b t}|b\rangle . \quad (4.19)$$

The Schrödinger equation for an atom in the presence of a laser field is

$$i\hbar\partial_t\psi(r, t) = [\hat{H}_A + \hat{H}_O(t)] \psi(r, t) . \quad (4.20)$$

The basis states $|a\rangle$ and $|b\rangle$ satisfy the orthonormality conditions and thus at all times t , we have $|c_a(t)|^2 + |c_b(t)|^2 = 1$. Defining $\omega_{ab} = (\omega_b - \omega_a) > 0$ as the transition frequency and inserting Eqs.(4.19) into Eq.(4.20) and multiplying the corresponding kets $\langle a, b|$, we get

$$i\dot{c}_a(t) = -\sum_b \frac{\Omega_{ab}}{2} \left(e^{i(\omega_L - \omega_{ab})t} + e^{-i(\omega_L + \omega_{ab})t} \right) c_b , \quad (4.21a)$$

$$i\dot{c}_b(t) = -\frac{\Omega_{ab}}{2} \left(e^{-i(\omega_L - \omega_{ab})t} + e^{i(\omega_L + \omega_{ab})t} \right) c_a . \quad (4.21b)$$

where $\Omega_{ab} = \langle b|\Omega|a\rangle$. Due to the odd parity of the Hamiltonian \hat{H}_O , we have used $\langle a|\hat{H}_O|a\rangle = \langle b|\hat{H}_O|b\rangle = 0$. The above equations can be solved analytically under certain approximations. When the laser frequency near resonance, then one can apply the so called rotating wave approximation. In which case, the fast rotating (counter rotating) terms such as $e^{\pm i(\omega_L + \omega_{ab})t}$ are ignored which is justified when $\omega_L - \omega_{ab} \ll \omega_L + \omega_{ab}$. This approximation does not hold anymore for a far-off resonant laser, which is the typical situation for an optical dipole trap. Assuming that the coupling of the electron to the light field given by the Rabi frequency is smaller compared than the transition frequency ω_{ab} , we treat $\hat{H}_O(t)$ as a perturbation to \hat{H}_A . Using Dirac's formulation of

time dependent perturbation theory, we take the integral form of the Eqs.(4.21a) and (4.21b), giving us

$$c_a(t) = c_a(0) - \sum_b \frac{\Omega_{ab}}{2i} \int_0^t \left(e^{i(\omega_{ab} + \omega_L)t'} + e^{-i(\omega_L - \omega_{ab})t'} \right) c_b(t') dt' , \quad (4.22)$$

$$c_b(t) = c_b(0) - \frac{\Omega_{ab}}{2i} \int_0^t \left(e^{i(\omega_{ab} + \omega_L)t'} + e^{-i(\omega_L - \omega_{ab})t'} \right) c_a(t') dt' . \quad (4.23)$$

By substituting the $c_{a,b}(t)$ back into the above equations repeatedly, one obtains an iterative expression for the coefficients as given below

$$c_a(t) = c_a^{(0)} + c_a^{(1)}(t) + c_a^{(2)}(t) + \dots , \quad (4.24)$$

$$c_b(t) = c_b^{(0)} + c_b^{(1)}(t) + c_b^{(2)}(t) + \dots . \quad (4.25)$$

Assuming that the initial state of the system is the ground state i.e. $c_a^{(0)}(t=0) = 1$, $c_b^{(0)}(t) = 0$ which yields $c_a^{(1)}(t) = 0$. The next non-zero term is the first order solution for c_b ,

$$\begin{aligned} c_b^{(1)}(t) &= -\frac{\Omega_{ab}}{2i} \int_0^t \left(e^{i(\omega_{ab} + \omega_L)t'} + e^{-i(\omega_L - \omega_{ab})t'} \right) dt' , \\ &= \frac{\Omega_{ab}}{2} \left[\frac{e^{i(\omega_{ab} + \omega_L)t}}{\omega_{ab} + \omega_L} - \frac{e^{-i(\omega_L - \omega_{ab})t}}{\omega_L - \omega_{ab}} \right] + \frac{\Omega_{ab}\omega_{ab}}{\omega_L^2 - \omega_{ab}^2} . \end{aligned} \quad (4.26)$$

From the above equation one can calculate the population in the excited state up to the first order which is ,

$$\langle |c_b(t)|^2 \rangle_t = \frac{\Omega_{ab}^2}{2} \frac{\omega_L^2 + 3\omega_{ab}^2}{(\omega_L^2 - \omega_{ab}^2)^2} . \quad (4.27)$$

The small population of the excited state induces a dipole moment to the atom given by

$$\begin{aligned} \mathbf{d}_a &= \langle \psi(r, t) | \boldsymbol{\mu} | \psi(r, t) \rangle \\ &= \sum_b c_a^* c_b \mu_{ab} e^{-i\omega_{ab}t} + c_b^* c_a \mu_{ba} e^{i\omega_{ab}t} \\ &\simeq \sum_b \frac{\mu_{ab}\Omega_{ab}}{2} \left[\frac{e^{i\omega_L t}}{\omega_{ab} + \omega_L} - \frac{e^{-i\omega_L t}}{\omega_L - \omega_{ab}} + \frac{e^{-i\omega_L t}}{\omega_{ab} + \omega_L} - \frac{e^{i\omega_L t}}{\omega_L - \omega_{ab}} + \frac{4 \cos(\omega_{ab}t)\omega_{ab}}{\omega_L^2 - \omega_{ab}^2} \right] . \end{aligned} \quad (4.28)$$

and thus the trapping potential for a given low lying level $|a\rangle$ evaluated from Eq.(4.3) is,

$$U_a(Z) = -\frac{1}{2} \langle \mathbf{d}_a \cdot \boldsymbol{\mathcal{E}}(Z, t) \rangle_t = \frac{1}{2} \alpha_a \mathcal{E}^2(Z) . \quad (4.29)$$

Within the perturbation expansion, all the states that contribute to dynamic polarizability α_a are added for a given state $|a\rangle$ and is

$$\alpha_a = \sum_b \alpha_a^b = \sum_b \frac{\mu_{ab}^2}{\hbar} \left(\frac{\omega_{ab}}{\omega_L^2 - \omega_{ab}^2} \right), \quad (4.30)$$

where α_a^b is the dynamic polarizability arising from optical dressing on a specific transition from ground state $|a\rangle$ to an excited state $|b\rangle$. The dipole matrix elements μ_{ab} are obtained from the lifetimes of the relevant states using the following equation [32],

$$\mu_{ab} = \sqrt{\frac{3\pi\epsilon_0\hbar c^3}{\omega_{ba}^3}} (\Gamma_a^b)^{-1}. \quad (4.31)$$

Here Γ_a^b denotes the rate of radiative decay from level $|b\rangle$ to $|a\rangle$. From Eq.(4.30), one can conclude that the dominant contribution to α_a comes from states that are energetically close to the state $|a\rangle$ and have large transition dipole moments. From Eq.(4.30), it is evident that the sign of the dynamic polarizability depends on the detuning of the laser $\Delta = \omega - \omega_{ab}$. Thus a blue detuned laser ($\Delta > 0 \implies \alpha_a > 0$) gives rise to a low field seeking potential while a red detuned laser ($\Delta < 0 \implies \alpha_a < 0$) gives high field seeking trapping potential (refer section 4.1.3). This was the polarizability for the deeply bound core electron. The frequency of the trapping laser (driving the low lying transitions) is so far away from any Rydberg state that the polarizability defined in Eq.(4.30) is negligible for the Rydberg electron. However the oscillating laser field of the trapping laser does provide a trapping potential for the Rydberg electron and is known as ‘ponderomotive potential’ which is discussed in the next section.

4.2.2 Rydberg polarizability

Ponderomotive potential is the potential experienced by a free charge due to an oscillating electric field. A classical derivation involves taking the time average of the kinetic energy of a charge q with mass m in an oscillating laser field which is given as [212],

$$\langle K.E. \rangle = \frac{\omega}{2\pi} \int_0^{2\pi/\omega} \frac{1}{2} m \dot{x}^2 dt = \frac{q^2 \mathcal{E}_0^2}{4m\omega^2}, \quad (4.32)$$

where the velocity of the electron is $\dot{x} = (-q\mathcal{E}_0)/(\omega m) \sin(\omega t)$ in an oscillating field with frequency ω . The ‘quivering’ motion which is induced by the oscillating laser field is along the polarization of the laser field of the form $\hat{\epsilon}_x \mathcal{E}_0(Z) \cos(\omega t)$.

Similarly the Rydberg polarizability is derived in a semi-classical treatment, where the valence electron of the Rydberg atom is considered to be (quasi)free and the light field is treated classically. For a trapped Rydberg atom in an optical lattice, the different dynamics involved are that of the trapped nuclei, the orbiting of the Rydberg electron and the ‘quivering’ motion of the Rydberg electron as shown in Fig.4.6. The fastest dynamics corresponds to the quivering motion and then the electronic dynamics which is generally faster than the nuclear dynamics. Thus one can separate out both, the electronic and the quivering dynamics from the center of mass dynamics by applying the

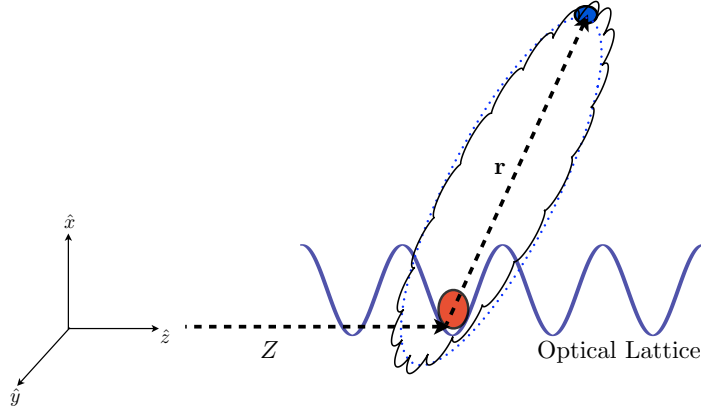


Figure 4.6: Semi-classical picture of the quivering motion of the Rydberg electron in the presence of oscillating laser field.

Born-Oppenheimer (BO) approximation [58]. Assuming that the optical lattice is along the \hat{z} axis and Z is the position of the nuclei from the origin (see Fig.4.6), then the BO potential V_p is the same as in Eq.(4.32) and is given as

$$V_p(\mathbf{Z} + \mathbf{r}) = \frac{\alpha_p \mathcal{E}(\mathbf{Z} + \mathbf{r})^2}{2}, \quad (4.33)$$

where α_p is the dynamical polarizability for a Rydberg electron defined as

$$\alpha_p = \frac{q^2}{2m\omega_L^2}. \quad (4.34)$$

The use of ponderomotive shift to trap alkali Rydberg atoms was first studied theoretically [211, 108] and experimentally implemented for Rb atoms [7, 6]. Typically Rydberg polarizabilities are much weaker than the core polarizabilities [204].

4.3 Magic trapping for ground and Rydberg atoms

Now we are in a position to calculate the trapping potential for strontium in the ground and Rydberg state. From Eqs.(4.30) and (4.34), we see that the polarizabilities are functions of the trapping wavelength. Therefore we need to find wavelengths for which the total ground state polarizability equals the total Rydberg polarizability,

$$\alpha_g = \alpha_c + \alpha_p = \alpha_m. \quad (4.35)$$

The wavelength for which this condition is satisfied is known as the *magic wavelength* (λ_m) and the corresponding frequency is the magic frequency $\omega_m = 2\pi c/\lambda_m$. For strontium, the additional core potential leads to a much deeper Rydberg atom lattice potential. The lifetimes and transition lines are given in Fig.4.7. In the case of strontium ground state, the relevant transitions are $5s^2 \rightarrow 5s5p$ and $5s^2 \rightarrow 5s6p$. Thus the total ground state dynamic polarizability is

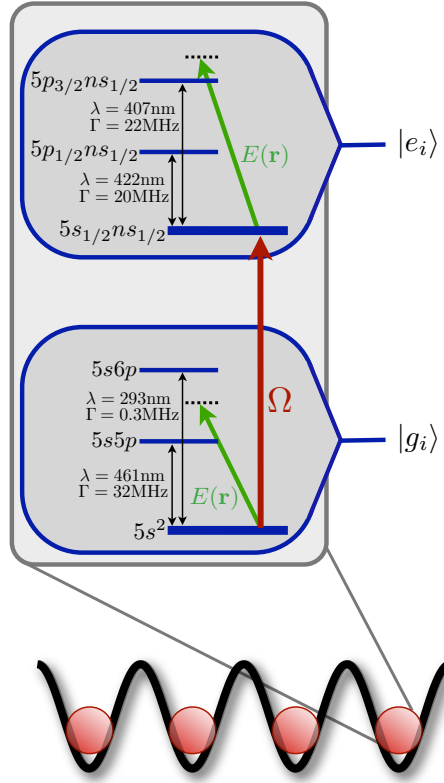


Figure 4.7: The figure shows the level scheme for optical dressing of the $\text{Sr}(5s^2 1S_0)$ ground state and the $\text{Sr}(ns 5s 1S_0)$ Rydberg state to provide an optical lattice for both states. $E(\mathbf{r})$ couples the ground state $|g\rangle_i$ and the also the core of the Rydberg atom to their corresponding low lying states at site i . The transitions and lifetimes are taken from [145, 71, 101].

$$\alpha_g = \alpha_{5s^2}^{5s5p} + \alpha_{5s^2}^{5s6p} . \quad (4.36)$$

For a range of laser wavelengths considered for the ground state atom, the dynamic polarizability for the strontium Rydberg core has significant contributions from the transitions $5s_{1/2} n s_{1/2} \rightarrow 5p_{1/2} n s_{1/2}$ and $5s_{1/2} n s_{1/2} \rightarrow 5p_{3/2} n s_{1/2}$ as shown in Fig.4.7. Thus the core polarizability for a strontium Rydberg atom is

$$\alpha_c = \alpha_{5s_{1/2} n s_{1/2}}^{5p_{1/2} n s_{1/2}} + \alpha_{5s_{1/2} n s_{1/2}}^{5p_{3/2} n s_{1/2}} . \quad (4.37)$$

The total polarizabilities of the ground (α_g) and Rydberg (α_e) states along with the individual contributions of the core resonances and the ponderomotive shift are shown in Fig.4.8. We find a broad range of wavelengths for which the ground and Rydberg state polarizabilities are nearly identical. This range is marked by the grey area in Fig.4.8. One finds the magic wavelengths at $\lambda_m = 323.4$ nm with $\alpha_m = 93.9$ in atomic units and one at $\lambda_m = 418.6$ nm with $\alpha_m = 460.3$ in atomic units which correspond to blue detuned

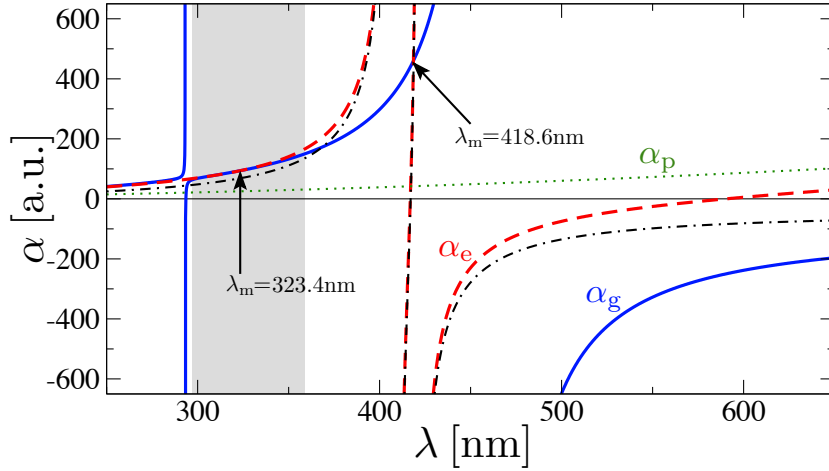


Figure 4.8: Scalar polarizability as a function of wavelength. Shown are the polarizability of $\text{Sr}(5s^2)$ ground state atoms (blue solid line), the total polarizability of the $\text{Sr}(5sns),ns$ Rydberg states (red dashed line) and the individual contributions of the Rydberg electron (green dotted line), and the core (black dash-dotted line). The two magic wavelengths at which the ground state and Rydberg state lattice potentials coincide are marked by the arrows.

lasers. Around the 323.4 nm, there is a broad range of wavelengths which contains the third harmonic of the Nd:YAG laser at $\lambda = 355$ nm, where single-frequency CW lasers are available with reasonable output power. The magic wavelength at 418.6 nm are reached using commercially available tunable frequency-doubled diode laser systems. Identifying blue magic wavelengths for the optical trap has the added benefit of suppressing various intensity dependent decay rate. A similar analysis for rubidium Rydberg states revealed a magic wavelength, based solely on the balance of the atomic ground state polarizability and the ponderomotive Rydberg atom potential [171]. Optical traps for alkali Rydberg atoms are much weaker than the traps for alkali ground state atoms. For this reason, it is difficult to confine both these internal states available in the same optical lattice without inducing motion of the atoms.

4.4 Decay processes in magic lattice

Lifetime of the magic lattice with ground and Rydberg atoms is limited by several additional decay channels apart from the spontaneous decay of the dressed ground state and the Rydberg state. There are transitions induced by blackbody radiation. Blackbody effects exist independent of the optical trap and have been measured for low and moderate principal quantum numbers. [84]. There are also decay processes such as autoionization for the weakly doubly excited state and photoionization, both of which are intensity dependent processes.

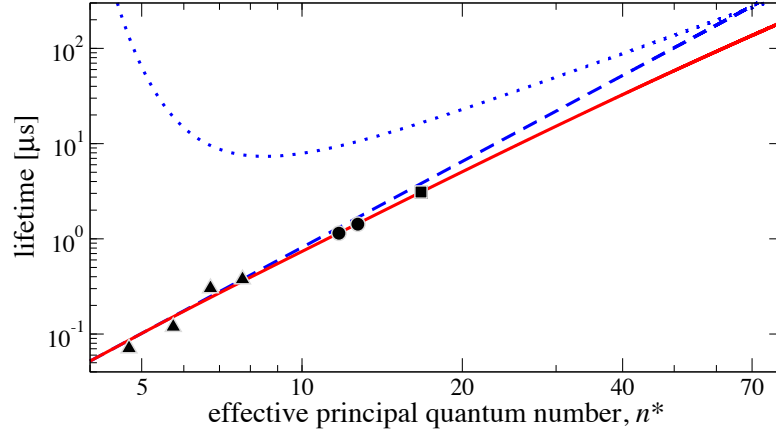


Figure 4.9: Experimental Sr(5sns) lifetimes from [78] (triangles), [84] (dots), and [140] (squares), extrapolated to high principal quantum numbers using (4.39) (solid red line). The dashed and dotted blue lines shows the separate contributions of spontaneous decay and black body radiation, respectively.

4.4.1 Spontaneous decay

For the magic frequency ω_m obtained in the previous section, the spontaneous decay for the relevant inter-mediate states ($5s5p$, $5s6p$) for ground state are given as (refer to Fig.4.7),

$$\Gamma_{5s^2}^{5s5p} = 32 \text{ MHz}, \quad \Gamma_{5s^2}^{5s6p} = 0.3 \text{ MHz} . \quad (4.38)$$

The core ground electrons are weakly dressed to the inter-mediate excited states. One notices that inter-mediate $5s5p$ state has significant decay rate. But the strength of the coupling to this state is determined by the Rabi frequency $\Omega_{5s^2, 5s5p}$ (see Eq.(4.17)) and hence the intensity of the laser.

The lifetime of Sr(5sns) Rydberg states due to spontaneous decay and black body radiation has been measured for low and moderate n in [140]. Lifetimes up to $n=11$ have been experimentally observed in [78] and MQDT calculations were performed in [43] for higher n 's (up to 40). In order to estimate lifetimes of higher excited states we have fitted this data to the expected behaviour at large effective principal quantum numbers n^* [23],

$$\gamma_{\text{ryd}} = \frac{\Gamma_s}{n^{*3}} + \frac{\Gamma_{\text{bbr}}}{n^{*5} (\exp(n_T^3/n^{*3}) - 1)} . \quad (4.39)$$

yielding $\Gamma_s = 2 \times 10^8 \text{ Hz}$, $\Gamma_{\text{bbr}} = 2 \times 10^9 \text{ Hz}$ and $n_T = 8.9$ (parameter dependent on the radiation temperature T). Spontaneous decay rates for Rydberg states typically follow the scaling law $\tau_{\text{ryd}}^{-1} \propto (n^*)^3$ and are independent of the laser intensity. As shown in Fig.??, this simple formula yields a rather good fit of the available experimental data.

4.4.2 Autoionization

The Rydberg atoms considered for trapping are essentially singly excited atoms with states belonging to the series for example $5sns$. These are bound states. But by applying a trapping laser, there is a small admixture of the inter-mediate $5s5p$ state to the Rydberg state due to the Rydberg core polarizability. This implies that the Rydberg atom is weakly dressed to a doubly excited state belonging to the series $5pns$, which has a strong coupling to the continuum (refer to section 3.2.1, Fig.3.1) due to the electron-electron interaction. Any perturbation to this discrete state will cause an interaction with the neighbouring continuum states resulting in a radiationless transition from the doubly excited state to a ionized configuration which is known as autoionization. Rydberg states have been shown to be unstable against autoionization [74]. The corresponding rates for $5pns$ have been measured over a broad range of principal quantum numbers [162, 210, 128] and were found to be well described by

$$\Gamma_{\text{ai}}^{5p_{1/2}} = \frac{6.0 \times 10^{14}}{n^*3} \text{ Hz}, \quad \Gamma_{\text{ai}}^{5p_{3/2}} = \frac{9.0 \times 10^{14}}{n^*3} \text{ Hz}. \quad (4.40)$$

A simple picture based on super elastic electron scattering of ionic core electron $5p$ gives the scaling law for autoionization rates with respect to n and l . In this semi-classical picture, the Rydberg electron orbits elliptically (depending on the l state), approaches the ionic core and gets scattered from it. From the scattering, the Rydberg electron gains enough energy to escape the Coulomb potential of Sr^+ leaving the core electron in the ground state. Thus the autoionization rates for high l states are lower than for low l states. In general autoionization rates can be much larger than the Rydberg spontaneous decay. But $\Gamma_{\text{ai}}^{5p_{1/2}}$ are dependent on the population of the excited state $5s5p$ (determined by Eq.(4.27)). This population depends on the strength of the coupling which is given as $\Omega_{5s^2, 5s5p}$ which in turn depends on the intensity of the laser $\mathcal{E}^2(z)$. We will return to this point in section 4.4.4.

4.4.3 Photoionization

It has been well known that for far off resonance traps, the laser field causes decay of the Rydberg state via photoionization [163, 204, 192, 134]. The photoionization rate is given by the general expression [70]

$$\Gamma_{\text{pi}} = \frac{\sigma I}{\hbar\omega}. \quad (4.41)$$

where I is the intensity of the field and σ is the cross section for a transition from a bound Rydberg state ψ_{nl} and to the continuum state $\phi_{\varepsilon l'}$. The cross section is defined as

$$\sigma = \left(\frac{2\pi\hbar q^2}{mc} \right) \frac{df}{dE} \Big|_{E=(E_{nl}+\hbar\omega)>0} = \left(\frac{2\pi\hbar q^2}{mc} \right) \sum_{l'=l-1}^{l'+1} \frac{2m\omega l_{>}}{3\hbar(2l+1)} \left| \int \psi_{nl}(r)r\phi_{\varepsilon l'}(r)r^2 dr \right|^2. \quad (4.42)$$

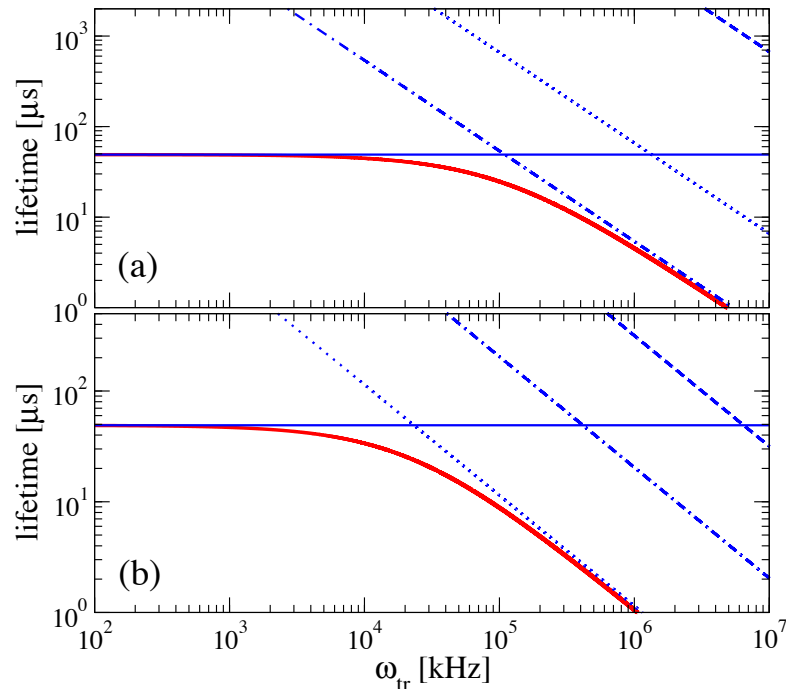


Figure 4.10: Lifetime of the trapped $\text{Sr}(5s^2s)$ ground state and $\text{Sr}(5s50s, ^1S_0)$ Rydberg atoms as a function of the local trapping frequency at (a) $\lambda_m = 323.4$ nm and (b) $\lambda_m = 418.6$ nm . The thick red solid line shows the total lifetime of the atoms obtained by summing all decay rates for both ground and Rydberg states. The thin blue lines show the individual contributions from radiative Rydberg states decay (solid line), spontaneous decay of the admixed p -states (dashed line), autoionization (dotted line) and photoionization (dash-dotted line).

The energy normalized continuous wave function is given by $\phi_{\epsilon l}(r) \sim \sqrt{\frac{2m}{\pi \hbar^2 k}} \sin(kr + \delta_{\epsilon l})$ with the continuum phase shift $\delta_{\epsilon l}$ and $k = \hbar^{-1} \sqrt{2mE}$. The oscillator strength distribution over the energy $\frac{df}{dE}$ with f is the oscillator strength for the corresponding transition is calculated by evaluating the bound-free radial matrix element using a semi-classical formula given in [59]. Photoionization at optical frequencies takes place far above threshold and the corresponding cross sections are expected to be small. The high l states have very little photoionization but for low l states it is significant. Using Eq.(4.42), the photoionization cross-section for Rb 50s is $9.45 \times 10^{-25} m^2$ which agrees with [204]. Similarly for Sr 50s one finds it to be $4.2 \times 10^{-25} m^2$ employing the quantum defects from [18].

4.4.4 Intensity dependent suppression of decay rates

For a tightly confined optical lattice, it is important to consider the effect of the intensity dependent losses. Since large trapping frequency requires large intensities, decay processes such as spontaneous decay of the $5s5p$ state, autoionization and photoionization

will affect the lifetime significantly. Our magic lattice however corresponds to a blue detuned laser (refer to Fig.4.8). As already discussed in section 4.3, a blue detuned trapping laser confines atoms in the low intensity field regions thereby minimizing the intensity dependent rates. For a given magic frequency ω_m , we know that the population of the excited state $5s5p$ from Eq.(4.27) and thus the admixed fraction of the excited state is given by [38]

$$S_{5s^2}^{5s5p}(Z) = \frac{\Omega_{5s^2,5s5p}^2(Z)}{2} \frac{\omega_m^2 + 3\omega_{5s^2,5s5p}^2}{\left(\omega_m^2 - \omega_{5s^2,5s5p}^2\right)^2}. \quad (4.43)$$

Assuming that the trapping potential is deep enough so that the confining atoms occupy the lowest motional state $|0\rangle$, the effective intensity experienced by the atoms is determined by the spatial average of the intensity over the motional states. Using Eq.(4.29) and the harmonic approximation in Eq.(4.14)

$$\begin{aligned} \langle 0|\mathcal{E}^2(Z)|0\rangle &= \frac{2U_m(Z)}{\alpha_m} \\ &= \frac{M}{\alpha_m} \omega_{\text{tr}}^2 \langle 0|Z^2|0\rangle \\ &= \frac{M}{\alpha_m} \omega_{\text{tr}}^2 \left[\frac{\hbar}{2M\omega_{\text{tr}}} \langle 0|\hat{a}^2 + \hat{a}^\dagger\hat{a} + \hat{a}\hat{a}^\dagger + (\hat{a}^\dagger)^2|0\rangle \right] \\ &= \frac{\hbar}{2\alpha_m} \omega_{\text{tr}} \left[2\left(0 + \frac{1}{2}\right)\delta_{0,0} \right] = \frac{\hbar\omega_{\text{tr}}}{2\alpha_m}. \end{aligned} \quad (4.44)$$

Here the position was expressed in terms of the creation/annihilation operators (\hat{a}^\dagger/\hat{a}) for the harmonic oscillator with its usual properties [70]. Using Eq.(4.43) and (4.44), one obtains a simple relation for the averaged suppression factor,

$$\begin{aligned} \bar{S}_{5s^2}^{5s5p} &= \langle 0|S_{5s^2}^{5s5p}(Z)|0\rangle \\ &= \frac{\omega_m^2 + 3\omega_{5s^2,5s5p}^2}{2\left(\omega_m^2 - \omega_{5s^2,5s5p}^2\right)^2} \langle 0|\Omega_{5s^2,5s5p}^2(Z)|0\rangle \\ &= \frac{\omega_m^2 + 3\omega_{5s^2,5s5p}^2}{2\left(\omega_m^2 - \omega_{5s^2,5s5p}^2\right)^2} \frac{\left(\omega_m^2 - \omega_{5s^2,5s5p}^2\right) \alpha_{5s^2}^{5s5p}}{\hbar\omega_{5s^2,5s5p}} \langle 0|\mathcal{E}^2(Z)|0\rangle \\ &= \left(\frac{\omega_m^2 + 3\omega_{5s^2,5s5p}^2}{\omega_m^2 - \omega_{5s^2,5s5p}^2} \right) \left(\frac{\omega_{\text{tr}}}{\omega_{5s^2,5s5p}} \right) \left(\frac{\alpha_{5s^2}^{5s5p}}{4\alpha_m} \right). \end{aligned} \quad (4.45)$$

The above expression will serve as a suppression factor for decay rates like spontaneous decay of the $5s5p$ state and autoionization. This is because the contribution from the quickly decaying excited state is minimized as it is not populated.

$$\gamma_{5s^2} = \Gamma_{5s^2}^{5s5p} \bar{S}_{5s^2}^{5s5p} + \Gamma_{5s^2}^{5s6p} \bar{S}_{5s^2}^{5s6p} , \quad (4.46)$$

$$\gamma_{ai} = \Gamma_{ai}^{5p_{1/2}} \bar{S}_{5s_{1/2}}^{5p_{1/2}} + \Gamma_{ai}^{5p_{3/2}} \bar{S}_{5s_{1/2}}^{5p_{3/2}} . \quad (4.47)$$

The suppression of the photoionization rate stems solely from the fact that it is intensity dependent and so for a blue detuned laser one obtains the following expression by using Eq.(4.44) in Eq.(4.41),

$$\gamma_{pi} = \langle 0 | \Gamma_{pi} | 0 \rangle = \frac{c \epsilon_0 \sigma \omega_{tr}}{4 \alpha_m \omega} . \quad (4.48)$$

where we used $I(z) = \frac{c \epsilon_0}{2} \mathcal{E}^2(z)$. We show our calculated lifetimes as a function of the local trap frequency for Sr(5s50s) Rydberg states for the two magic wavelengths (see Fig.4.10). The relevance of the different decay processes strongly depends on the wavelength of the optical lattice. Most importantly, we find that the atomic lifetime is not affected by the additional trapping fields for typical lattice parameters. Even for very large trap frequencies of $\omega_{tr} \sim 1$ MHz the total lifetime at both magic wavelengths is solely limited by the Rydberg state decay.

4.5 Summary

A magic lattice that permits simultaneous trapping of the ground and Rydberg state atom was possible only with alkaline-earth atoms due to the extra valence electron. Alkali Rydberg atoms lack the core polarizability. Hence they are trapped optically solely on the merit of the ponderomotive force which is much weaker than the trap for the ground state atom. Whereas for strontium, we identify broad ranges of trapping frequencies that are in the blue detuned region. Blue detuned trapping lasers have experimental challenges to construct one and two dimensional traps compared to a red detuned trap, however three dimensional traps are easily made [26]. An essential advantage of a blue detuned trap is that the intensity dependent processes that lead to the ionization of the Rydberg atom are highly suppressed. The study of the different loss mechanisms show that the entire Rydberg lattice setup decays with its natural Rydberg lifetime for fairly large range of trap frequencies.

The Rydberg lattice established in this chapter offers new possibilities to explore many-body physics in ultra-cold systems. Two particular many-body systems will be discussed in the subsequent chapters, one is about implementing multi-particle entanglement and the other deals with coherent ion transport in an optical lattice.

Multi-particle entanglement in strontium Rydberg lattice

Contents

5.1	Rydberg atoms in optical lattice	53
5.2	Atomic motion in optical lattice	54
5.3	Many body energy spectrum	56
5.4	Generating entanglement: Double sweep protocol	57
5.5	Geometry effects of the lattice	59
5.6	Quantum Ising model	60
5.7	Summary	63

In this chapter, we propose to create a many-body superposition state for a large number of particles, more specifically a GHZ (Greenberger, Horne and Zeilinger) state known to have applications in quantum information [96]. In general to have a large scale entanglement, one requires strong interactions between the particles which in this case is provided by the long range Rydberg interactions of strontium atoms (see section 3.3.2). We consider a situation where ground state strontium atoms are confined in the magic lattice and are optically coupled to strongly interacting Rydberg states. We study the the spatial dependence of the Rabi frequency and the effect of the strong interactions on the motion of the trapped particles in the magic lattice. The energy spectrum for the zero laser field case shows an interesting cross over between the many-body all ground state atoms and many-body all excited state atoms for attractive Rydberg interactions. We propose a protocol for multi-particle entanglement where the dynamics is similar to the one in a quantum Ising model. We also study the effect on the scheme of entanglement by considering trapped atoms arranged in different optical lattice geometries.

5.1 Rydberg atoms in optical lattice

Consider a setup where N strontium atoms are confined in an optical lattice with one particle per site. Each atom is coupled to a Rydberg state with the help of an excitation laser (see Fig.5.1). The underlying Hamiltonian for such a system is given by

$$\hat{H} = \hat{H}_{\text{opt}} + \hat{H}_{\text{CoM}} + \hat{H}_{\text{I}} . \quad (5.1)$$

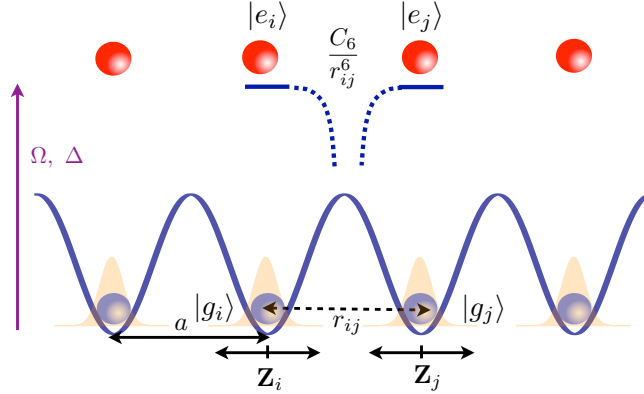


Figure 5.1: The position of the atoms are given by $\mathbf{r}_i = ai + \mathbf{Z}_i$. Atoms in the ground state $|g_i\rangle$ are shown in blue and the corresponding Rydberg state $|e_i\rangle$ are shown in red. The two internal states are coupled with a Rabi frequency Ω and detuning Δ giving rise to a strongly correlated excitation dynamics due to the strong van der Waals interactions between atoms in states $|e_{i,j}\rangle$. The shaded orange region represents the motional states.

where \hat{H}_{opt} describes the coupling of an atom in ground state $|g\rangle$ to its Rydberg state $|e\rangle$ at every site. It is written in terms of the projection operators defined by the two internal states,

$$\hat{H}_{\text{opt}} = \frac{\hbar\Omega}{2} \sum_{i=1}^N \left(e^{ikZ_i} |e_i\rangle\langle g_i| + e^{-ikZ_i} |g_i\rangle\langle e_i| \right) - \hbar\Delta \sum_{i=1}^N |e_i\rangle\langle e_i|. \quad (5.2)$$

where Ω and Δ are the Rabi frequency and detuning respectively determined by the laser. The Hamiltonian \hat{H}_{CoM} corresponds to the center-of-mass (CoM) dynamics of the trapped atoms within the optical trap. Assuming that the optical lattice is one dimensional (along the \hat{z} -axis) where the harmonic approximation is valid at every site of the lattice (refer to section 4.1.2), then \hat{H}_{CoM} is simply a sum of harmonic oscillators given as

$$\hat{H}_{\text{CoM}} = \sum_{i=1}^N \frac{\hbar^2 \nabla_{Z_i}^2}{2M} + \sum_{i=1}^N \frac{1}{2} M \omega_{\text{tr}}^2 Z_i^2. \quad (5.3)$$

ω_{tr} is the trapping frequency of the optical lattice and Z_i is the relative atomic displacement at the corresponding site as introduced in section 4.1.2. The van der Waals interaction between the Rydberg atoms is represented by \hat{H}_1 ,

$$\hat{H}_1 = \sum_i \sum_{j>i} \frac{C_6}{|a(i-j) + \mathbf{Z}_i - \mathbf{Z}_j|^6} |e\rangle_i \langle e| \otimes |e\rangle_j \langle e|. \quad (5.4)$$

where a is the lattice spacing along the z-axis and C_6 are determined from Eq.(3.37) derived in section 3.3.2. The presence of strong Rydberg interactions between the atoms can lead to the excitation of higher motional states. Populating higher motional states

within the trap implies heating of atoms. An important question in the dynamics of any many-body Hamiltonian such as in Eq.(5.1) is how to minimize decoherence effects caused by the heating of atoms in optical lattices [209].

5.2 Atomic motion in optical lattice

In this section, we will show that for sufficiently strong confinement, interaction-induced coupling to higher motional states are adiabatically eliminated. This gives rise to an effective lattice Hamiltonian for spatially frozen atoms. Both the Hamiltonians, \hat{H}_{opt} and \hat{H}_{CoM} are dependent on the position of the nuclei. Expressing \hat{H}_{opt} in terms of creation (\hat{a}_i^\dagger) and annihilation (\hat{a}_i) operators of the harmonic oscillator (refer to section 4.1.2), we obtain

$$\hat{H}_{\text{opt}} = \frac{\hbar\Omega}{2} \sum_{i=1}^N \left(e^{i\eta_0(\hat{a}_i^\dagger + \hat{a}_i)} |e_i\rangle \langle g_i| + e^{-i\eta_0(\hat{a}_i^\dagger + \hat{a}_i)} |g_i\rangle \langle e_i| \right) - \hbar\Delta \sum_{i=1}^N |e_i\rangle \langle e_i|. \quad (5.5)$$

where $\eta_0 = \frac{k\sigma_0}{\sqrt{2}}$ is the Lamb Dicke parameter of the optical lattice with $\sigma_0 = \sqrt{\hbar/M\omega_{\text{tr}}}$ is the extent of the ground state motional wave function $|0\rangle$. In general, the matrix element for the diagonal and off-diagonal coupling of the motional states via the Rabi frequency is given as [117],

$$\Omega_{0,0} = \Omega \langle 0 | e^{i\eta_0(\hat{a}_i^\dagger + \hat{a}_i)} | 0 \rangle = \Omega e^{-\eta_0^2/2} \simeq \Omega \left(1 - \frac{\eta_0^2}{2} + \dots \right), \quad (5.6)$$

$$\Omega_{0,1} = \Omega \langle 1 | e^{i\eta_0(\hat{a}_i^\dagger + \hat{a}_i)} | 0 \rangle = \Omega e^{-\eta_0^2/2} \eta_0 \simeq \Omega \left(\eta_0 - \frac{\eta_0^3}{2} + \dots \right). \quad (5.7)$$

Lamb Dicke regime is where $\eta_0 \ll 1$ which implies that both the wave number of the laser k and the size of the motional ground state σ_0 must be small. The latter is small for large trapping frequencies. However, often exciting an atom to a Rydberg state is a two photon process and the resultant wave number given as $\mathbf{k}_1 + \mathbf{k}_2$ can be large if they are in the same direction. In such a case, the two photon excitation is achieved by having the two lasers in opposite directions. This gives a resultant wave number that is small. Using second order perturbation theory and assuming $\Omega < \hbar\omega_{\text{tr}}$, we can estimate the energy correction resulting from the coupling to excited motional states due to the spatial variation of the Rabi frequency as

$$E^{(2)} = \frac{\hbar|\Omega_{0,1}|^2}{\omega_{\text{tr}}} = \frac{\hbar\Omega^2}{\omega_{\text{tr}}}\eta_0^2. \quad (5.8)$$

Consider the example of $\omega_{\text{tr}} = 500$ kHz which gives $\sigma_0 = 15$ nm for strontium atoms ($M=87.2$ a.u.). Typical optical transitions to Rydberg states are of the order of few 1000 nm [95] and so $\eta_0^2 = 0.004$. Tight confinement of the optical lattice ensures that the above correction $E^{(2)}$ is small. In such an optical lattice, where the extent of the local atomic CoM wave functions is much smaller than the lattice spacing ($|Z_i - Z_j| \ll a(i-j)$), we

can expand the van der Waals potential in terms of Taylor series to leading order in the atomic CoM displacements \mathbf{Z}_i ,

$$\begin{aligned}
 V_{ee} &= \frac{C_6}{|\mathbf{a}_i + \mathbf{Z}_i - \mathbf{a}_j - \mathbf{Z}_j|^6} \\
 &\approx \frac{C_6}{a^6(i-j)^6} \left[1 - 6 \frac{Z_i - Z_j}{a(i-j)} \right] \\
 &= \frac{C_6}{a^6(i-j)^6} + \frac{6C_6}{a^7(i-j)^7} \frac{\sigma_0}{\sqrt{2}} \left(\hat{a}_j^\dagger - \hat{a}_i^\dagger + \hat{a}_j - \hat{a}_i \right) \\
 &= \frac{V_0}{(i-j)^6} + \frac{\tilde{V}_0}{(i-j)^7} \left(\hat{a}_j^\dagger - \hat{a}_i^\dagger + \hat{a}_j - \hat{a}_i \right) . \tag{5.9}
 \end{aligned}$$

Here $V_0 = C_6/a^6$ is the nearest neighbour interaction between adjacent sites. We see that the Rydberg interactions not only yield the desired level shifts of excited pair states, but also lead to intra-band coupling with a coupling strength $\tilde{V}_0 = 6\sigma V_0/(a\sqrt{2})$. This coupling can however be strongly suppressed by realizing sufficiently strong trapping potentials, for which the vibrational splitting $\hbar\omega_{\text{tr}}$ exceeds the coupling strength \tilde{V}_0 . Similar to Eq.(5.8), we the energy correction for interacting atoms located at i and j respectively to be

$$\begin{aligned}
 E_{ij}^{\text{int},(2)} &= \frac{\langle 01 | \tilde{V}_0 \left(\hat{a}_j^\dagger - \hat{a}_i^\dagger + \hat{a}_j - \hat{a}_i \right) | 00 \rangle|^2}{(i-j)^7 \hbar\omega_{\text{tr}}} \\
 &= \frac{V_0^2}{2(i-j)^7 \hbar\omega_{\text{tr}}} \left(\frac{6\sigma}{a} \right)^2 \\
 &= \frac{V_0^2 \eta_{ij}^2}{2\hbar\omega_{\text{tr}}(i-j)^7} . \tag{5.10}
 \end{aligned}$$

The motional intra-band coupling simply yields a correction $\eta_{ij} = \left(\frac{6\sigma}{a}\right)$ to the van der Waals shifts. The above energy correction has an explicit dependence on the lattice spacing. Small lattice spacings are required to reach the blockade limit (half a μm for 60s Rb [182]) which is often required for certain applications in quantum information [172]. In such a limit, the van der Waals interaction V_0 can be considerably higher counteracting the small η_{ij} . Nevertheless, for a typical Rydberg state with $n = 50$ and a lattice spacing of $a = 3 \mu\text{m}$, one obtains an interaction of strength $V_0 = 9.6 \text{ MHz}$ and using the preceding trapping frequency of 500 kHz, the resulting correction factor $\eta_{ii+1} = 0.02$ is indeed negligibly small. Multiplying by 2 to Eq.(5.8) and Eq.(5.10) in order to take into account the coupling to $|10\rangle$ as well, the effective single-band Hamiltonian for the lowest band of the atomic lattice is

$$\begin{aligned} \hat{H} = & \frac{\hbar\Omega}{2} \sum_{i=1}^N (|e\rangle_i \langle g| + |g\rangle_i \langle e|) \left[1 - \frac{\eta_0^2}{2} \right] - \hbar\Delta \sum_{i=1}^N |e\rangle_i \langle e| \\ & + V_0 \sum_i \sum_{j>i} \frac{|e\rangle_i \langle e| \otimes |e\rangle_j \langle e|}{(i-j)^6} \left[1 + \frac{V_0}{\hbar\omega_{tr}(i-j)} \eta_{ij}^2 \right] + \frac{\hbar\Omega^2}{\omega_{tr}} \eta_0^2. \end{aligned} \quad (5.11)$$

This simple discussion shows that despite the presence of strong interactions that greatly exceed the energy scale of the lattice confinement, for reasonable experimental parameters, atomic motion can be practically frozen out. Such large interactions are essential to assure a sufficiently short timescale for the many-body dynamics of the internal states, which must be faster than the decay of the Rydberg lattice.

5.3 Many body energy spectrum

Henceforth we assume that the trapping potential is deep enough such that the intra-band coupling between motional states are suppressed. The many-body Hamiltonian in Eq.(5.11) can be scaled by the Rydberg interactions by introducing dimensionless quantities for the detuning $\tilde{\Delta} = \hbar\Delta/|V_0|$ and the Rabi frequency $\tilde{\Omega} = \hbar\Omega/|V_0|$. We then have,

$$\hat{H} = \frac{\tilde{\Omega}}{2} \sum_i (|e_i\rangle \langle g_i| + |g_i\rangle \langle e_i|) - \tilde{\Delta} \sum_i |e_i\rangle \langle e_i| - \sum_i \sum_{j>i} \frac{|e_i\rangle \langle e_i| \otimes |e_j\rangle \langle e_j|}{(i-j)^6}. \quad (5.12)$$

Let us study the features of the many-body spectrum when the laser field is switched off ($\tilde{\Omega} = 0$). Each atom can either be in the ground state or Rydberg state. Thus for N atoms in an optical lattice, we have 2^N possible many-body states. The energy for a configuration where there are n Rydberg atoms is given as

$$E_n = -n\tilde{\Delta} - \sum_i \sum_{j>i} \frac{1}{(i-j)^6}. \quad (5.13)$$

For an arbitrary configuration of $0 < n < N$ Rydberg atoms in a lattice of N atoms, there maybe a set of degenerate states. For example, the many-body configuration state $|ggg\dots\rangle$ has a N -fold degeneracy as it corresponds to any one atom in Rydberg state with all the others in the ground state. Nevertheless the configuration where all atoms are in the ground state ($n = 0$) or when all atoms are in the Rydberg state ($n = N$) are unique. We denote these two many-body states as $|G\rangle \equiv |ggg\dots\rangle$ and $|E\rangle \equiv |eee\dots\rangle$ respectively. Depending on the sign of the V_0 , there are two interesting scenarios. For repulsive Rydberg interactions, the energy spectrum show a step-wise crossing between $|n\rangle$ and $|n+1\rangle$ state as the detuning is varied from a large negative value to zero (see Fig.5.2(a)). It was shown in [160] that a using an excitation laser with a chirped pulse, one can adiabatically prepare a crystal of $n < N$ Rydberg states starting from a $|G\rangle$ configuration. Due to the repulsive nature of the interaction, the ground state of the

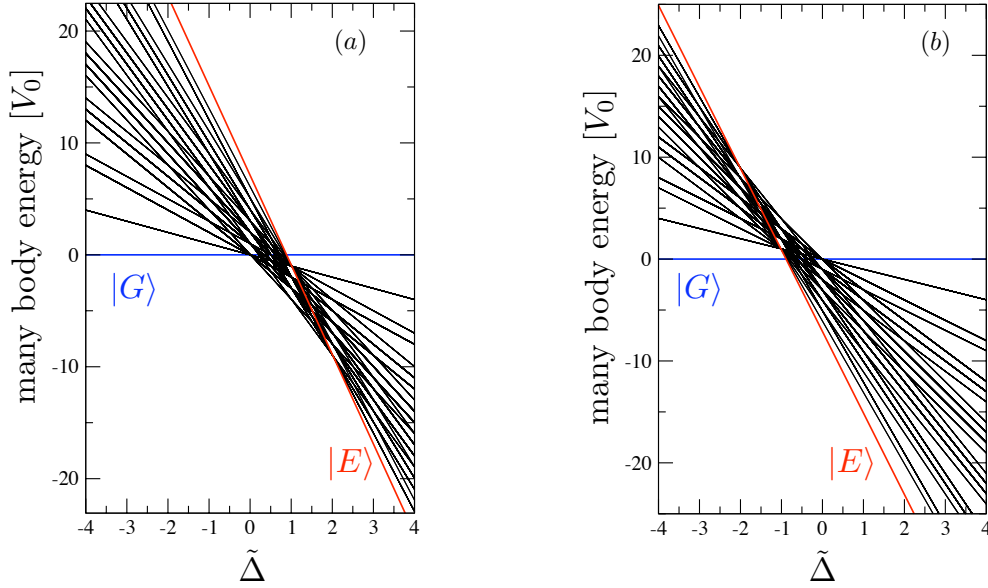


Figure 5.2: Many body spectrum for $\tilde{\Omega} = 0$ with $N=8$ particles: (a) for repulsive interactions and (b) for attractive interactions. The crossover between $|G\rangle$ and $|E\rangle$ occurs for attractive interactions only.

configuration at every step corresponds to the case where Rydberg atoms are maximally separated giving rise to the crystal structure.

In this chapter we explore the effect of *attractive* interactions. In the many-body spectrum, we find that there is a real crossing between the many-body state $|G\rangle$ and $|N\rangle$, which did not exist for the repulsive case. For a finite one dimensional lattice, the value of the detuning ($\tilde{\Delta}_C$) at which this crossing occurs can be calculated from the condition $E_N = 0$, where E_N is the energy corresponding to $|E\rangle$ given by Eq.(5.13). Thus,

$$\begin{aligned}
 E_N &= -N\tilde{\Delta}_C - \sum_i \sum_{j>i} \frac{1}{(i-j)^6} \simeq -N\tilde{\Delta}_C - (N-1) = 0, \\
 \Rightarrow \tilde{\Delta}_C &= -\frac{N-1}{N}.
 \end{aligned} \tag{5.14}$$

Here we have assumed that number of Rydberg atoms N is large enough to ignore edge effects and that the nearest neighbour interactions are the dominant ones. This particular detuning $\tilde{\Delta}_C$ at which the cross over between $|G\rangle$ and $|E\rangle$ occurs takes an interesting interpretation in the context of the quantum Ising model discussed in section 5.6. For now, we proceed to examine a scheme that generates many-body entanglement between the states $|G\rangle$ and $|E\rangle$.

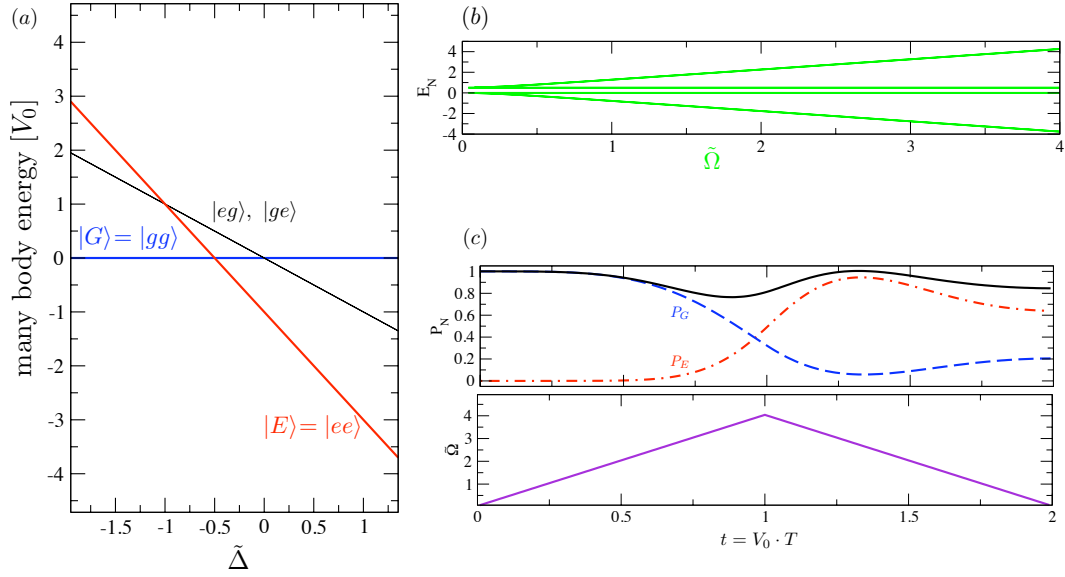


Figure 5.3: (a) The figure shows the crossing between $|G\rangle$ and $|E\rangle$ for the energy spectrum of two particles. (b) Here it shows the variation in the energy of the four instantaneous states (green lines) as a function of the scaled Rabi frequency for a two particle system. (c) The double sweep protocol is applied for the two particle system and the corresponding overlap states P_G and P_E are shown.

5.4 Generating entanglement: Double sweep protocol

A maximally entangled state of three or more particles is a GHZ (Greenberger, Horne and Zeilinger) state [19, 214]. The non-classical properties of a GHZ state and its applications have been extensively studied [200]. The simplest three entangled state qubit is

$$|\psi^E\rangle = \frac{1}{\sqrt{2}} (|ggg\rangle + |eee\rangle) . \quad (5.15)$$

In the above state, there is an equal probability to measure a state either in $|ggg\rangle$ or in $|eee\rangle$. Bouwmeester was the first to create a three particle GHZ state by entangling the polarizations of three individually separated photons [30]. This can be generalized to a larger manifold of qubits with $N > 3$,

$$|\psi^{GHZ}\rangle = \frac{1}{\sqrt{2}} (|g\rangle^{\otimes N} + |e\rangle^{\otimes N}) \equiv \frac{1}{\sqrt{2}} (|G\rangle + |E\rangle) . \quad (5.16)$$

One of the challenges is to have a scalable multi-particle entanglement. With the help of a temporally varying laser profile (see Fig.5.3), we investigate the dynamics of the Hamiltonian in Eq.(5.12). The laser is switched on and its intensity is increased to a certain value and then decreased back to zero. The duration of this entire pulse is given by pulse width (T). At the beginning of the pulse, the degeneracy between $|G\rangle$ and $|E\rangle$ is lifted creating an avoided crossing (See Fig.5.3(a)) which then closes at the end of the pulse. During this process, one can have a Landau-Zener transition [215] between the

two many-body states and finally end up with a collective state of N atoms which is a superposition of the $|G\rangle$ and $|E\rangle$ states controlled by the pulse width and the intensity of the laser. Thus the Hamiltonian $\hat{H}(t)$ in Eq.(5.12) is time dependent. At any given instant t , the time dependent eigenstates are expressed in terms of the many-body basis states,

$$|m(t)\rangle = \sum_n (c_0(t)|ggg\dots\rangle + c_1(t)|egg\dots\rangle + \dots + c_{2^N}(t)|eee\dots\rangle) . \quad (5.17)$$

If $|\Psi(t)\rangle$ is the full many-body wave function at any instant t , then expressed in terms of the new eigenstates, it is given as

$$\Psi(t) = \sum_m b_m |m(t)\rangle . \quad (5.18)$$

We can evaluate the overlap of the full wave function with the GHZ state given in Eq.(5.16) as follows

$$\begin{aligned} & |\langle \Psi(t) | \psi^{\text{GHZ}} \rangle|^2 \\ &= \frac{1}{2} [\langle \Psi(t) | G \rangle + \langle \Psi(t) | E \rangle]^2 \\ &= \frac{1}{2} [P_G + P_E + 2\sqrt{P_G}\sqrt{P_E}] . \end{aligned} \quad (5.19)$$

where $P_G = |\langle \Psi(t) | G \rangle|^2$ and $P_E = |\langle \Psi(t) | E \rangle|^2$. If the dynamics were entirely adiabatic then we get back close to the same un-entangled state we started with. This is because the overlap of the instantaneous eigenstates of the time evolving Hamiltonian with the time evolving wave function are all conserved according to the adiabatic theorem. In Fig.5.3, we implement the scheme of double sweep of the field for a system of two particles. In (a), we see that there is a crossing between the states $|gg\rangle$ and $|ee\rangle$ at $\tilde{\Delta}_C = -0.5$ as expected from Eq.(5.14). The next higher states are the degenerate states $|eg\rangle$ and $|ge\rangle$. On turning on the field, there is an avoided crossing and the time dependent states $|m(t)\rangle$ (shown in green lines in Fig.5.3(b)) are a superposition of the all the four basis states with which we started. At the end of the double ramp with a pulse width of $2 V_0 \cdot T$, we get a two particle GHZ state with 0.94 % fidelity. Using the same procedure for different pulse widths, we show the creation of GHZ state for 15 particles in Fig.5.4.

When the laser field is on, other many-body states (such as the ones $|eg\rangle$, $|ge\rangle$ for the two atom) from energy spectrum will also get shifted. In the case of a finite chain one dimensional lattice, the next excited many-body state $|N-1\rangle$ corresponding to the configuration of $(N-1)$ Rydberg atoms will come closer to the state $|E\rangle$. This is not favourable as the coupling of $|G\rangle$ to other excited many-body states (apart from $|E\rangle$) will spoil the fidelity of the GHZ state. This depends on the intensity of the laser field and the energy gap between the state $|E\rangle$ and $|N-1\rangle$. One obvious way to increase this energy gap is to have more interacting atoms for every single Rydberg atom.

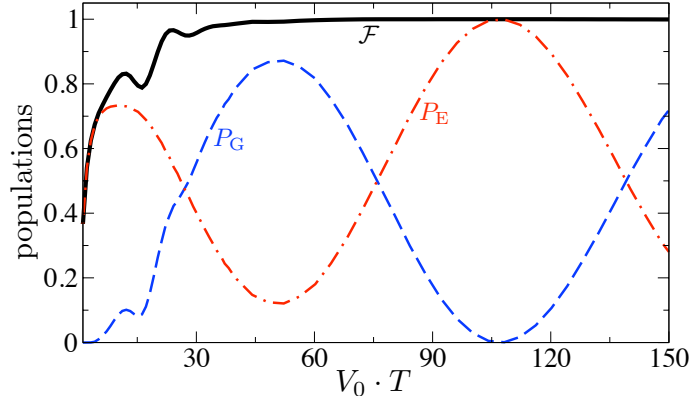


Figure 5.4: The final population P_G (blue dashed line) and P_E (red dot-dashed line) for the many-body ground $|G\rangle$ and excited state $|E\rangle$ are plotted as a function of the excitation pulse duration for $N=15$ atoms. We find a GHZ state for 15 atoms with a fidelity of 95 % in a short pulse length of $V_0 T \simeq 27$ and a fidelity of 99.9 % in $V_0 T \simeq 76$.

5.5 Geometry effects of the lattice

The difference between the many-body state $|E\rangle$ and $|N-1\rangle$ is that one of the Rydberg atom in $|E\rangle$ is de-excited to a ground state atom. Thus the energy gap between these two many-body states depends on the number of Rydberg interaction links lost on de-exciting one Rydberg atom. By considering different arrangements of the Rydberg atoms in the lattice, we can modify the number of interacting Rydberg atoms and thus the energy gap. Let the energy of $|N-1\rangle$ denoted by E_{N-1} is calculated using Eq.(5.13). We first calculate the energy gap for the one dimensional finite case and then we repeat the same calculations for a periodic chain (ring), square lattice and three dimensional cubic lattice. Adopting a more general notation for atomic distances, we switch i, j to r_i, r_j . Thus the energy of the many-body state $|E\rangle$ in a lattice of any geometry is given as

$$E_N = -N\tilde{\Delta}_C - \sum_i \sum_{j>i} \frac{1}{(r_i - r_j)^6} . \quad (5.20)$$

Using the condition $E_N = 0$ and similar to Eq.(5.14), the value of the detuning for the cross over between $|G\rangle$ and $|E\rangle$ in a lattice of any geometry is given as

$$\tilde{\Delta}_C = -\frac{1}{N} \sum_i \sum_{j>i} \frac{1}{(r_i - r_j)^6} . \quad (5.21)$$

As shown in Fig.5.5, the Rydberg atom that gets de-excited are from the edges. Thus the energy of the state $|N-1\rangle$ at detuning $\tilde{\Delta}_C$ is given as

$$E_{N-1} = -(N-1)\tilde{\Delta}_C - \sum_i \sum_{j>i} \frac{1}{(r_i - r_j)^6} + L , \quad (5.22)$$

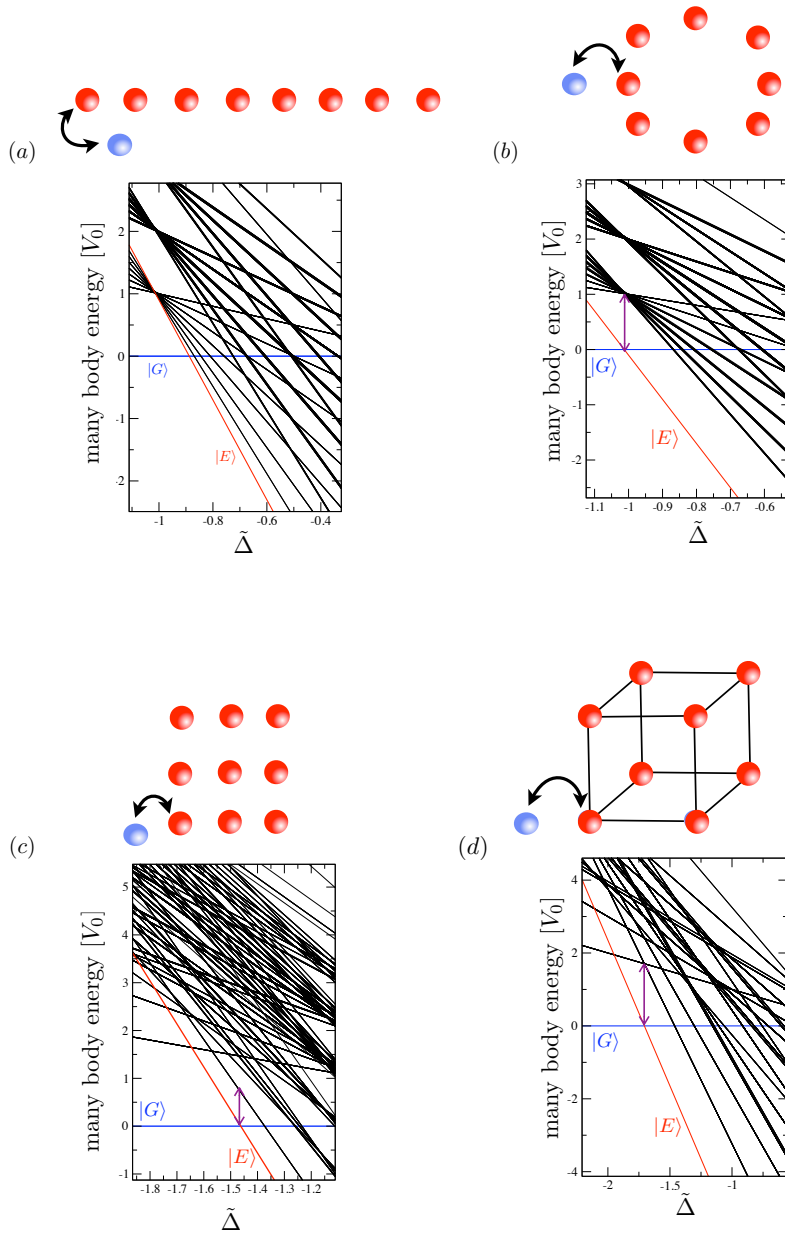


Figure 5.5: The figure shows the many-body spectrum for $\tilde{\Omega} = 0$ and the corresponding energy difference to the next excited state at $\tilde{\Delta}_C$ (in purple double arrow): (a) 1D finite lattice ($N=8$ particles) (b) 1D periodic lattice ($N=8$ particles) (c) 2D square lattice ($N=9$ particles) (d) 3D cubic lattice ($N=8$ particles).

where L is constant parameter depending on the type of geometry considered. It represents the change in the Rydberg interaction energy as one Rydberg atom from the edge is de-excited. Thus using Eq.(5.20) and (5.22) in general the energy gap at $\tilde{\Delta}_C$ is given as

$$E_{N-1} - E_N = \tilde{\Delta}_C + L . \quad (5.23)$$

The main results are summarized in Table 5.1.

Geometry	N	$\tilde{\Delta}_C$	L	$ E_{N-1} - E_N $
1D open lattice	8	-0.88773	1	0.112
1D periodic lattice	8	-1.01	2	0.987
2D square lattice	9	-1.462	$2 + (\frac{1}{\sqrt{2}})^6 = 2.125$	0.663
3D cubic lattice	8	-1.706	$3 + 3(\frac{1}{\sqrt{2}})^6 + (\frac{1}{\sqrt{3}})^6 = 3.41$	1.704

Table 5.1: For different lattice geometries we calculate the gap energy between many-body state $|E\rangle$ and $|N-1\rangle$ at the detuning $\tilde{\Delta}_C$.

Thus for the open chain the energy difference between the last and penultimate energy levels at $\tilde{\Delta}_C$ scales inversely with N. For very large number of atoms, this energy gap vanishes. This severely restricts in obtaining an entangled state purely in terms of many-body states $|G\rangle$ th and $|E\rangle$.

5.6 Quantum Ising model

Rydberg atoms and trapped ions have often been used to model spin systems [180, 102, 110]. The Hamiltonian in Eq.(5.12) can be studied as an effective quantum Ising model. Using the transition operators of a two level system, one can define the Pauli spin matrices as follows

$$\sigma_x = \frac{1}{2} (|e_i\rangle\langle g_i| + |g_i\rangle\langle e_i|) , \quad (5.24)$$

$$\sigma_y = \frac{-i}{2} (|e_i\rangle\langle g_i| - |g_i\rangle\langle e_i|) , \quad (5.25)$$

$$\sigma_z = \frac{1}{2} (|g_i\rangle\langle g_i| - |e_i\rangle\langle e_i|) . \quad (5.26)$$

The Hamiltonian Eq.(5.12) can be re-written to obtain the general quantum Ising model,

$$H = \sum_i^N \left[\sum_{j>i}^N -J_{ij} \sigma_z^i \sigma_z^j + h_i^z \sigma_z^i + h^x \sigma_x^i \right] + \text{constant term} . \quad (5.27)$$

where

$$J_{ij} = \tilde{V}_{ij} = \frac{1}{(i-j)^6} , \quad (5.28)$$

$$h^x = \tilde{\Omega} , \quad (5.29)$$

$$h_i^z = \tilde{\Delta} + \sum_{j>i}^N \frac{\tilde{V}_{ij}}{2} . \quad (5.30)$$

The study of the transverse Ising model with non-zero longitudinal field is nontrivial and quite interesting in itself. At the particular value of detuning $\tilde{\Delta}_C$, where the many-body state $|G\rangle$ and $|E\rangle$ have a cross over, the shift due to the interaction cancels with the detuning setting the second term (the longitudinal term) in Eq.(5.27) to zero. This reduces the above equation to a transverse Ising model given as

$$H = \sum_i^N \left[\sum_{j>i}^N J_{ij} \sigma_z^i \sigma_z^j + h^x \sigma_x^i \right]. \quad (5.31)$$

The two atomic internal state can correspond to the spin $|\uparrow(\downarrow)\rangle_i$ at site i . There are two ferromagnetic ground states ($|E\rangle \equiv |\uparrow\uparrow\uparrow \dots\rangle$, $|G\rangle \equiv |\downarrow\downarrow\downarrow \dots\rangle$) that are degenerate in the absence of the field. For a non-zero field, there exists a critical point in the thermodynamic limit which corresponds to $g = \frac{h^x}{J_{ij}} = 1$. For $g > 1$, there is spontaneous symmetry breaking resulting in a phase transition to the paramagnetic state. One dimensional quantum Ising model is the simplest model to study ferromagnetism and is known to show second order quantum phase transition [168]. Analytical solutions are known for the one dimensional transverse Ising model by mapping it to the classical (1+1) dimension Ising chain [168]. These analytical results may provide a useful insight to the dynamics of the many-body entanglement process.

The effectiveness of the double sweep protocol described in section 5.4 can be assessed from the following intuitive picture. Thus one starts with the symmetry breaking unentangled ground states of H_z and increases the transverse field h_x from zero to a finite value pass the critical point and then ramp it back to zero. In the end, it is numerically shown (Fig.5.4) that the final state has significant overlap with the GHZ state. The memory of the initial state is retained in the final state despite crossing the critical point where all the symmetry breaking ground states ($|G\rangle$, $|E\rangle$) have a substantial overlap with the wave function $\psi(t)$. However the introduction of non-adiabacity into the dynamics helps weakening this memory bias by exciting higher energy states. Thus by ramping the field faster it is possible to generate entangled states. But to perform this protocol in a systematic manner is difficult since the properties of high energy excitations are fully not understood and the dynamics is extremely complicated.

5.7 Summary

We study a Hamiltonian that describes the excitation of ground state strontium atoms to Rydberg states confined in a magic optical lattice with one particle at every site. We show that for deep enough lattices (few hundred KHz) and with large lattice spacings (few μm), it is sufficient to guarantee that the trapped atoms remain in their motional ground states. As a result of attractive Rydberg interactions, at a particular detuning, the many-body energy spectrum for the zero field case exhibits a cross over between the state with all atoms in the ground state and all atoms in the Rydberg state. These two many-body states correspond to the two degenerate ferromagnetic ground states of the quantum Ising model. A phase transition occurs by applying a temporally varying laser field from the ferromagnetic phase to the paramagnetic phase and dynamics of

the many-body system culminated with an entangled state. The crossing of the critical point in a non-adiabatic manner is the key element for entanglement generation. This is verified in Fig.5.4 where we see that that the final state is remarkably close to a GHZ state.

Coherent charge transport in optical lattice

Contents

6.1	Setup for ion transport	67
6.2	Rydberg states of molecular ion	67
6.2.1	Perturbative treatment	69
6.2.2	Non-perturbative treatment	69
6.3	Optical coupling of electronic states	73
6.3.1	Dressed state	76
6.3.2	Adiabatic optical coupling	77
6.4	Ion transport in a double well	80
6.4.1	Population of the excited states	81
6.4.2	Lifetime of the system	82
6.4.3	Condition for coherent dynamics	82
6.5	Analytical expressions for dynamical parameters	83
6.5.1	Constant laser field	84
6.5.2	Spatially varying laser field	86
6.6	Ion transport in an optical lattice	90
6.6.1	Many-body Hamiltonian	91
6.6.2	Numerical simulation	93
6.7	Summary	94

Dynamics of charged particles in a gas of neutral atoms/BEC have been studied before [41, 178, 42, 149]. The question of controlling and ensuring coherent charge transport is still open. This chapter studies yet another application of strontium Rydberg atom, specifically the possibility of ion dynamics immersed among strontium atoms. By weakly exciting the atom to a Rydberg state, we show that the probability for the electron to hop onto its neighbouring ion is enhanced. The ion-atom system is studied for small distances using a non-perturbative treatment. Since the dynamics is strongly dependent on the inter-nuclear distance of the particles, any motion of the particle would result in de-phasing of the dynamics. To control the de-phasing issue, we propose to optically trap the ion-atom system. A compact set of dynamical equations are derived that ensure coherent hopping. These equations are solved numerically and compared with analytical

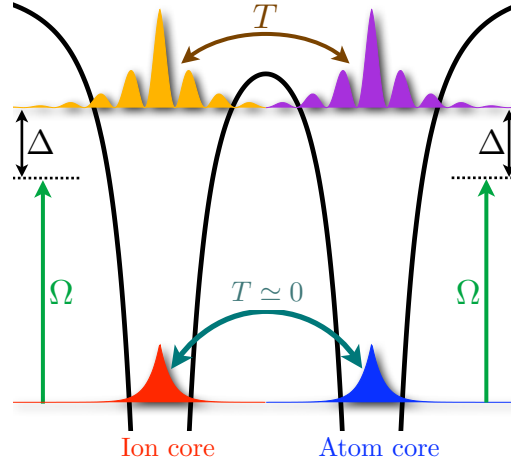


Figure 6.1: The ionic potentials are shown corresponding to the ion (red) and atom core (blue). The ground state is optically coupled to its Rydberg state for which the tunneling T is higher since it has a stronger overlap with the neighbouring core.

results. Finally we test the coherence of the dynamics for a two site case which is later generalized to many-sites. With the help of a spatially dependent laser field, we are able to choose the direction of the transport. We conclude with a discussion on the relevant time scales and the possibility of experimental realization of the system.

6.1 Setup for ion transport

Consider the simple case of an ion placed next to an atom. If the atom is in its ground state, then the electron is highly localized with its atomic core. While for a Rydberg atom, the wave function of the electron has a large spatial extension (refer to section 2.2) and thus crosses the ionic potential barrier as shown in Fig.6.1. Thus having the atom in its Rydberg state enhances the hopping probability. One can also view this process as the transport of the ion (hole) with an effective mass of the electron. It is important to have the dynamical time scale for the ion transport much smaller than the lifetime of the system, which is partly determined by the lifetime of the Rydberg atoms. One enhances the lifetime of the Rydberg state by a fraction $(2\Delta/\Omega)^2$, where Δ is the detuning of the laser and Ω is the Rabi frequency. In the forthcoming sections, we determine the Rydberg spectrum of the ion-atom system and study the process of optically coupling the ground state to the Rydberg state of the ion-atom.

6.2 Rydberg states of molecular ion

A typical Hamiltonian that describes any molecular ion system (as in our case Sr_2^+) consists of the kinetic energy of the electron, the attractive ionic potential experienced by the electron with respect to each of the nuclei and the repulsive potential between

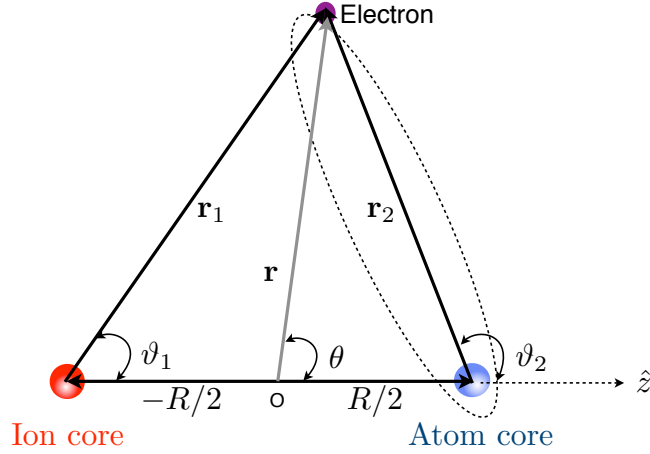


Figure 6.2: A schematic diagram showing the different electronic and nuclear interactions co-ordinates of an atom and ion.

the two nuclei as shown schematically in Fig.6.2. Explicitly it is written as

$$\hat{H}_{\text{el}} = -\frac{\nabla_r^2}{2} - \frac{1}{|\mathbf{r}_1|} - \frac{1}{|\mathbf{r}_2|} + \frac{1}{|\mathbf{R}|} . \quad (6.1)$$

The distance between the atom and the ion is denoted by R . If \mathbf{r} is the co-ordinate for the electron, then the relative position with respect to the ion is $\mathbf{r}_1 = \mathbf{r} - \mathbf{R}/2$ and that to the atom, $\mathbf{r}_2 = \mathbf{r} + \mathbf{R}/2$ (See Fig.6.2). \hat{H}_{el} is invariant with respect to the exchange of $\mathbf{r}_1 \leftrightarrow \mathbf{r}_2$. This exchange symmetry is used to define a symmetric (gerade) and anti-symmetric (ungerade) basis. Thus the Rydberg molecular ion wave function expressed in terms of the localized (un)gerade basis is given as

$$|e^{(\pm)}\rangle = c^{(\pm)} [|\psi_{nlm_l}(\mathbf{r}_1)\rangle \pm |\psi_{nlm_l}(\mathbf{r}_2)\rangle] . \quad (6.2)$$

where $|e^{(\pm)}\rangle$ are the excited states of the molecular ion corresponding to each symmetry. $\psi_{nlm_l}(\mathbf{r}_{i=1,2}) = \mathcal{R}_{nl}(r)\mathcal{Y}_{lm_l}(\vartheta, \varphi)$ are the bare atomic strontium Rydberg states calculated in section 3.3.1. Note that here $\mathbf{r}_{i=1,2}$ denotes the position of the excited valence electron of strontium while the position for the second valence electron is suppressed compared to Eq.(3.21). We choose the inter-nuclear axis along the z-axis and focus on $m_l = 0$ (henceforth we omit this label). Using Eq.(6.1), we now calculate the hopping rate of the Rydberg electron perturbatively.

6.2.1 Perturbative treatment

Assuming that the ion-atom distance (R) is much larger compared to the size of the Rydberg wave function ($\mathbf{r}_{1,2}$), then we can apply multipole expansion upto the second order to $\left(\frac{1}{r_1} + \frac{1}{r_2}\right)$ about the center (O in Fig.6.2) of the inter-nuclear distance. Defining the hopping rate of the Rydberg electron as

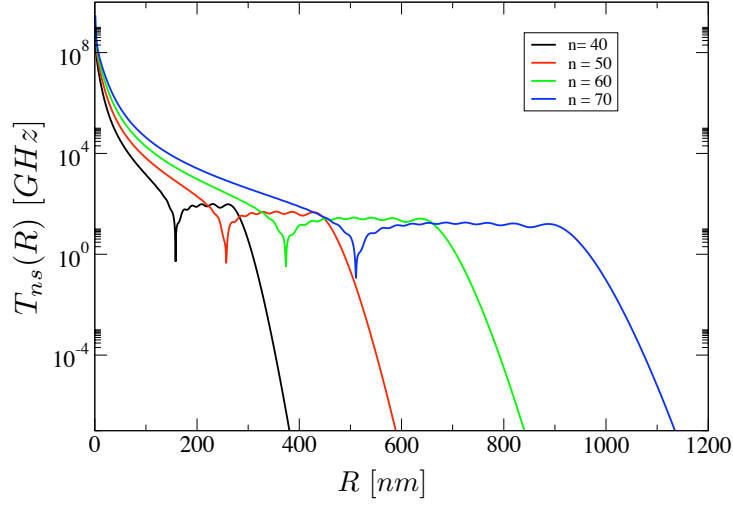


Figure 6.3: Perturbative calculations of hopping rate $T_{nl}(R)$ for different Rydberg states as a function of inter-nuclear distance.

$$\begin{aligned}
 T_{nl}(R) &= \frac{1}{2} \left[\langle \psi_{nl}(\mathbf{r}_1) | \hat{H}_{el} | \psi_{nl}(\mathbf{r}_2) \rangle + \langle \psi_{nl}(\mathbf{r}_2) | \hat{H}_{el} | \psi_{nl}(\mathbf{r}_1) \rangle \right] \\
 &= \left(\varepsilon_{nl} - \frac{1}{R} \right) \langle \psi_{nl}(\mathbf{r}_1) | \psi_{nl}(\mathbf{r}_2) \rangle + \langle \psi_{nl}(\mathbf{r}_2) | \frac{4r^2(1 - 3 \cos \theta)}{R^3} | \psi_{nl}(\mathbf{r}_2) \rangle . \quad (6.3)
 \end{aligned}$$

Owing to the the non-orthogonality of the wave functions defined at different locations, there is a small non-zero overlap function $\langle \psi_{nl}(\mathbf{r}_1) | \psi_{nl}(\mathbf{r}_2) \rangle$. To evaluate $T_{nl}(R)$, we express $\mathbf{r}_{1,2}$ in terms of \mathbf{r} and \mathbf{R} . The purpose of weakly exciting to Rydberg states is to have large hopping rates for fast dynamical time scales. As we see in Fig.6.4, one can achieve large hopping rate (order of GHz) but only for small inter-nuclear spacings. For example, the 60s state has few GHz hopping rate for an inter-nuclear distance of 750 nm, after which it drops exponentially. The exponential drop comes from the overlap of the tails ends of the Rydberg wave functions. This means that we need to calculate the ion-atom interaction for distances for which the coupling to other Rydberg states is greater than the energy differences between the states. At such small distances, the validity of multipole expansion comes into question and perturbative calculations break down.

6.2.2 Non-perturbative treatment

Since we are dealing in the regime where strong coupling causes mixing of different states, more than one Rydberg state is included into the basis Eq.(6.2). The molecular ion wave function expressed in terms of the different bare atomic Rydberg states $|\psi_{nl}\rangle$ of the strontium atom is given as

$$|e^{\alpha,(\pm)}\rangle = \sum_{n,l} c_{nl}^{\alpha,(\pm)} [|\psi_{nl}(\mathbf{r}_1)\rangle \pm |\psi_{nl}(\mathbf{r}_2)\rangle] . \quad (6.4)$$

which satisfies the following eigenvalue equation

$$\hat{H}_{\text{el}}|e^{\alpha,(\pm)}\rangle = \hbar\omega_{\text{el}}^{\alpha,(\pm)}(R)|e^{\alpha,(\pm)}\rangle . \quad (6.5)$$

The index $\alpha = 1, 2, \dots$ represents the different excited states of the molecular ion. The corresponding matrix elements in the (un)gerade basis are

$$\begin{aligned} & \langle e^{\alpha,(\pm)} | \hat{H}_{\text{el}} | e^{\alpha,(\pm)} \rangle \\ &= \sum_{n,l} \sum_{n',l'} (c_{nl}^{\alpha,(\pm)}) (c_{n'l'}^{\alpha,(\pm)}) \left[\langle \psi_{n'l'}(\mathbf{r}_1) \pm \psi_{n'l'}(\mathbf{r}_2) | \hat{H}_{\text{el}} | \psi_{nl}(\mathbf{r}_1) \pm \psi_{nl}(\mathbf{r}_2) \rangle \right] \\ &= \sum_{n,l} \sum_{n',l'} (c_{nl}^{\alpha,(\pm)}) (c_{n'l'}^{\alpha,(\pm)}) \left[\langle \psi_{n'l'}(\mathbf{r}_1) | \hat{H}_{\text{el}} | \psi_{nl}(\mathbf{r}_1) \rangle + \langle \psi_{n'l'}(\mathbf{r}_2) | \hat{H}_{\text{el}} | \psi_{nl}(\mathbf{r}_2) \rangle \right. \\ & \quad \left. \pm \langle \psi_{n'l'}(\mathbf{r}_2) | \hat{H}_{\text{el}} | \psi_{nl}(\mathbf{r}_1) \rangle \pm \langle \psi_{n'l'}(\mathbf{r}_1) | \hat{H}_{\text{el}} | \psi_{nl}(\mathbf{r}_2) \rangle \right] . \end{aligned} \quad (6.6)$$

Thus there are two kinds of matrix elements, the one center matrix elements and the two center matrix elements given in the last line of the above equation. Similarly it can be shown that

$$\langle e^{\alpha,+} | \hat{H}_{\text{el}} | e^{\alpha,-} \rangle = \langle e^{\alpha,-} | \hat{H}_{\text{el}} | e^{\alpha,+} \rangle = 0 . \quad (6.7)$$

The advantage of expressing the basis in the (un)gerade basis is that they can be solved separately by diagonalization. The larger the basis size, the more accurate are the eigenvalues for smaller distances. For the calculations shown here, we used a basis size consisting of all Rydberg states within the energy band of 5×10^{-5} a.u. around the 50s atomic Rydberg energy. This amounted to 476 different Rydberg states with n ranging from 46 to 56 along with all the relevant angular momentum states. In the next section we discuss the details for evaluating the specific matrix elements.

Matrix elements

Calculating the matrix elements involves performing a two dimensional numerical integration, one for the radial part and the other for the angular part. The coupling between states of an atom located at the same position and is given as

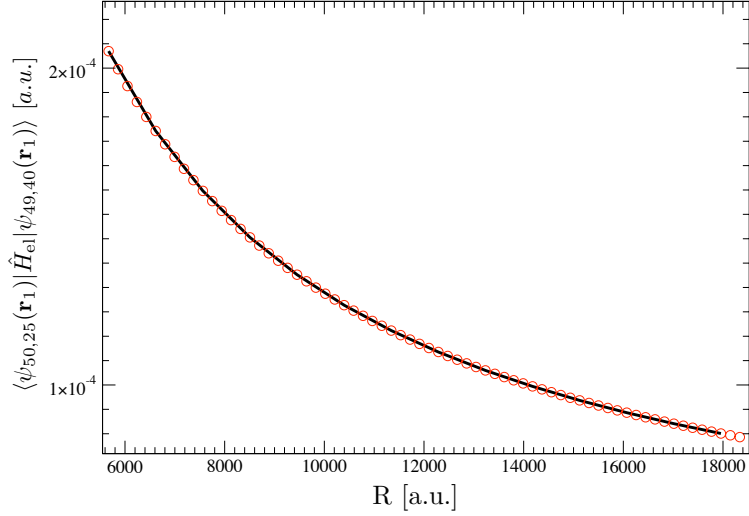


Figure 6.4: The plot evaluates the single center matrix element for a specific case using Eq.(6.8) where the sum was terminated on convergence (red circles) and the full calculation (black).

$$\begin{aligned}
& \langle \psi_{n'l'}(\mathbf{r}_1) | \hat{H}_{\text{el}} | \psi_{nl}(\mathbf{r}_1) \rangle \\
&= \left(\varepsilon_{nl} + \frac{1}{R} \right) \delta_{nl}^{n'l'} + \langle \psi_{n',l'}(\mathbf{r}_1) | \frac{1}{r_2} | \psi_{n,l}(\mathbf{r}_1) \rangle \\
&= \left(\varepsilon_{nl} + \frac{1}{R} \right) + \int_0^\pi \int_0^\infty \frac{\psi_{nl}(r_1) \psi_{n'l'}(r_1) \mathcal{Y}_{l,0}^*(\cos \vartheta_1) \mathcal{Y}_{l',0}(\cos \vartheta_1)}{r_2} r_1^2 dr_1 d\Omega_1 \\
&= \left(\varepsilon_{nl} + \frac{1}{R} \right) + \sum_{l_p=|l-l'|}^{l+l'} \sqrt{\frac{\pi(2l+1)(2l'+1)}{(2l_p+1)}} \langle ll'00 | l_p 0 \rangle^2 \\
&\times \int_0^\pi \int_0^\infty \frac{\psi_{nl}(r_1) \psi_{n'l'}(r_1) \mathcal{Y}_{l_p,0}^*(\cos \vartheta_1)}{r_2} r_1^2 dr_1 \sin \vartheta_1 d\vartheta_1 .
\end{aligned} \tag{6.8}$$

where the big angular brackets correspond to the Clebsch-Gordan coefficients (refer to Appendix B). Similar expressions are obtained for $\psi_{n,l}(\mathbf{r}_2)$. In the last line we used the standard properties for the product of spherical harmonics [32]. The coupling between states for atoms at two different locations and is given as

$$\langle \psi_{n'l'}(\mathbf{r}_1) | \hat{H}_{\text{el}} | \psi_{nl}(\mathbf{r}_2) \rangle = \left(\varepsilon_{nl} + \frac{1}{R} \right) \langle \psi_{n',l'}(\mathbf{r}_1) | \psi_{n,l}(\mathbf{r}_2) \rangle + \langle \psi_{n',l'}(\mathbf{r}_1) | \frac{1}{r_2} | \psi_{n,l}(\mathbf{r}_2) \rangle . \tag{6.9}$$

The above equation is a two center integrals. Evaluating two center matrix elements especially for small distances can be quite demanding [167]. This is because at every step of the integration, one has to transform the position of the electron defined at one of the centers to the other center. Also for small distances, the Rydberg wave functions are

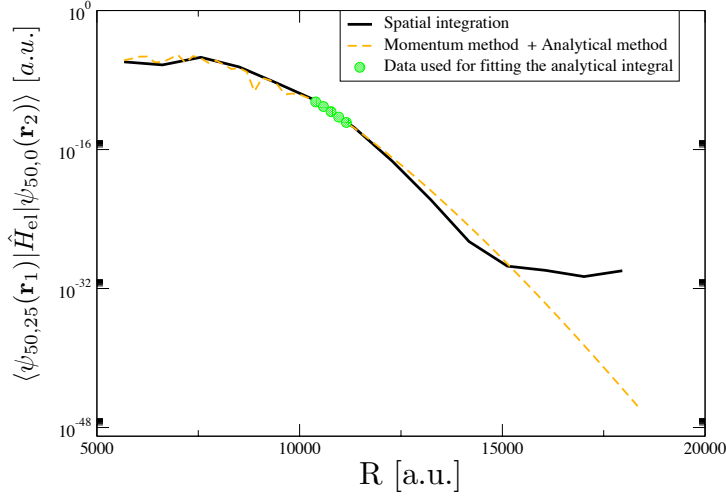


Figure 6.5: The dashed orange line is the combined result of Eq.(6.12) for small distances and Eq.(6.13) for large distance. The green dots were also calculated using Eq.(6.12) used for fitting Eq.(6.13). The bold black line corresponds to spatial integration. At large distances, the spatial integration becomes inaccurate due to the limitation in step-size.

highly oscillatory and to resolve them requires a very fine grid size. To do this repeatedly for a very large basis size is inefficient.

These integrals can however be easily solved in momentum space for small and intermediate distances as is often done in the study of ion-atom scattering processes [173]. The advantage in solving the two center integrals in momentum space is that the angular part can be separated out which simplifies the integration to two one dimensional integrals. If ψ_{nl} is spatial wave function then the momentum counterpart is given by its Fourier transform,

$$\begin{aligned}
 \tilde{\psi}_{nl}(\mathbf{k}) &= \frac{1}{(2\pi)^{3/2}} \int_0^\infty e^{-i\mathbf{k}\cdot\mathbf{r}} \psi_{nl}(\mathbf{r}) d^3\mathbf{r} \\
 &= \sqrt{\frac{2}{\pi}} i^l \mathcal{Y}_{l0}(\vartheta_k, \varphi_k) \int_0^\infty \psi_{nl}(r) j_l(kr) r^2 dr \\
 &= \sqrt{\frac{2}{\pi}} i^l \mathcal{Y}_{l0}(\vartheta_k, \varphi_k) \tilde{\psi}_{nl}(k) .
 \end{aligned} \tag{6.10}$$

where we used the fact that generalized spherical harmonics are orthonormal and the following expansion,

$$e^{i\mathbf{k}\cdot\mathbf{r}} = 4\pi \sum_{L=0}^{\infty} i^L j_L(kr) \sum_{M=-L}^L \mathcal{Y}_{LM}^*(\vartheta, \varphi) \mathcal{Y}_{LM}(\vartheta_k, \varphi_k) . \tag{6.11}$$

j_L are the Bessel functions [70]. For the overlap integral, we have we define the momentum representation of $\psi_{nl}(\mathbf{r}_1)$ and $\psi_{n'l'}(\mathbf{r}_2)$ as $e^{i\mathbf{k}\cdot\mathbf{R}} \tilde{\psi}_{nl}(\mathbf{k})$ and $\tilde{\psi}'_{n'l'}(\mathbf{k})$ respectively.

$$\begin{aligned}
\langle \psi_{nl}(\mathbf{r}_1) | \psi_{n'l'}(\mathbf{r}_2) \rangle &= \langle \psi_{nl}(\mathbf{r}_2 + \mathbf{R}) | \psi_{n'l'}(\mathbf{r}_2) \rangle \\
&= \int_0^\infty e^{i\mathbf{k}\cdot\mathbf{R}} \tilde{\psi}_{nl}^*(\mathbf{k}) \tilde{\psi}'_{n'l'}(\mathbf{k}) d^3\mathbf{k} \\
&= \sum_L 2i^{l'-l+L} \sqrt{4\pi(2l+1)(2l'+1)(2L+1)} \langle ll'00 | L0 \rangle^2 \mathcal{Y}_{L0}^*(\vartheta, \varphi) \\
&\quad \times \int_0^\infty \tilde{\psi}_{nl}(k) \tilde{\psi}'_{n'l'}(k) j_L(kR) k^2 dk .
\end{aligned} \tag{6.12}$$

The attraction integral (second term in Eq.(6.9)) is solved in the similar manner as above by defining $\tilde{\psi}'_{n'l'}(\mathbf{k})$ for $\psi_{n'l'}(\mathbf{r}_2)/\mathbf{r}_2$ instead of just $\psi_{n'l'}(\mathbf{r}_2)$. As seen from Fig.6.5, the two center integrals from the momentum method agree with the spatial integration up to an intermediate distance. To calculate the Bessel functions accurately for large distances is inefficient. So for large distances ($> (n^2 + n'^2)$), there exists analytical formulae for two center integrals which are expressed in terms of the Slater like wave functions [112, 152]. The analytical formulae involve the evaluation of factorials which are dependent on the principal and angular quantum numbers. Since these can be quite large (~ 45 -55) for Rydberg states, it is also inefficient to calculate them explicitly. Instead for large inter-nuclear distances, we express the two center integrals in terms of the Slater like wave function using a simplified formula given as

$$\langle \psi_{nl}(\mathbf{r}_1) | \frac{1}{r_2} | \psi_{n'l'}(\mathbf{r}_2) \rangle = C_0 \left(\frac{\rho}{2} \right) e^{C_1} \left[e^{-u(1-v)} + e^{-u(1+v)} \right] . \tag{6.13}$$

Coefficients C_0 and C_1 are fitted linearly from the matrix elements calculated for intermediate values of R using Eq.(6.12). The prolate spheroidal co-ordinates (u, v) are defined as

$$u = \frac{R}{2}(\xi_1 + \xi_2), \quad v = \frac{\xi_1 - \xi_2}{\xi_1 + \xi_2} \quad \text{where} \quad \xi_i = \frac{Z}{n_i} . \tag{6.14}$$

In Fig.6.5, the evaluation of the two center integrals is shown using the three different methods. Combining the results from Eq.(6.12) for small and inter-mediate distances and Eq.(6.13) for large distances, we obtain the dashed orange curve in Fig.6.5.

Numerical results

The strontium Rydberg molecular ion potential curves ($\hbar\omega_{\text{el}}^{\alpha,\pm}$) are represented in pairs, each corresponding to a symmetry group of (un)gerade basis as shown in Fig.6.6. Potential curves belonging to the same symmetry group have avoided crossings while potentials from different symmetry groups cross. The strong mixing of the different l states is reflected in the potential curves as multiple avoided crossings particularly at small distances giving a ‘spaghetti’ like spectrum (see Fig.6.6). From the eigenvalue energies obtained, one defines the splitting energy between the gerade and ungerade state as

$$T^\alpha(R) = \frac{\hbar(\omega_{\text{el}}^{\alpha,+}(R) - \omega_{\text{el}}^{\alpha,-}(R))}{2} . \tag{6.15}$$

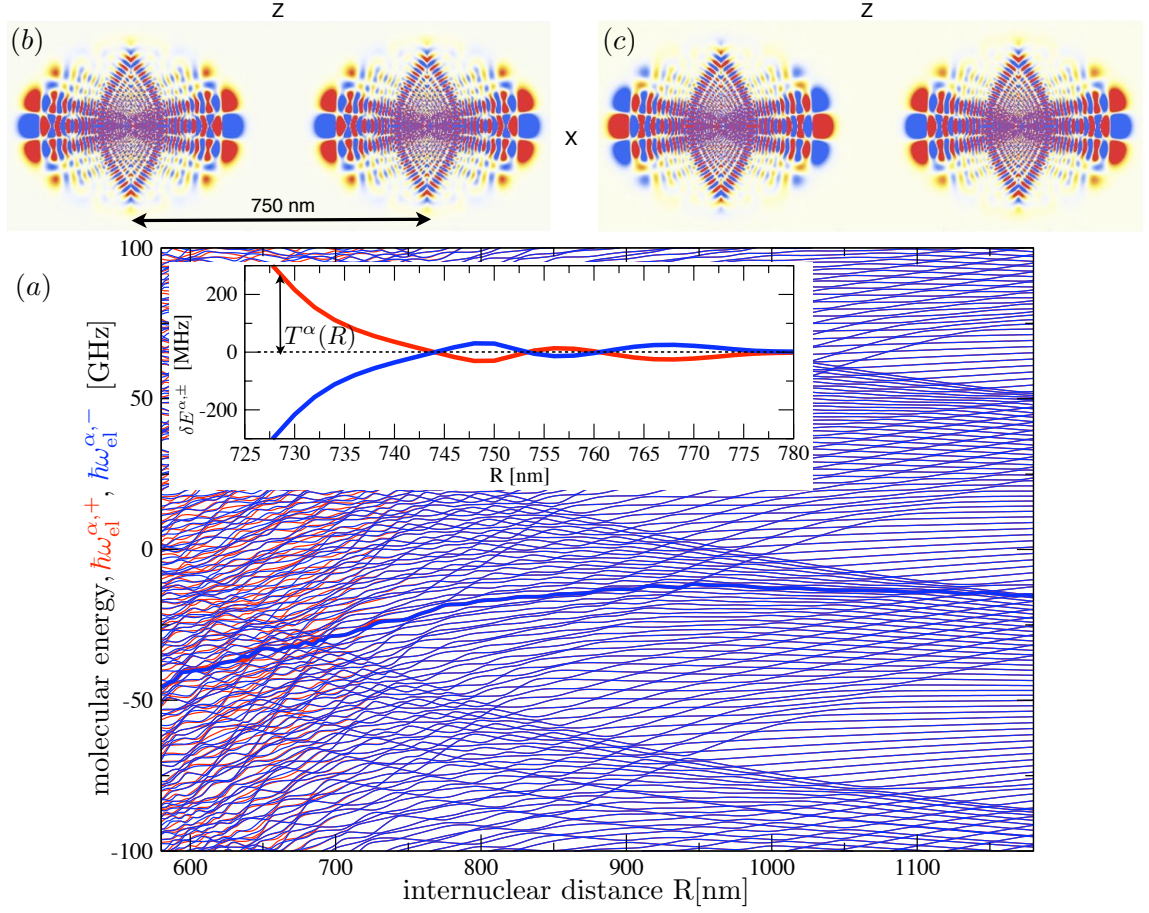


Figure 6.6: Potential curves for high lying Rydberg states of a Sr_2^+ molecular ion. The molecular energies are given relative to the $\text{Sr}_2^+(50S)$ asymptote. The relative energies, $\delta E^{\alpha, \pm} = \hbar\omega_{\text{el}}^{\alpha, (\pm)} - (\hbar\omega_{\text{el}}^{\alpha, (+)} + \hbar\omega_{\text{el}}^{\alpha, (-)})/2$, of a selected pair ($\alpha = 243$, thick lines) with (un)gerade symmetry is shown in the inset. Panels (b) and (c) show the corresponding (un)gerade electronic wave functions at an internuclear distance of $R = 750$ nm. At this distance the tunnel splitting is as large as several 100 MHz, while the electronic wave function is well localized at each ionic core.

for a given excited molecular ion state α (see Fig.6.6(a)). T^α is the non-perturbative hopping rate and has contributions from a large number of Rydberg states particularly at small distances unlike the T in Eq.(6.3). The inset of Fig.6.6 shows that for small distances (less than 700 nm), T^α has significant oscillations before it decreases. Different l states polarize differently and since all the l states contribute in the wave function, there is a rich complexity of the wave functions shown in Fig.6.7. The Rydberg molecular ion wave function shown in Fig.6.7(a) shows some higher probability for the electron to be between the two centers of the nuclei while the other wave functions ((b)-(e)) are for inter-nuclear distances where the Rydberg molecular ionic state is not over the ionic

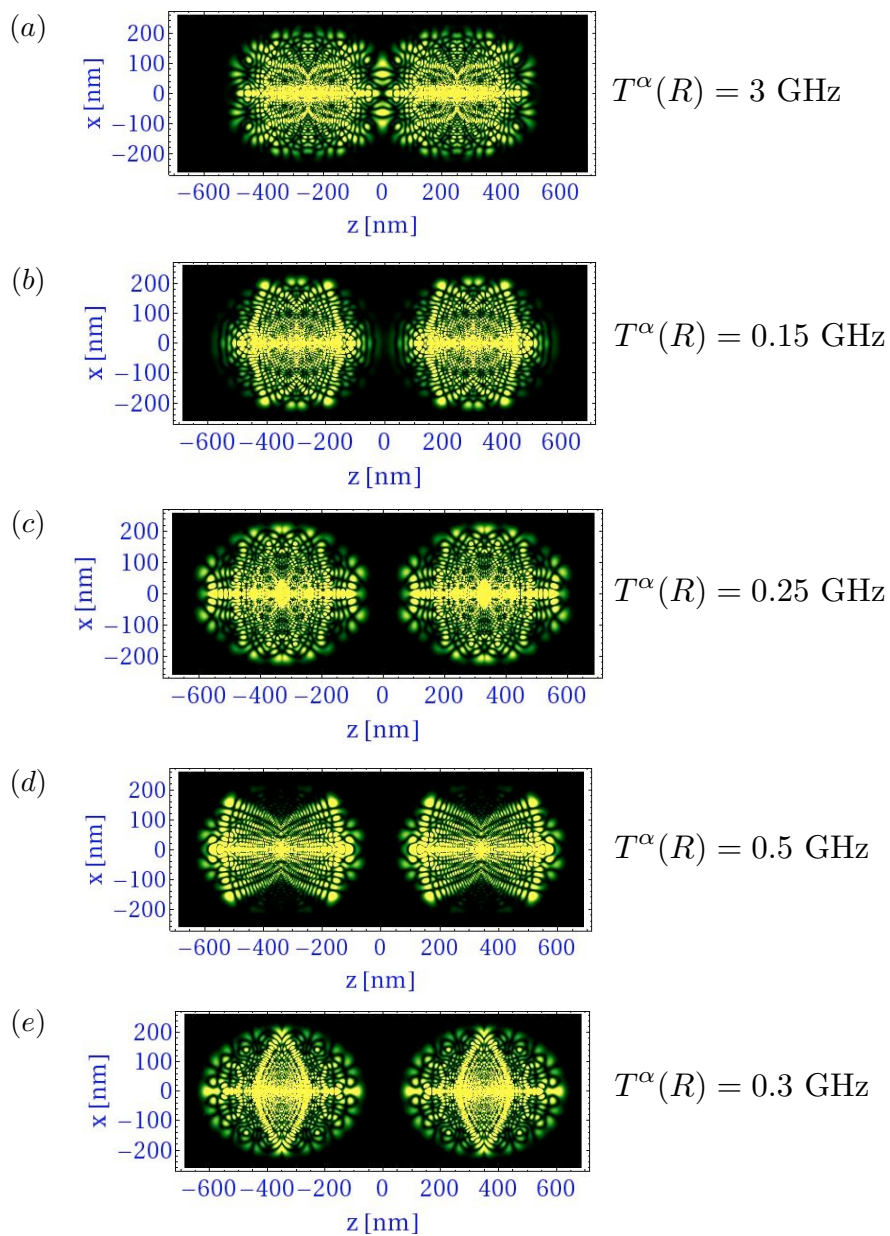


Figure 6.7: The figure shows plots of the molecular ion wave functions ($|e^{\alpha,(\pm)}|^2$) for a selected pair of curves ($\alpha = 243$) at different inter-core distances: (a) $R = 500 \text{ nm}$ (b) $R = 600 \text{ nm}$ (c) $R = 640 \text{ nm}$ (d) $R = 670 \text{ nm}$ (e) $R = 700 \text{ nm}$.

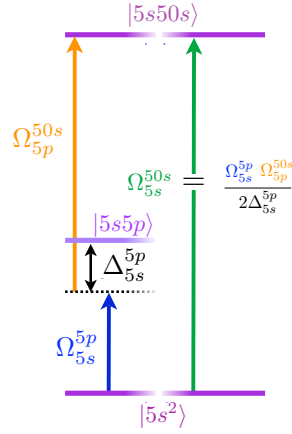


Figure 6.8: Two photon excitation to a Rydberg state via the inter-mediate state $|5s5p\rangle$.

potential barrier.

6.3 Optical coupling of electronic states

The ground states of the molecular ion is coupled to the excited molecular ion states $|e^{\alpha,(\pm)}\rangle$ with the help of an excitation laser. Adopting a two particle state notation, we have

$$|ie^{\alpha}\rangle = \frac{1}{\sqrt{2}} (|e^{\alpha,+}\rangle + |e^{\alpha,-}\rangle), \quad |e^{\alpha}i\rangle = \frac{1}{\sqrt{2}} (|e^{\alpha,+}\rangle - |e^{\alpha,-}\rangle) . \quad (6.16)$$

where $|i\rangle$ represents the ionic state of a particle. By using this two particle state, we explicitly show whether the atom is to left or right of the ion. Similarly the ground state of the molecular ion is given as $|ig\rangle$ and $|gi\rangle$ where where $|g\rangle = |5s^2\rangle$. The energy of the ground state is set to zero. The full wave function of the molecular ion with all its states is given as

$$|\psi\rangle = c^{ig}(t)|ig\rangle + c^{gi}(t)|gi\rangle + \sum_{\alpha} (c^{ie,\alpha}(t)|ie^{\alpha}\rangle + c^{ei,\alpha}(t)|e^{\alpha}i\rangle) \quad (6.17)$$

and the corresponding time dependent Schrödinger equation is

$$i\hbar \frac{d|\psi\rangle}{dt} = \hat{H}_{\text{opt}}|\psi\rangle . \quad (6.18)$$

where \hat{H}_{opt} is the Hamiltonian for optical coupling similar to Eq.(5.12) introduced in the earlier chapter but now for more number of Rydberg states and including T^{α} of Eq.(6.15),

$$\hat{H}_{\text{opt}} = \hbar \sum_{\alpha} \left[-\Delta^{\alpha} (|ie^{\alpha}\rangle\langle ie^{\alpha}| + |e^{\alpha}i\rangle\langle e^{\alpha}i|) + \frac{\Omega^{\alpha}}{2} (|ie^{\alpha}\rangle\langle ig| + |e^{\alpha}i\rangle\langle gi| + \text{h.c.}) + \frac{T^{\alpha}}{\hbar} (|ie^{\alpha}\rangle\langle e^{\alpha}i| + \text{h.c.}) \right]. \quad (6.19)$$

The above Hamiltonian considers that a laser with frequency ω_L is detuned with respect to a particular excited molecular ion state $|e^{\alpha}\rangle$ given by $\Delta^{\alpha} = \omega_L - (\omega_{\text{el}}^{\alpha,-} + \omega_{\text{el}}^{\alpha,+})/2$. The corresponding Rabi frequency is given by Ω^{α} assuming that the intensity of the laser field is spatially constant. Later in section 6.5.2, we will generalize \hat{H}_{opt} for a spatially varying laser field.

The coupling of the ground state atom to the excited molecular ion state is achieved via a two photon excitation (See Fig.6.8). We define a reference Rabi frequency which corresponds to the coupling of the ground state to the 50s Rydberg state via the intermediate state 5s5p. Assuming that the second laser is largely detuned (Δ_{5s}^{5p}) from the inter-mediate 5p state, we have an effective Rabi frequency to the 50s state given by Ω_{5s}^{50s} . For our calculations we take the reference frequency to be $\Omega_{5s}^{50s} = 20$ MHz. Thus we have,

$$\Omega^{\alpha}(R) = \frac{\mu^{\alpha}(R)}{\mu_{50s}^{50s}} \Omega_{5s}^{50s}, \quad (6.20)$$

where $\mu^{50s} = \langle 5p|\mu|50s\rangle$ and $\mu^{\alpha}(R) = \langle 5p|\mu|e^{\alpha}(R)\rangle$. Since the coupling to the excited state is via the inter-mediate state 5s5p state, the contribution to the Rabi frequencies for any given $|e^{\alpha}\rangle$ is determined by the strength of the coupling to ns and nd components of molecular ion state. The Rabi frequencies depend on inter-nuclear distance R as the dipole moments vary with R as do the molecular ion wave functions (see Fig.6.7). Solving Eq.(6.18) gives the following dynamical equations

$$i\partial_t c^{ig} = \frac{\Omega^{\alpha}}{2} c^{ie}, \quad (6.21a)$$

$$i\partial_t c^{gi} = \frac{\Omega^{\alpha}}{2} c^{ei}, \quad (6.21b)$$

$$i\partial_t c^{ie,\alpha} = -\Delta^{\alpha} c^{ie,\alpha} + \frac{\Omega^{\alpha}}{2} c^{ig} + \frac{T^{\alpha}}{\hbar} c^{ei,\alpha}, \quad (6.21c)$$

$$i\partial_t c^{ei,\alpha} = -\Delta^{\alpha} c^{ei,\alpha} + \frac{\Omega^{\alpha}}{2} c^{gi} + \frac{T^{\alpha}}{\hbar} c^{ie,\alpha}. \quad (6.21d)$$

For a constant laser field, it is more convenient to work in the (un)gerade basis as the above set of dynamical equations decouple to two independent sets of dynamical equations, each corresponding to a symmetry group. We solve the two sets of dynamical equations numerically to obtain instantaneous states that are a superposition of the ground and Rydberg states.

6.3.1 Dressed state

Defining the ground states in the (un)gerade basis similar to the ones for the excited molecular states in Eq.(6.4), we have

$$|g^\pm\rangle = \frac{1}{\sqrt{2}} (|ig\rangle \pm |gi\rangle) . \quad (6.22)$$

Using the following change of variables

$$c^{g,\pm} = 1/\sqrt{2}(c^{ig} \pm c^{gi}), \quad c^{\alpha,\pm} = 1/\sqrt{2}(c^{ie,\alpha} \pm c^{ei,\alpha}) . \quad (6.23)$$

we re-write dynamical equations in Eqs.(6.21a)-(6.21d) in the (un)gerade basis

$$i\partial_t c^{g,+} = \frac{\Omega^\alpha}{2} c^{\alpha,+} , \quad (6.24a)$$

$$i\partial_t c^{g,-} = \frac{\Omega^\alpha}{2} c^{\alpha,-} , \quad (6.24b)$$

$$i\partial_t c^{\alpha,+} = -\Delta^{\alpha,+} c^{\alpha,+} + \frac{\Omega^\alpha}{2} c^{g,+} , \quad (6.24c)$$

$$i\partial_t c^{\alpha,-} = -\Delta^{\alpha,-} c^{\alpha,-} + \frac{\Omega^\alpha}{2} c^{g,-} . \quad (6.24d)$$

where $\Delta^{\alpha,\pm} = \omega_L - \omega_{\text{el}}^{\alpha,(\pm)} = \Delta^\alpha \mp \frac{T^\alpha}{\hbar}$. Defining the transition operators in terms of the internal states $|g^{(\pm)}\rangle$ and $|e^{\alpha,(\pm)}\rangle$, we re-write the \hat{H}_{opt} in Eq.(6.19), which is

$$\hat{H}_{\text{opt}}^\pm = \hbar \sum_\alpha \left[-\Delta^{\alpha,(\pm)} |e^{\alpha,(\pm)}\rangle \langle e^{\alpha,(\pm)}| + \frac{\Omega^\alpha}{2} (|e^{\alpha,(\pm)}\rangle \langle g^{(\pm)}| + \text{h.c.}) \right] . \quad (6.25)$$

At any given time t , the instantaneous eigenstates of the above Hamiltonian will be a superposition of the ground and excited molecular ion states given as

$$|\xi^{\beta,(\pm)}\rangle = c_\beta^{g,(\pm)} |g^{(\pm)}\rangle + \sum_\alpha c_\beta^{\alpha,(\pm)} |e^{\alpha,(\pm)}\rangle . \quad (6.26)$$

These states $|\xi^{\beta,(\pm)}\rangle$ are known as *dressed states* [38]. They satisfy the following eigenvalue equation

$$\hat{H}_{\text{opt}}^{(\pm)} |\xi^{\beta,(\pm)}\rangle = \hbar\omega_{\text{opt}}^{\beta,(\pm)}(R) |\xi^{\beta,(\pm)}\rangle , \quad (6.27)$$

The energies of the corresponding dressed states are given as $\hbar\omega_{\text{opt}}^{\beta,(\pm)}(R)$, where $\beta = 1, 2, \dots$ represents excited dressed states and are ordered according to states with increasing energy. The energy levels of the dressed states obtained numerically are shown in Fig.6.9. At resonance, there is equal mixture of the electronic ground state and the Rydberg molecular ion states in the dressed ground state. Thus in Fig.6.9(a), we see that the contribution of the electronic ground state drop to 0.5 whenever the laser hits a potential curve at different distances. Similarly the ground dressed energies are inversely related to the detuning. At resonances, the dressed energies spike up as shown in Fig.6.9(b).

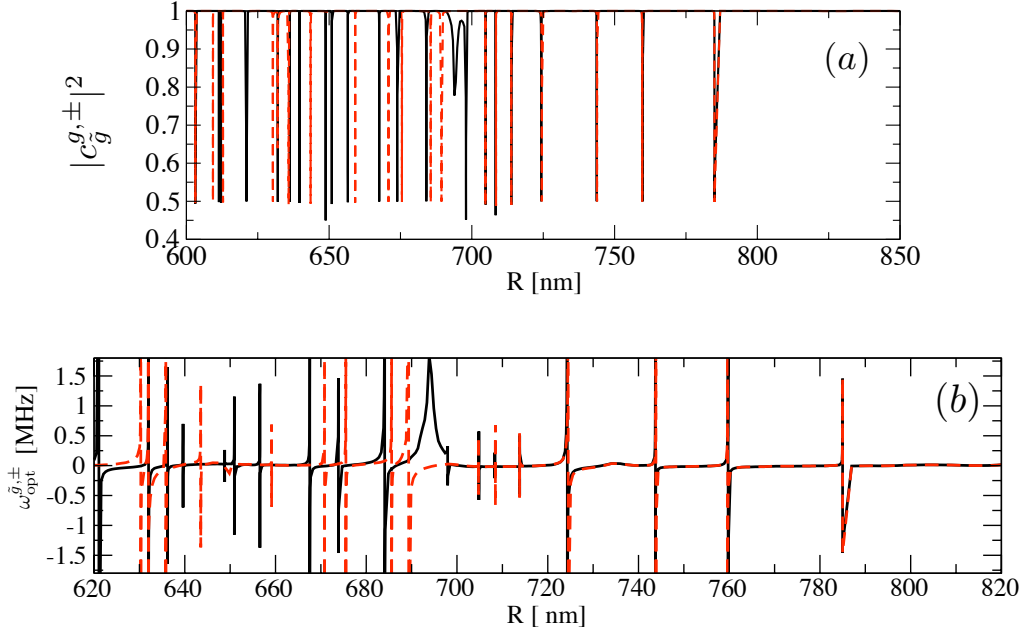


Figure 6.9: For $\Delta = -60.2$ GHz: (a) Contribution of the gerade (black) and ungerade (dashed red) electronic ground state to the dressed ground state at different distances R calculated numerically in Eq.(6.34). (b) Dressed ground state energies obtained numerically from Eq.(6.35).

6.3.2 Adiabatic optical coupling

In the previous section, we discussed about coupling the electronic ground states to the molecular excited states using an excitation laser. The excitation laser is gradually switched on and thus the Rabi frequency varies temporally till it achieves its final value. This introduces a time dependence in the Hamiltonian $\hat{H}_{\text{opt}}^{(\pm)}(t)$. Thus the dressed eigenstates are also time dependent.

$$\hat{H}_{\text{opt}}^{(\pm)}(t)|\xi^{\beta,(\pm)}(t)\rangle = \hbar\omega_{\text{opt}}^{\beta,(\pm)}(R,t)|\xi^{\beta,(\pm)}(t)\rangle. \quad (6.28)$$

Since the dressed eigenstates are orthonormal at every instant of time, the general solution for each symmetry independently expressed in terms of the instantaneous eigenstates $\xi^{\beta,(\pm)}(t)$ is

$$|\psi^{(\pm)}\rangle = \sum_{\beta} \left[c_{\beta}^{\pm}(t) |\xi^{\beta,(\pm)}(t)\rangle e^{-i \int_0^t \omega_{\text{opt}}^{\beta,(\pm)}(t') dt'} \right]. \quad (6.29)$$

Solving the corresponding time dependent Schrödinger equation for each symmetry, we have

$$\begin{aligned}
& i\hbar \sum_{\beta} \left[\dot{c}_{\beta}^{\pm}(t) |\xi^{\beta,\pm}(t)\rangle + c_{\beta}^{\pm}(t) |\dot{\xi}^{\beta,\pm}(t)\rangle - i c_{\beta}^{\pm}(t) |\xi^{\beta,\pm}(t)\rangle \omega_{\text{opt}}^{\beta,\pm} \right] e^{-i \int_0^t \omega_{\text{opt}}^{\beta,\pm}(t') dt'} \\
& = \sum_{\beta} c_{\beta}^{\pm}(t) \hat{H}_{\text{opt}}^{\pm} |\xi^{\beta,\pm}(t)\rangle e^{-i \int_0^t \omega_{\text{opt}}^{\beta,\pm}(t') dt'} .
\end{aligned} \tag{6.30}$$

The dot represents time derivative in the above equations. The third term in the L.H.S. cancels with the R.H.S. giving,

$$\sum_{\beta} \dot{c}_{\beta}^{\pm}(t) |\xi^{\beta,\pm}(t)\rangle e^{-i \int_0^t \omega_{\text{opt}}^{\beta,\pm}(t') dt'} = - \sum_{\beta} c_{\beta}^{\pm}(t) |\dot{\xi}^{\beta,\pm}(t)\rangle e^{-i \int_0^t \omega_{\text{opt}}^{\beta,\pm}(t') dt'} \tag{6.31}$$

Taking inner product with $\langle \xi^{\alpha,\pm}(t) |$, gives

$$\begin{aligned}
\dot{c}_{\alpha}^{\pm}(t) & = -c_{\alpha}^{\pm} \langle \xi^{\alpha,\pm}(t) | \dot{\xi}^{\alpha,\pm}(t) \rangle - \sum_{\beta \neq \alpha} c_{\beta}^{\pm} \langle \xi^{\alpha,\pm}(t) | \dot{\xi}^{\beta,\pm}(t) \rangle e^{-i \int_0^t (\omega_{\text{opt}}^{\beta,\pm}(t') - \omega_{\text{opt}}^{\alpha,\pm}(t')) dt} \\
& = -c_{\alpha}^{\pm} \langle \xi^{\alpha,\pm}(t) | \dot{\xi}^{\alpha,\pm}(t) \rangle - \sum_{\beta \neq \alpha} c_{\beta}^{\pm} \frac{\langle \xi^{\alpha,\pm}(t) | \hat{H}_{\text{opt}}^{\pm} | \xi^{\beta,\pm}(t) \rangle}{\hbar(\omega_{\text{opt}}^{\beta,\pm} - \omega_{\text{opt}}^{\alpha,\pm})} e^{-i \int_0^t (\omega_{\text{opt}}^{\beta,\pm}(t') - \omega_{\text{opt}}^{\alpha,\pm}(t')) dt} .
\end{aligned} \tag{6.32}$$

In the above equations, going from the first line to the next, we used the Hellmann-Feynman theorem for time dependent wave functions [67] which states,

$$i\hbar \frac{d}{dt} \langle \xi^{\alpha,\pm} | \frac{d}{d\lambda} \xi^{\beta,\pm} \rangle = \langle \xi^{\alpha,\pm} | \frac{d}{d\lambda} \hat{H}_{\text{opt}}^{\pm} | \xi^{\beta,\pm} \rangle , \tag{6.33}$$

In our case the parameter $\lambda \equiv t$. The second term in Eq.(6.32) couples a state starting initially in $|\xi^{\alpha,\pm}(t)\rangle$ to other states $|\xi^{\beta \neq \alpha,\pm}(t)\rangle$. If the process of switching on the laser is done very slowly then adiabatic approximation states that the time derivative of the Hamiltonian in Eq.(6.32) is small. The only time dependent term in the Hamiltonian is the Rabi frequency in Eq.(6.25). Let us assume that the time taken to increase $\Omega^{\alpha,\pm}(t=0) = 0$ to its final value is τ_p . At $t = 0$, the instantaneous ground state are the electronic ground states since the laser is off and there is no coupling to the Rydberg states. However on switching on the laser adiabatically, the instantaneous ground state of the system will be the *dressed ground states*. Dressed ground state is the dressed eigenstate with the lowest energy in absolute magnitude (since electronic ground state energy is taken to be zero) and is denoted by $|\xi^{\beta=0,(\pm)}\rangle \equiv |\tilde{g}^{(\pm)}\rangle$. Thus following Eq.(6.26),

$$|\tilde{g}^{(\pm)}\rangle = c_{\tilde{g}}^{g,(\pm)} |g^{(\pm)}\rangle + \sum_{\alpha} c_{\tilde{g}}^{\alpha,(\pm)} |e^{\alpha,(\pm)}\rangle , \tag{6.34}$$

and from Eq.(6.27), the dressed ground states satisfy the following eigenvalue equation,

$$\hat{H}_{\text{opt}}^{(\pm)} |\tilde{g}^{(\pm)}\rangle = \hbar \omega_{\text{opt}}^{\tilde{g},\pm}(R) |\tilde{g}^{(\pm)}\rangle . \tag{6.35}$$

Thus for the instantaneous state of the system to be the dressed ground state, we require the second term in Eq.(6.32) to be negligible and this is the case if

$$\tau_p \gg \frac{\Omega^{\alpha,\pm}(t = \tau_p) - \Omega^{\alpha,\pm}(t = 0)}{\omega_{\text{opt}}^{\beta=1,\pm} - \omega_{\text{opt}}^{\tilde{g},\pm}} . \quad (6.36)$$

Typical Rabi frequencies considered in Eq.(6.20) are in the order of tens of MHz. Numerically the energy difference between the closest excited dressed state ($\beta = 1$) to the dressed ground state ($\tilde{g} \equiv \beta = 0$) is of the order of at least few hundreds of MHz. Hence as an estimate, if the time taken for the excitation laser to reach its final value of intensity is more than 0.1 s, then by the adiabatic approximation, the instantaneous state of the system is the sum of the dressed ground states,

$$|\psi(t)\rangle = (c^{\tilde{g},+}(t) |\tilde{g}^+\rangle + c^{\tilde{g},-}(t) |\tilde{g}^-\rangle) . \quad (6.37)$$

Solving the time dependent Schrödinger equation for the Hamiltonian $\hat{H}_{\text{opt}}^{(\pm)}$, we get dynamical equations in terms of the dressed ground states,

$$i\partial_t c^{\tilde{g},+} = \omega_{\text{opt}}^{\tilde{g},+} c^{\tilde{g},+} \quad (6.38a)$$

$$i\partial_t c^{\tilde{g},-} = \omega_{\text{opt}}^{\tilde{g},-} c^{\tilde{g},-} \quad (6.38b)$$

The above dynamical equations can be expressed in the left/right basis using the following definition,

$$c^{i\tilde{g}} = 1/\sqrt{2}(c^{\tilde{g},+} + c^{\tilde{g},-}), \quad c^{\tilde{g}i} = 1/\sqrt{2}(c^{\tilde{g},+} - c^{\tilde{g},-}) . \quad (6.39)$$

where $|c^{i\tilde{g},\tilde{g}i}|^2$ gives the probability of the ion to be to the left/right of the atom in the molecular ion. It should be noted that the $c^{i\tilde{g},\tilde{g}i}$ are not the same as $c^{ig,gi}$ given in Eqs.(6.21a)-(6.21d) because the states $|i\tilde{g}, \tilde{g}i\rangle$ contain the ground states $|ig\rangle, |gi\rangle$ as well as the Rydberg states $|ie^\alpha\rangle, |e^\alpha i\rangle$ (see Eq.(6.34) and Fig.6.9). Substituting the above coefficients into Eq.(6.38a) give

$$i\partial_t c^{i\tilde{g}} = U(R)c^{i\tilde{g}} + J(R)c^{\tilde{g}i} , \quad (6.40a)$$

$$i\partial_t c^{\tilde{g}i} = U(R)c^{\tilde{g}i} + J(R)c^{i\tilde{g}} . \quad (6.40b)$$

where

$$U(R) = \frac{\omega_{\text{opt}}^{\tilde{g},+}(R) + \omega_{\text{opt}}^{\tilde{g},-}(R)}{2}, \quad J(R) = \frac{\omega_{\text{opt}}^{\tilde{g},+}(R) - \omega_{\text{opt}}^{\tilde{g},-}(R)}{2} . \quad (6.41)$$

The dynamics of the charge between the instantaneous ground states is thus determined by the dynamical parameters $U(R)$ and $J(R)$. $U(R)$ is the self-energy of the molecular ion with inter-nuclear distance R , while $J(R)$ is the energy required for the electron to hop to the neighbouring ion. $J(R)$ is the hopping rate between the dressed ground states

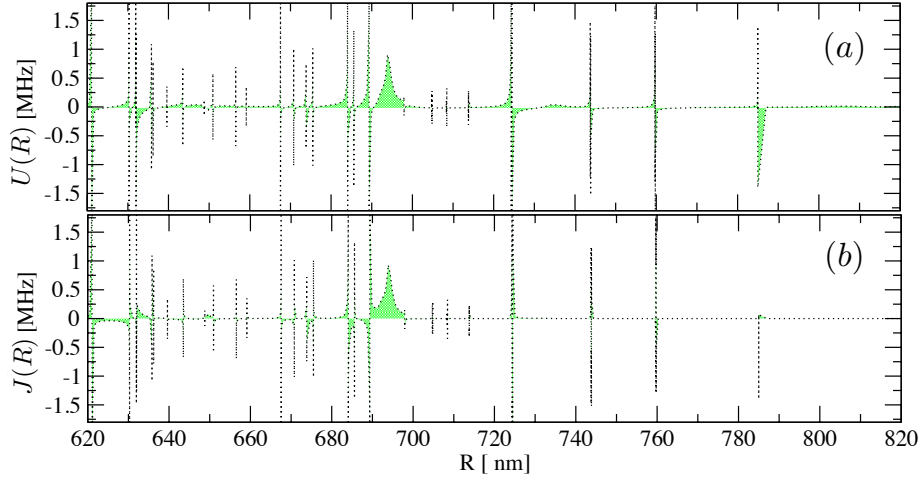


Figure 6.10: Plot of the dynamical parameters for $\Delta = -60.2$ GHz as a function of inter-nuclear distance: (a) $U(R)$ and (b) $J(R)$ from Eq.(6.41). Asymmetric contributions to $U(R)$ and $J(R)$ occurs (see at 690 nm) where the slope of the potential curve changes significantly.

which is different from T^α of Eq.(6.15), which is the hopping rate between the electronic Rydberg states located at different centers.

These dynamical parameters are calculated using the numerically obtained energies from Eq.(6.35). $U(R)$ and $J(R)$ are large when the laser frequency is near or on resonance as shown in Fig.6.10. The parameters take negative and positive values depending on the sign of the detuning. For a potential curve with a fixed slope, these positive and negative contributions are symmetrical and effectively cancel out. However for potential curves with a relatively large change in its slope across the resonance, there is more contribution of either region (positive/negative), for example near $R = 690$ nm in Fig.6.10.

6.4 Ion transport in a double well

The dynamical equations Eqs.(6.40a)-(6.40b) discussed in the previous section describe the hopping of the Rydberg electron from an atom to its neighbouring ion in their dressed ground states. But the dynamical parameters $U(R)$ and $J(R)$ are dependent on distance and so any change in distance will lead to dephasing of the transport process. Thus to control the motion of the particles, we propose to trap the ion and the atom in a double well optical trap. In Fig.4.8 (referring to section 4.3 of chapter 4), the black dash-dotted line corresponds to the polarizability of the ground state strontium ion. At magic wavelengths, this polarizability of the ion matches with the Rydberg atom and the ground state atom. Hence one can use the same optical lattice to trap the ion and the Rydberg dressed ground state atom. The trapping frequency of the optical lattice can be used as a control knob to alter the energy gap between the motional states. Large trapping frequencies ensure that higher motional states of the trapped nuclei are not

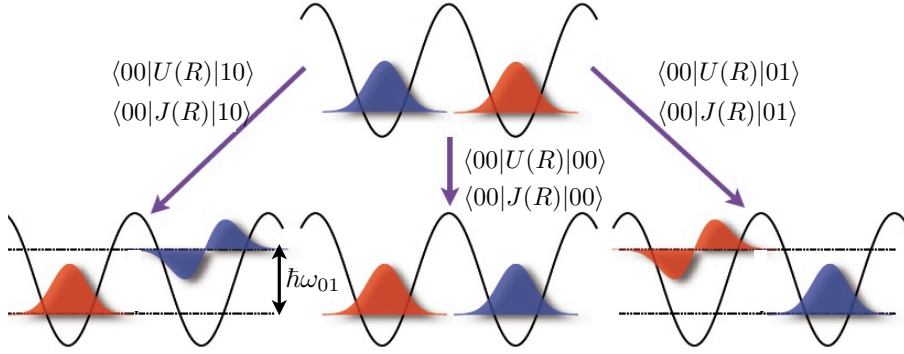


Figure 6.11: The figure represents the idea of using the trapping frequency as a control parameter to suppress the coupling to excited motional states.

excited during the hopping process of the Rydberg electron as shown in Fig.6.11. We write the Hamiltonian for the nuclear motion for our two site model as a sum of two harmonic oscillators (refer to Eq.(5.3) in section 5.1),

$$\hat{H}_{CoM}|n_1n_2\rangle = \sum_{i=1,2} \left[-\frac{\hbar^2 \nabla_{Z_i}^2}{2M} + \omega_{n_1n_2}^2 Z_i^2 \right] |n_1n_2\rangle = \hbar\omega_{n_1n_2} |n_1n_2\rangle. \quad (6.42)$$

where $|n_{i=1,2}\rangle$ is the motional state at the corresponding site and $|n_1n_2\rangle$ is the two particle motional eigenstate. The eigenvalue for the two particle motional state is defined as $\omega_{n_1n_2} = (n_1 + n_2)\omega_{tr}$, where ω_{tr} is the trapping frequency of the lattice. $Z_{(1,2)}$ is the relative motion of the corresponding trapped nuclei at each site. The time dependent Schrödinger equation for the full quantum dynamics is

$$i\hbar \frac{d|\Psi\rangle}{dt} = (\hat{H}_{opt}^+ + \hat{H}_{opt}^- + \hat{H}_{CoM})|\Psi\rangle. \quad (6.43)$$

$|\Psi\rangle$ given as a product state of the electronic eigenstates (also known as internal states) and the motional states (also known as external states) is,

$$|\Psi\rangle = \sum_{n_1, n_2} (c_{n_1n_2}^{\tilde{g}^+}(t) |\tilde{g}^+\rangle + c_{n_1n_2}^{\tilde{g}^-}(t) |\tilde{g}^-\rangle) |n_1n_2\rangle. \quad (6.44)$$

Switching to left/right basis and multiplying with $\langle n_1n_2|$ throughout we get the dynamical equations in terms of the left/right dressed ground states,

$$i\partial_t c_{n_1n_2}^{i\tilde{g}} = (\langle n_1n_2|U(R)|n_1n_2\rangle + \omega_{n_1n_2}) c_{n_1n_2}^{i\tilde{g}} + (\langle n_1n_2|J(R)|n_1n_2\rangle) c_{n_1n_2}^{i\tilde{g}} \quad (6.45a)$$

$$+ \sum_{n_1, n_2 \neq n'_1 n'_2} [\langle n'_1 n'_2|U(R)|n_1n_2\rangle] c_{n'_1 n'_2}^{i\tilde{g}} + \sum_{n_1, n_2 \neq n'_1 n'_2} [\langle n'_1 n'_2|J(R)|n_1n_2\rangle] c_{n'_1 n'_2}^{i\tilde{g}},$$

$$i\partial_t c_{n_1n_2}^{i\tilde{g}} = (\langle n_1n_2|U(R)|n_1n_2\rangle + \omega_{n_1n_2}) c_{n_1n_2}^{i\tilde{g}} + (\langle n_1n_2|J(R)|n_1n_2\rangle) c_{n_1n_2}^{i\tilde{g}} \quad (6.45b)$$

$$+ \sum_{n_1, n_2 \neq n'_1 n'_2} [\langle n'_1 n'_2|U(R)|n_1n_2\rangle] c_{n'_1 n'_2}^{i\tilde{g}} + \sum_{n_1, n_2 \neq n'_1 n'_2} [\langle n'_1 n'_2|J(R)|n_1n_2\rangle] c_{n'_1 n'_2}^{i\tilde{g}}.$$

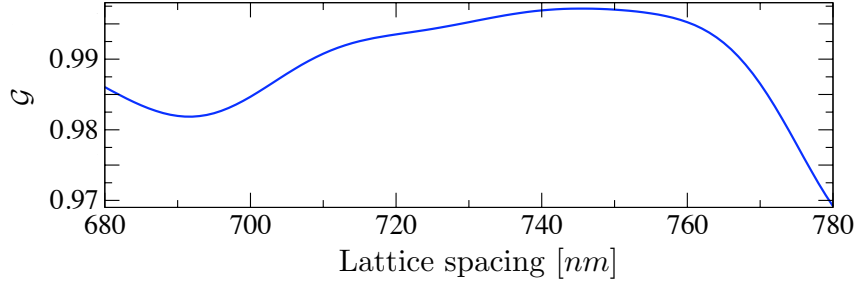


Figure 6.12: The figure shows the plot of \mathcal{G} as defined in Eq.(6.47). Despite the resonances in Fig.(6.9), it verifies that on averaging over the motional states, there is no significant population of the electronic excited states.

Here we used the transformation defined in Eqn.(6.39). In the above set of equations, we observe that higher motional states are coupled via the dynamical parameters $U(R)$, $J(R)$. These are the non-adiabatic couplings due to the spatial variation of the dynamical parameters. There is yet another type of non-adiabatic coupling that arises due to the spatial variation of the dressed electronic wave functions. However we have assumed the Born Oppenheimer (BO) approximation to derive the above sets of dynamical equations where the derivatives of the dressed ground state with respect to the inter-nuclear distance is assumed to be negligible. The validity of the BO approximation for our problem has been addressed in detail in Appendix D.

6.4.1 Population of the excited states

For a given detuning, one observes many resonances in the spectrum (see Fig.6.9(a)). This would imply that there is a significant population of the Rydberg states in the dressed ground states $|\tilde{g}^{(\pm)}\rangle$. But if one averages the dressed ground state over the motional states then one finds that the cross section of exciting a Rydberg atom is indeed very small as shown in Fig.6.12. Evaluating the expectation value of the Rydberg and ground state population with respect to the motional states $|n_1 n_2\rangle$, the following condition,

$$\langle n_1 n_2 | (c_{\tilde{g}}^{g,\pm}(R))^2 | n_1 n_2 \rangle \gg \langle n_1 n_2 | (c_{\tilde{g}}^{e,\pm}(R))^2 | n_1 n_2 \rangle \quad \forall n_1, n_2. \quad (6.46)$$

The above condition is evaluated for different values of detuning and lattice spacing by averaging over the ground motional state using the following quantity,

$$\mathcal{G} = \langle 00 | \frac{(c_{\tilde{g}}^{g,+})^2 + (c_{\tilde{g}}^{g,-})^2}{2} | 00 \rangle. \quad (6.47)$$

\mathcal{G} will be less than one if the laser frequency is resonant with the potential of either symmetry. In the density plot shown in Fig.6.13(a), one sees that $\mathcal{G} \simeq 1$ for small lattice spacings. This is because at small lattice spacings, the potential curves have a steeper slope. A potential curve with a steep slope when averaged over the extent of the ground motional state, then the effect of the resonance is negligible. This aspect is again verified

where one observes a drop in \mathcal{G} (red regions) for flatter potential curves (for example around 760 nm at $\Delta = -57$ GHz). Wherever $\mathcal{G} \simeq 1$, we have $|\tilde{g}^\pm\rangle \simeq |g^\pm\rangle$ (see Eq.(6.34). This is important for the lifetime of the system. By not strongly populating the Rydberg state, we have a larger lifetime since the dressed state is dominated by the electronic ground state.

6.4.2 Lifetime of the system

It is important that the dynamics of the electron is fast enough within the life time of the system to have transport over significant distance. There are two main decay rates play an important role for the life time of the system. One is the decay rate of the intermediate 5s5p state ($\Gamma_{5s5p} = 32$ MHz) which has a life time of 4.97 ns. Assuming that the dressing for the intermediate state as strong as $\frac{\Omega_{5s}^{5p}}{2\Delta_{5s}^{5p}} = 0.005$ (refer to Eq.(6.20)), then the lifetime of the inter-mediate state is enhanced to 200 μ s. The life time of the Rydberg state (ignoring black body radiation) is (from Eq.(4.39)),

$$\tau_\alpha = \sum_{nl} |c_{nl}|^2 \times \frac{(n^*)^3}{2\pi \times 2 \times 10^8}, \quad (6.48)$$

where α is one of the excited molecular potential curves and

$$n^* = \begin{cases} n - \delta_l & \text{for } l=0,1,2, \\ \frac{n^9}{(\frac{3n^2}{2} - \frac{l(l+1)}{2})^2} & \text{for } l>2. \end{cases} \quad (6.49)$$

where δ_l is the quantum defects calculated for strontium. The pre-factor in the denominator was taken from [74]. Eq.(6.48) gives the bare lifetime to be 25 ms for a particular potential curve and with dressing it amounts to 250 ms (since $\langle 00|(c_g^{\epsilon_j^\pm})^2|00\rangle \simeq 0.1$). This implies that the real bottle neck in terms of the life time is the decay rate of the intermediate 5p singlet state. A way around this is to populate the meta-stable triplet 5p state with the help of a sufficiently strong laser (and has been achieved in cases for strontium clock). Our molecular potential curves ignore the spin exchange energy since its quite negligible for the Rydberg states therefore valid for both the singlet and triplet states. Another way around it is to have a single photon Rydberg excitation skipping the intermediate 5p state.

6.4.3 Condition for coherent dynamics

We are not only interested in the electronic ground states but also in the motional ground state. Hence from the general dynamical equations in (6.45), those specific to the motional ground state are

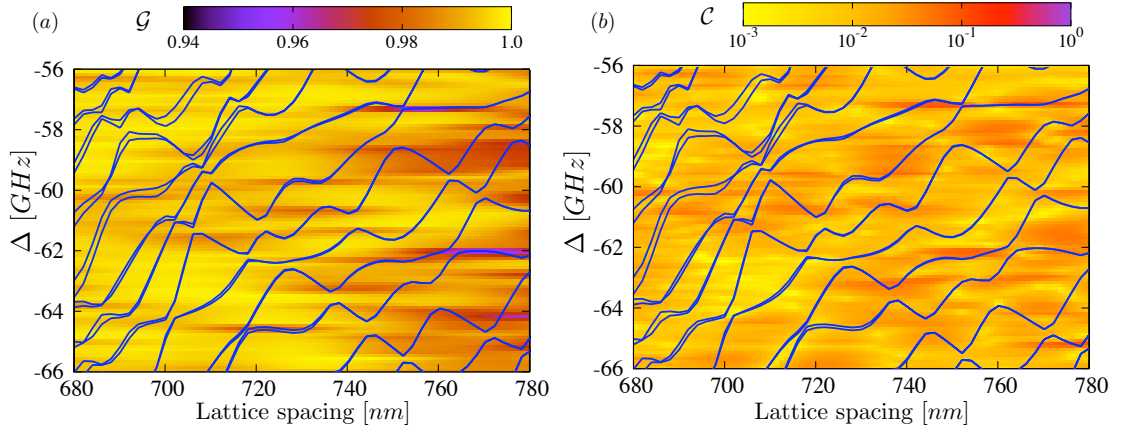


Figure 6.13: The figure shows two density plots to test conditions given in Eq.(6.46) and Eq.(6.51) in the parameter space of detuning (Δ) and lattice spacing. Molecular potential curves are plotted on top. In (a), we plot \mathcal{G} represents the population of the dressed ground state and in (b) we plot the quantity \mathcal{C} defined in Eq.(6.52).

$$i\partial_t c_{00}^{i\tilde{g}} = (\langle 00|U(R)|00\rangle + \omega_{00}) c_{00}^{i\tilde{g}} + \langle 00|J(R)|00\rangle c_{00}^{\tilde{g}i} + \sum_{n'_1 n'_2 \neq 00} \left[\langle 00|U(R)|n'_1 n'_2\rangle c_{n'_1 n'_2}^{i\tilde{g}} + \langle 00|J(R)|n'_1 n'_2\rangle \right] c_{n'_1 n'_2}^{\tilde{g}i}, \quad (6.50a)$$

$$i\partial_t c_{00}^{\tilde{g}i} = (\langle 00|U(R)|00\rangle + \omega_{00}) c_{00}^{\tilde{g}i} + \langle 00|J(R)|00\rangle c_{00}^{i\tilde{g}} + \sum_{n'_1 n'_2 \neq 00} \left[\langle 00|U(R)|n'_1 n'_2\rangle c_{n'_1 n'_2}^{\tilde{g}i} + \langle 00|J(R)|n'_1 n'_2\rangle \right] c_{n'_1 n'_2}^{i\tilde{g}}. \quad (6.50b)$$

The set of dynamical equations can be further simplified by finding a condition of coherence which when satisfied ensures that the higher motional states are never populated and hence can be thrown away from the dynamical equations. For a given ω_L and lattice spacing R , the condition for not populating the first excited motional state (as higher motional states will be further suppressed if the first excited state is not populated) within the same site or the neighbouring site is

$$\langle 01|U(R)|01\rangle - (\langle 00|U(R)|00\rangle + \omega_{tr}) \gg \langle 01|U(R)|00\rangle, \langle 01|J(R)|00\rangle. \quad (6.51)$$

where $\omega_{tr} = \omega_{10} - \omega_{00}$. To verify this condition for the first motional state, we define

$$\mathcal{C} = \frac{\langle 10|U(R)|00\rangle + \langle 10|J(R)|00\rangle}{\langle 10|U(R)|10\rangle - (\langle 00|U(R)|00\rangle + \omega_{tr})}. \quad (6.52)$$

If $\mathcal{C} \ll 1$ for the first excited motional state, then the probability to excite higher motional states is even lower. Thus the density plot in Fig.6.13(b) that coherent dynamics

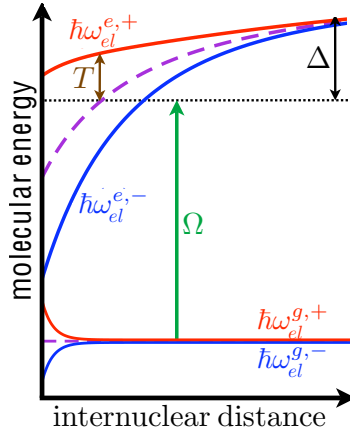


Figure 6.14: A schematic figure showing that though the the ground states are coupled to a large set of Rydberg states, there is always one Rydberg state of either symmetry (gerade or ungerade potential curve) which is closest to the laser frequency and can thus be simplified into a pair of two levels.

can be achieved for a wide range of detuning and lattice spacing. One reason for which the coherence condition is so easily satisfied is because we have chosen a relatively large trapping frequency of 1 MHz. If this condition of coherence holds, then a simple analytical form of a set of closed equations in ground states can be written down.

$$i\partial_t c_{00}^{\tilde{g}}(t) = \langle 00|U(R)|00\rangle c^{\tilde{g}}(t) + \langle 00|J(R)|00\rangle c^{\tilde{g}^i}(t) , \quad (6.53a)$$

$$i\partial_t c_{00}^{\tilde{g}^i}(t) = \langle 00|U(R)|00\rangle c^{\tilde{g}^i}(t) + \langle 00|J(R)|00\rangle c^{\tilde{g}}(t) . \quad (6.53b)$$

So now we have closed form of dynamical equations purely in terms of the ground states. Whenever adiabatic elimination of the Rydberg states is possible, analytical expressions are derived for the dynamical parameters.

6.5 Analytical expressions for dynamical parameters

In this section, we derive analytical expressions for the dynamical parameters $U(R)$ and $J(R)$. Previously we calculated the dynamical parameters in Eq.(6.41) using dressed ground state energies that were obtained numerically and considered contributions from all the Rydberg states. However the dominant contribution comes from the pair that is closest to the laser frequency and one can reduce the basis to a four level system as shown in Fig.6.14. We thus write the full wave function in terms of the relevant electronic states as follows,

$$\Psi = c^{g,+}|g^+\rangle + c^{g,-}|g^-\rangle + c^{e,+}|e^+\rangle + c^{e,-}|e^-\rangle . \quad (6.54)$$

Since there is only one Rydberg state, we have dropped the superscript α .

6.5.1 Constant laser field

Since we are considering only one Rydberg state (or a single pair of (un)gerade Rydberg states), the Hamiltonian for optical coupling given in Eq.(6.25) is reduced to the following

$$\hat{H}_{\text{red}}^{\pm} = \hbar \left[-\Delta^{(\pm)} |e^{(\pm)}\rangle \langle e^{(\pm)}| + \frac{\Omega}{2} (|e^{(\pm)}\rangle \langle g^{(\pm)}| + \text{h.c.}) \right]. \quad (6.55)$$

The advantage of the (anti)symmetric basis is that for a constant Rabi frequency, we get two independent sets of dynamical equations, one for each symmetry group,

$$i\partial_t \begin{pmatrix} c^{g,\pm} \\ c^{e,\pm} \end{pmatrix} = \begin{pmatrix} 0 & \frac{\Omega}{2} \\ \frac{\Omega}{2} & -\Delta^{\pm} \end{pmatrix} \begin{pmatrix} c^{g,\pm} \\ c^{e,\pm} \end{pmatrix}. \quad (6.56)$$

We are required to find analytical expressions for the lowest eigenvalues since those are the ones that correspond to the dressed ground states $|\tilde{g}_{\text{red}}^{(\pm)}\rangle$ and thus satisfying

$$\hat{H}_{\text{red}}^{(\pm)} |\tilde{g}_{\text{red}}^{(\pm)}\rangle = \lambda_{\text{red}}^{\tilde{g},\pm} |\tilde{g}_{\text{red}}^{(\pm)}\rangle. \quad (6.57)$$

I. Four levels

The analytical expressions for the smallest eigenvalues for each of the two level system (one for gerade and the other for ungerade) is given by [4]

$$\lambda_{\text{red}}^{\tilde{g},\pm}(R) = \begin{cases} \frac{-\Delta^{\pm} + \sqrt{(\Delta^{\pm})^2 + \Omega^2}}{2} & \text{if } \Delta^{\pm} > 0, \\ \frac{-\Delta^{\pm} - \sqrt{(\Delta^{\pm})^2 + \Omega^2}}{2} & \text{if } \Delta^{\pm} < 0. \end{cases} \quad (6.58)$$

These eigenvalues are valid for all ranges of detuning, that is near resonance and also away from resonances as schematically shown in Fig.6.15. We call it the effective four level system because both the pair of ground states and the pair of excited states are relevant.

II. Effective three level system

For an arbitrary detuning, its often that the laser frequency is near resonance to only one potential (gerade or ungerade) out of the pair (see Fig.6.15(a)). In such cases, it is possible to reduce the four level system to an effective three level system by adiabatically eliminating one of the excited states (either gerade or ungerade) depending on the detuning of the laser. If the gerade pair is adiabatically eliminated then

$$\lambda_{\text{red}}^{\tilde{g},+}(R) \simeq \frac{\Omega^2}{4\Delta^+} \quad \text{assuming } \Delta^+ \gg \Omega \quad (6.59a)$$

$$\lambda_{\text{red}}^{\tilde{g},-}(R) = \begin{cases} \frac{-\Delta^- + \sqrt{(\Delta^-)^2 + \Omega^2}}{2} & \text{if } \Delta^- > 0, \\ \frac{-\Delta^- - \sqrt{(\Delta^-)^2 + \Omega^2}}{2} & \text{if } \Delta^- < 0. \end{cases} \quad (6.59b)$$

If the un-gerade pair is adiabatically eliminated then

$$\lambda_{\text{red}}^{\tilde{g},-}(R) \simeq \frac{\Omega^2}{4\Delta^-} \quad \text{assuming } \Delta^- \gg \Omega \quad (6.60a)$$

$$\lambda_{\text{red}}^{\tilde{g},+}(R) = \begin{cases} \frac{-\Delta^+ + \sqrt{(\Delta^+)^2 + \Omega^2}}{2} & \text{if } \Delta^+ > 0, \\ \frac{-\Delta^+ - \sqrt{(\Delta^+)^2 + \Omega^2}}{2} & \text{if } \Delta^+ < 0. \end{cases} \quad (6.60b)$$

This approximation is not valid when the laser frequency is equidistant from the gerade and ungerade potential curve which happens when the laser frequency $\omega_L = T/2$ is half-way through the splitting or at large enough distances where both the gerade and ungerade potentials have similar variation over R .

III. Effective two level system

A further simplification is if both the excited states can be adiabatically eliminated giving rise to an effective two level system. In such a case both the eigenvalues are obtained perturbatively, where we assume $\Delta^{(\pm)} \gg \Omega$,

$$\lambda_{\text{red}}^{\tilde{g},\pm}(R) \simeq \frac{\Omega^2}{4\Delta^\pm} \quad \text{assuming } \Delta^{(\pm)} \gg \Omega. \quad (6.61)$$

This approximation is not valid at and near by the resonances. In general, for an arbitrary detuning, the most commonly occurring scenario is where the laser frequency is close to one of the two pair of Rydberg states as shown in Fig.6.15. In such a case, the effective three and four level approximation works well. However for small distances (where the potential curves are steep), the positive and the negative contributions to U and J around the resonance cancel out. Often the Rydberg spectrum of the molecular ion contain potential curves alternate between steeply sloped and flat sloped curves (see the blue potential curves in Fig.6.13) along R . During such a transition, an asymmetric contribution will show in $U(R)$ and $J(R)$ (as seen in Fig.6.9). Major contribution to U and J comes from regions where there is this asymmetry and again for these regions the effective three and four level approximation works well. This explains why the averaged values of dynamical parameters from the effective three and four level approximation fits better with the full numerical calculation in Fig.6.16.

Similar to the equations in (6.53), we get the following dynamical parameters,

$$U(R) = \frac{\lambda_{\text{red}}^{\tilde{g},+}(R) + \lambda_{\text{red}}^{\tilde{g},-}(R)}{2}, \quad J(R) = \frac{\lambda_{\text{red}}^{\tilde{g},+}(R) - \lambda_{\text{red}}^{\tilde{g},-}(R)}{2}. \quad (6.62)$$

In Fig.6.17, we show that the dynamics for two particles for different cases where the coherent condition is satisfied in the density plot Fig.6.13. The dynamical parameters from the analytical results (Eqs.(6.59), (6.60) in (6.62)) and from numerics (Eq.6.41) are used in Eq.(6.50) and compared. The overall timescales of the dynamics obtained from both methods agree.

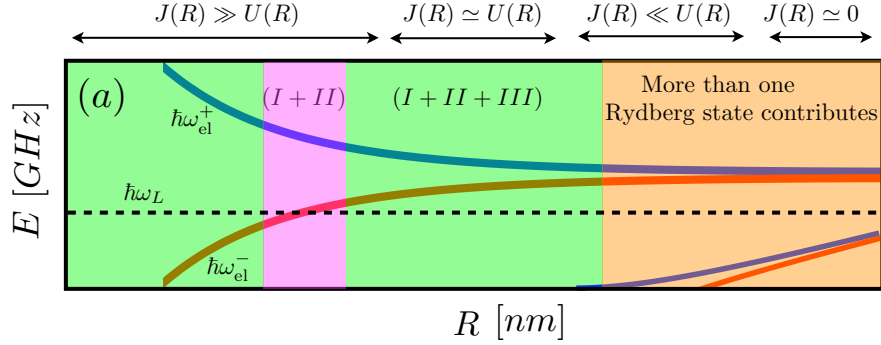


Figure 6.15: The figure shows the regions where the different analytical approximations are valid for a given pair of (un)gerade potential curves. The dashed line corresponds to the laser frequency ω_L . When is the laser is closest to one of the Rydberg state, then the effective four and three level approximation are valid (shown in magenta). Away from the resonance the effective two level approximation is valid (shown in green).

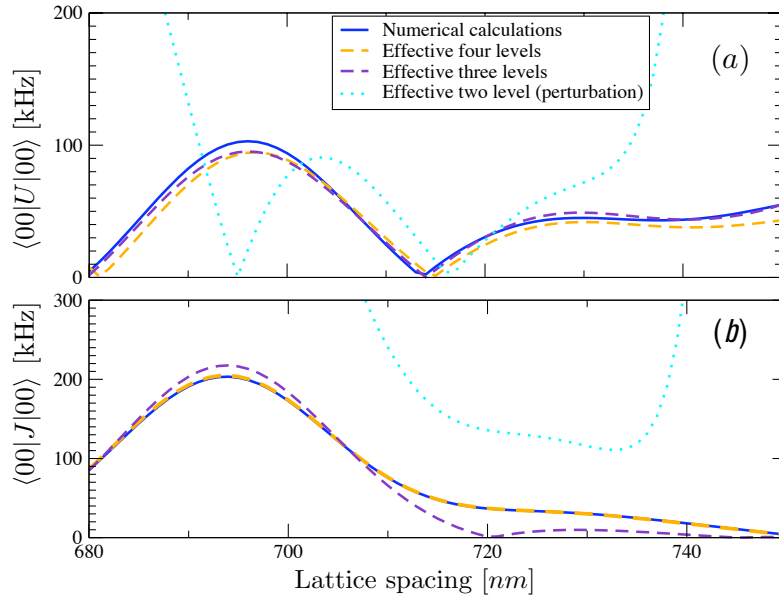


Figure 6.16: Comparison of different analytical approximations for $\Delta = -60.2$ GHz: Average of the dynamical parameters $U(R)$ and $J(R)$ are calculated from Eqs.(6.61) in (6.62)(dotted cyan), Eqs.(6.59), (6.60) in (6.62) (dashed indigo), Eqs.(6.58) in (6.62) (dashed orange) and compare it with the calculation of $U(R)$ and $J(R)$ from the full Hamiltonian having all the Rydberg states using Eqs.(6.41)(dark blue).

6.5.2 Spatially varying laser field

If the intensity of the laser is to be used as a control knob for the transport process of the Rydberg electron, then we need to allow to vary the intensity profile of the laser

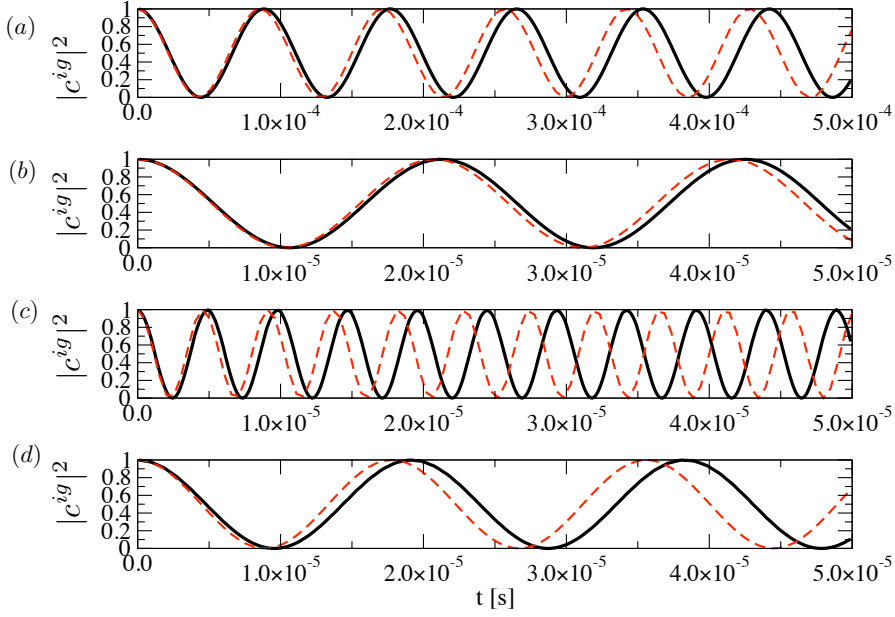


Figure 6.17: The figure shows the converged results of the dynamics obtained numerically from Eq.(6.50) for 8 motional states with U, J taken from Eqs.(6.59), (6.60) in (6.62)(dashed red) and Eq.(6.41) (black) respectively. (a) At $\Delta = -67.3$ GHz, $R = 771$ nm (b) At $\Delta = -60.1$ GHz, $R = 768$ nm (c) At $\Delta = -60.2$ GHz, $R = 690$ nm (d) At $\Delta = -60.2$ GHz, $R = 715$ nm.

with distance. Hence analytical solutions for the spatially varying Rabi frequency will be useful to characterize the dynamics. Generalizing the Hamiltonian in (6.19) for a spatially varying laser field, we get

$$\hat{H}_{\text{vary}} = \hbar \left[-\Delta (|ie\rangle\langle ie| + |ei\rangle\langle ei|) + \left(\frac{\Omega_2}{2} |ie\rangle\langle ig| + \frac{\Omega_1}{2} |ei\rangle\langle gi| + \text{h.c.} \right) + \frac{T}{\hbar} (|ie\rangle\langle ei| + \text{h.c.}) \right]. \quad (6.63)$$

Parameters: $\Delta = -60.2$ GHz, lattice spacing $R = 690$ nm	$\langle 00 U 00\rangle [s^{-1}]$	$\langle 00 J 00\rangle [s^{-1}]$
Full calculations (Eq.(6.41))	$36444.9 \times 2\pi$	$109434 \times 2\pi$
Effective four levels (Eqs.(6.58) in (6.62))	$30786.4 \times 2\pi$	$110341 \times 2\pi$
Effective three levels (Eqs.(6.59), (6.60) in (6.62))	$30788.5 \times 2\pi$	$110344 \times 2\pi$
Effective two level (Eqs.(6.61) in (6.62))	$32898 \times 2\pi$	$188420 \times 2\pi$

Table 6.1: Comparing the averaged values of the onsite energies and hopping rates calculated from different approximation methods.

Solving the time dependent Schrödinger equation using $|\psi\rangle = c^{ig}(t)|ig\rangle + c^{gi}(t)|gi\rangle + c^{ie}(t)|ie\rangle + c^{ei}(t)|ei\rangle$, gives the following dynamical equations

$$i\partial_t c^{ig} = \frac{\Omega_2}{2} c^{ie}, \quad (6.64a)$$

$$i\partial_t c^{gi} = \frac{\Omega_1}{2} c^{ei}, \quad (6.64b)$$

$$i\partial_t c^{ie} = -\Delta c^{ie} + \frac{\Omega_2}{2} c^{ig} + \frac{T}{\hbar} c^{ei}, \quad (6.64c)$$

$$i\partial_t c^{ei} = -\Delta c^{ei} + \frac{\Omega_1}{2} c^{gi} + \frac{T}{\hbar} c^{ie}. \quad (6.64d)$$

The subscripts in the Rabi frequencies $\Omega_{1,2}$ correspond to the case if the laser field intensity varies spatially and hence the atom to the left of the ion will couple to the Rydberg state differently than for the atom to the right of the ion. The variation is determined by changing the intensity profile of the laser along the sites. This is independent from the variation in R due to the change in the dipole moments as defined in Eq.(6.20). Unlike for the constant field case, there is no advantage in defining the above equations in (un)gerade basis as the equations do not de-couple to their corresponding symmetry. Instead we express only the excited states in the (un)gerade basis and we obtain

$$i\partial_t \begin{pmatrix} c^{ig} \\ c^{gi} \\ c^{e,+} \\ c^{e,-} \end{pmatrix} = \begin{pmatrix} 0 & 0 & \frac{\Omega_2}{2\sqrt{2}} & \frac{\Omega_2}{2\sqrt{2}} \\ 0 & 0 & \frac{\Omega_1}{2\sqrt{2}} & -\frac{\Omega_1}{2\sqrt{2}} \\ \frac{\Omega_2}{2\sqrt{2}} & \frac{\Omega_1}{2\sqrt{2}} & -\Delta^+ & 0 \\ \frac{\Omega_2}{2\sqrt{2}} & -\frac{\Omega_1}{2\sqrt{2}} & 0 & -\Delta^- \end{pmatrix} \begin{pmatrix} c^{ig} \\ c^{gi} \\ c^{e,+} \\ c^{e,-} \end{pmatrix}. \quad (6.65)$$

However it is hard to find analytical expressions for the full 4×4 matrix unless certain approximations are made. In Fig.6.16, it was shown that the assumption that at least one of the excited states can be eliminated is valid for most lattice spacings. Let us assume that the gerade Rydberg state can be adiabatically eliminated ($\Delta^+ \gg \frac{\Omega_{1,2}}{2\sqrt{2}}$) giving the resultant matrix Hamiltonian as

$$i\partial_t \begin{pmatrix} c^{ig} \\ c^{gi} \\ c^{e,-} \end{pmatrix} = \begin{pmatrix} \frac{\Omega_2^2}{8\Delta^+} & \frac{\Omega_1\Omega_2}{8\Delta^+} & \frac{\Omega_2}{2\sqrt{2}} \\ \frac{\Omega_2\Omega_1}{8\Delta^+} & \frac{\Omega_1^2}{8\Delta^+} & -\frac{\Omega_1}{2\sqrt{2}} \\ \frac{\Omega_2}{2\sqrt{2}} & -\frac{\Omega_1}{2\sqrt{2}} & -\Delta^- \end{pmatrix} \begin{pmatrix} c^{ig} \\ c^{gi} \\ c^{e,-} \end{pmatrix}. \quad (6.66)$$

Of course it could also be ungerade that is adiabatically eliminated and the analysis would remain the same. Even if one of the excited states is adiabatically eliminated, one requires additional approximations to Eq.(6.66) and reduce it to a form of effective three level system where analytical results can be derived. Since $\Delta^+ \gg \frac{\Omega_{1,2}}{2\sqrt{2}}$, we approximate terms like $\frac{\Omega_{1,2}^2}{8\Delta^+}$ and $\frac{\Omega_2\Omega_1}{8\Delta^+}$ as negligible compared to the other matrix elements. Thus the approximate matrix is

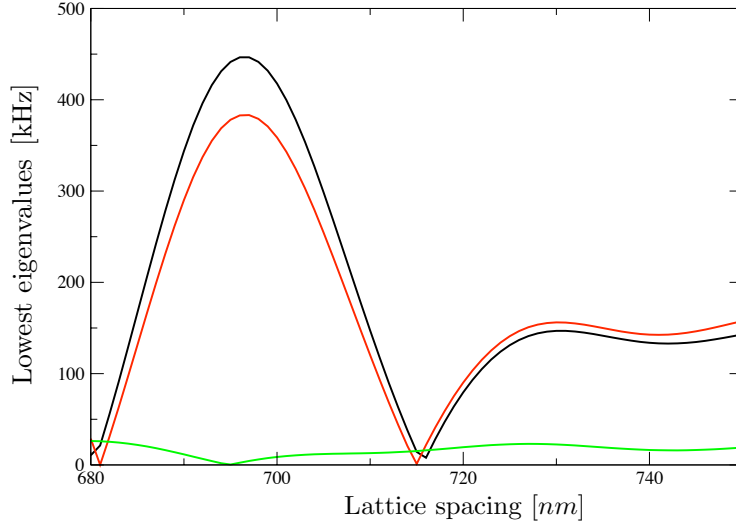


Figure 6.18: The plot compares the two lowest eigenvalues (red and green) obtained numerically by solving Eq.(6.65) and analytical eigenvalue (black) for the approximated matrix given in Eq.(6.67). The parameters are $\Delta = -60.2$ GHz and $\Omega_2 = 2\Omega_1$.

$$i\partial_t \begin{pmatrix} c^{ig} \\ c^{gi} \\ c^{e,-} \end{pmatrix} = \begin{pmatrix} 0 & 0 & \frac{\Omega_2}{2\sqrt{2}} \\ 0 & 0 & -\frac{\Omega_1}{2\sqrt{2}} \\ \frac{\Omega_2}{2\sqrt{2}} & -\frac{\Omega_1}{2\sqrt{2}} & -\Delta^- \end{pmatrix} \begin{pmatrix} c^{ig} \\ c^{gi} \\ c^{e,-} \end{pmatrix}. \quad (6.67)$$

With these approximations, our matrix reduces to a standard lambda level system with analytical solutions used in electromagnetic induced transparency [68]. The solution consists of three dressed states, one of which is considered a *dark state*. It is a state which has no contribution of the excited state. By varying the couplings (Rabi frequencies) adiabatically in a systematic manner, one can achieve a coherent population transfer from one ground state to the other [21]. The dressed ground states for this case will correspond to the dark state of our approximated system and the state with the smallest non-zero eigenvalue. The dark state for our three level system is

$$\lambda_{\text{vary}}^- = 0, \quad (6.68)$$

$$|\tilde{g}_{\text{vary}}^-\rangle = \cos \sigma |ig\rangle - \sin \sigma |gi\rangle. \quad (6.69)$$

The eigenstate with the lowest non-zero eigenvalue depending on the sign of the detuning for our system is

$$\lambda_{\text{vary}}^+ = \begin{cases} \frac{-\Delta^- + \sqrt{(\Delta^-)^2 + (\Omega_1^2 + \Omega_2^2)}}{2} & \text{if } \Delta^- > 0, \\ \frac{-\Delta^- - \sqrt{(\Delta^-)^2 + (\Omega_1^2 + \Omega_2^2)}}{2} & \text{if } \Delta^- < 0, \end{cases} \quad (6.70)$$

$$|\tilde{g}_{\text{vary}}^+\rangle = \sin \sigma \sin \rho |ig\rangle + \cos \rho |e^-\rangle + \cos \sigma \sin \rho |gi\rangle. \quad (6.71)$$

with the following definitions,

$$\begin{aligned}\tan \sigma &= \frac{\Omega_2}{\Omega_1}, \\ \tan 2\rho &= \frac{\sqrt{(\Omega_1^2 + \Omega_2^2)/2}}{\Delta^-}.\end{aligned}$$

Consider the case where $\Omega_1 = \Omega_2$, then we have $\sigma = \pi/4$, giving $|\tilde{g}_{\text{vary}}^-\rangle = |g^-\rangle$ and $|\tilde{g}_{\text{vary}}^+\rangle = \sin \rho |g^+\rangle + \cos \rho |e^-\rangle$ with the same eigenvalues as in the effective three level case for constant field. If we have $\Omega_1 = \Omega_2$ and $\Delta^- \gg \Omega_{1,2}$ then we get $\rho \simeq \pi/2$ giving $|\tilde{g}_{\text{vary}}^-\rangle = |g^-\rangle$ and $|\tilde{g}_{\text{vary}}^+\rangle = |g^+\rangle$, which is the effective two level for a constant field as expected. Assuming that both the conditions (6.46) and (6.51) are satisfied and the averaging over the motional states, we have $\langle 00 | \cos \rho | 00 \rangle \simeq 0$ and $\langle 00 | \sin \rho | 00 \rangle \simeq 1$ as the excited states are not populated (see Fig.6.12). Assuming that the total wave function for the effective three level system for the spatially varying Rabi frequency is given as,

$$|\Psi\rangle = c_{\text{vary}}^-(t) |\tilde{g}_{\text{vary}}^-\rangle + c_{\text{vary}}^+(t) |\tilde{g}_{\text{vary}}^+\rangle. \quad (6.72)$$

then we obtain the same dynamical equations as in (6.53) with,

$$U_{ig}(R) = \lambda_{\text{vary}}^{\tilde{g},+}(R) \cos^2 \sigma + \lambda_{\text{vary}}^{\tilde{g},-}(R) \sin^2 \sigma, \quad (6.73a)$$

$$U_{gi}(R) = \lambda_{\text{vary}}^{\tilde{g},+}(R) \sin^2 \sigma + \lambda_{\text{vary}}^{\tilde{g},-}(R) \cos^2 \sigma, \quad (6.73b)$$

$$J(R) = \frac{\lambda_{\text{vary}}^{\tilde{g},-}(R) - \lambda_{\text{vary}}^{\tilde{g},+}(R)}{2} \sin 2\sigma. \quad (6.73c)$$

where we used Eq.(6.39) and the following transformation of basis,

$$\begin{pmatrix} c_{\text{vary}}^- \\ c_{\text{vary}}^+ \end{pmatrix} = \begin{pmatrix} \cos \sigma & -\sin \sigma \\ \sin \sigma & \cos \sigma \end{pmatrix} \begin{pmatrix} c^{ig} \\ c^{gi} \end{pmatrix}. \quad (6.74)$$

6.6 Ion transport in an optical lattice

In generalizing the two site model to N sites, the essential physics of the charge hopping is the same but now there is the additional van der Waal's interaction between the Rydberg atoms. In the presence of the laser field, all the atoms are dressed to the Rydberg states and the Rydberg-Rydberg interaction will lead to a shift in energy of the dressed states. By choosing the laser frequency ω_L close to a particular Rydberg state $|e\rangle$, we ensure that atoms that are nearest neighbours to the ion are strongly dressed to their Rydberg state while all the others are far away from resonance. The next nearest atoms are located at about little more than a micrometer ($>19000 a_0$) away. This means that the Rydberg states for these atoms correspond to the bare atomic states with the effect of the ion treated perturbatively ($\frac{n^7}{R^4}$) on them. An atom being accidentally excited far away from the ion despite choosing the laser off resonant from any bare atomic state (due

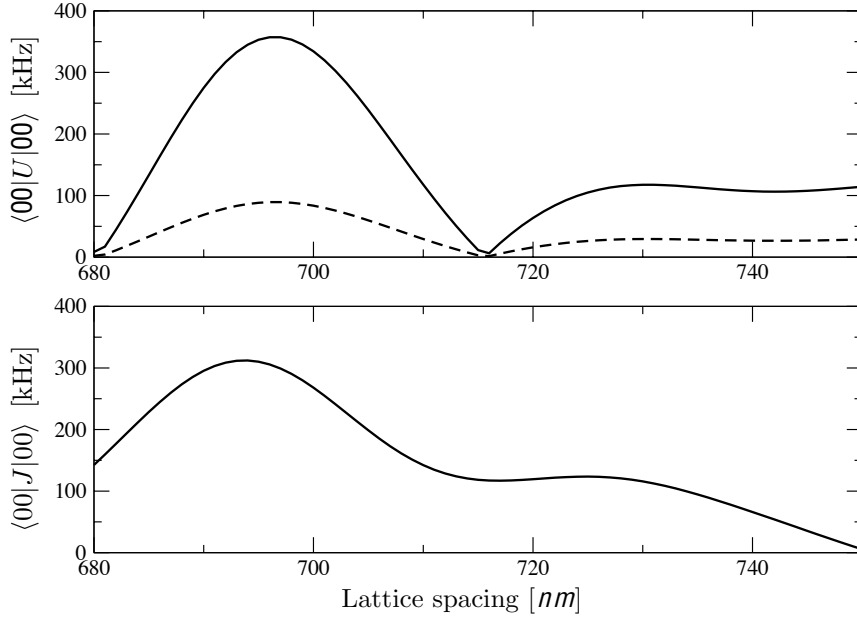


Figure 6.19: The averaged values of the dynamical parameters are plotted for the spatially varying case of $\Omega_2 = 2\Omega_1$ and $\Delta = -60.2$ GHz using Eq.(6.73). The dashed and bold lines in top plot corresponds to averaged values of U_{ig} and U_{gi} respectively.

to Rydberg shifts), will anyways not contribute to the dynamics. Also the probability of two atoms to be excited simultaneously to dressed Rydberg states of energy is given by $|c_g^{e,\pm}|^2 \times |c_g^{e',\pm}|^2 \simeq 10^{-4}$, which is extremely low.

6.6.1 Many-body Hamiltonian

Thus the basis consists of three types, all atoms in the ground state with an ion at site k ($|I^{(k)}\rangle$), a Rydberg atom to the right of the ion ($|R^{(k)}\rangle$) and a Rydberg atom to the left of the ion ($|L^{(k)}\rangle$). Thus the reduced basis set for the many-body Hamiltonian is

$$|I^{(k)}\rangle = |g_1 \dots g_{k-1} i_k g_{k+1} \dots g_N\rangle, \quad (6.75a)$$

$$|R^{(k)}\rangle = |g_1 \dots g_{k-1} i_k e_{k+1} \dots g_N\rangle, \quad (6.75b)$$

$$|L^{(k)}\rangle = |g_1 \dots e_{k-1} i_k g_{k+1} \dots g_N\rangle. \quad (6.75c)$$

The full many-body wave function is given as a linear combination of the three different basis,

$$\Psi = \sum_k \left(C_k^I |I^{(k)}\rangle + C_k^R |R^{(k)}\rangle + C_k^L |L^{(k)}\rangle \right). \quad (6.76)$$

Generalizing the two site Hamiltonian in Eq.(6.63) to the many-body body Hamiltonian for N particles describing the charge(ion) transport within the optical lattice, we have

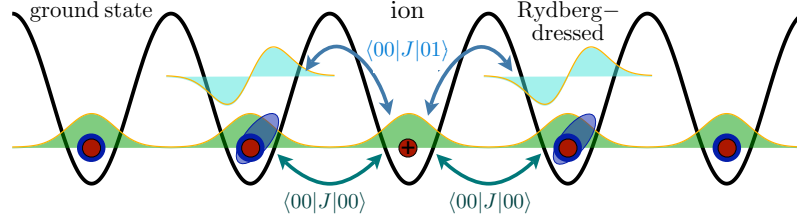


Figure 6.20: Ground state strontium atoms (green) and an ion (red) are trapped in the optical lattice. Due to optical coupling, only the nearest neighbouring strontium atoms are strongly dressed Rydberg dressed (blue) while all the others are off-resonant due to Rydberg interaction. J is the effective coherent hopping between sites while J is the incoherent hopping between sites.

$$\begin{aligned}
\hat{H}_{\text{Many sites}} = & \sum_{k=1}^{N-1} \left[-\hbar\Delta |R^{(k)}\rangle\langle R^{(k)}| + \frac{\hbar\Omega_{k+1}}{2} (|R^{(k)}\rangle\langle I^{(k)}| + \text{h.c.}) \right] \\
& + \sum_{k=2}^N \left[-\hbar\Delta |L^{(k)}\rangle\langle L^{(k)}| + \frac{\hbar\Omega_{k-1}}{2} (|L^{(k)}\rangle\langle I^{(k)}| + \text{h.c.}) \right] \\
& + \sum_{k=1}^{N-1} \frac{T}{2} [|R^{(k)}\rangle\langle L^{(k+1)}| + \text{h.c.}] .
\end{aligned} \tag{6.77}$$

T is the hopping between the Rydberg states of neighbouring sites. It is to be noted that the states $|R^{(N)}\rangle$ and $|L^{(1)}\rangle$ does not exist for a finite size optical lattice. The set of dynamical equations determining the motion of the ion placed at site k are

$$i\partial_t C_k^I = \frac{\Omega_{k-1}}{2} C_k^L + \frac{\Omega_{k+1}}{2} C_k^R , \tag{6.78a}$$

$$i\partial_t C_k^R = -\Delta C_k^R + \frac{\Omega_{k+1}}{2} C_k^I + \frac{T}{\hbar} C_{k+1}^L , \tag{6.78b}$$

$$i\partial_t C_k^L = -\Delta C_k^L + \frac{\Omega_{k-1}}{2} C_k^I + \frac{T}{\hbar} C_{k-1}^R . \tag{6.78c}$$

Defining a (un)grade amplitudes for the many-body excited states

$$C_k^{E,\pm} = \frac{1}{\sqrt{2}} (C_k^R \pm C_{k+1}^L) , \tag{6.79}$$

with which we obtain,

$$i\partial_t C_k^{E,+} = -\Delta^+ C_k^{E,+} + \frac{\Omega_{k+1}}{2\sqrt{2}} C_k^I + \frac{\Omega_k}{2\sqrt{2}} C_{k+1}^I , \tag{6.80a}$$

$$i\partial_t C_k^{E,-} = -\Delta^- C_k^{E,-} + \frac{\Omega_{k+1}}{2\sqrt{2}} C_k^I - \frac{\Omega_k}{2\sqrt{2}} C_{k+1}^I . \tag{6.80b}$$

where $\Delta^\pm = \Delta \mp \frac{T}{\hbar}$. For the more non-trivial case of spatially varying laser field over N sites is derived in Appendix E. Here we do the simpler case where we assume that both the excited states can be adiabatically eliminated $\Delta^\pm \gg \Omega$ and use the following basis transformation to get the left/right basis for the excited states,

$$C_k^R = \frac{1}{\sqrt{2}} \left(C_k^{E,+} + C_k^{E,-} \right), \quad (6.81)$$

$$C_k^L = \frac{1}{\sqrt{2}} \left(C_{k-1}^{E,+} - C_{k-1}^{E,-} \right). \quad (6.82)$$

and averaging over the motional states for lattice spacings and detunings where the conditions (6.46) and (6.51) are satisfied, we obtain the dynamical equations for the ground states,

$$i\partial_t C_k^I = \langle 00 | (U_{k-1} + U_{k+1}) | 00 \rangle C_k^I + \langle 00 | J_{k,k-1} | 00 \rangle C_{k-1}^I + \langle 00 | J_{k,k+1} | 00 \rangle C_{k+1}^I. \quad (6.83)$$

and the dynamical parameters are

$$U_k(R) = \left(\frac{\Omega_k^2}{8\Delta^+} + \frac{\Omega_k^2}{8\Delta^-} \right), \quad J_{k,k+1}(R) = \left(\frac{\Omega_k \Omega_{k+1}}{8\Delta^+} - \frac{\Omega_k \Omega_{k+1}}{8\Delta^-} \right). \quad (6.84)$$

One can re-write the Eq.(6.83) in terms of h_k^\dagger/h_k which represent creation and annihilation operators for the ion at site k . Thus we have,

$$\hat{H} = \sum_k U_k h_k^\dagger h_k + \sum_k J_{k,k+1} \left(h_{k+1}^\dagger h_k + \text{h.c.} \right). \quad (6.85)$$

This is a more compact form of the transport equation for the ion with similarities to the effective Hubbard model.

6.6.2 Numerical simulation

Parameters	\mathcal{C}	$\frac{\langle 00 J 00 \rangle}{\langle 00 U 00 \rangle}$	$\langle 00 J 00 \rangle [s^{-1}]$
$\Delta = -57.3$ GHz, lattice spacing 771 nm	0.23	0.84	$5843 \times 2\pi$
$\Delta = -60.1$ GHz, lattice spacing 768 nm	10^{-2}	132	$24108 \times 2\pi$
$\Delta = -60.2$ GHz, lattice spacing 690 nm	10^{-1}	3	$109434 \times 2\pi$
$\Delta = -60.2$ GHz, lattice spacing 715 nm	2×10^{-2}	7.35	$28105 \times 2\pi$

Table 6.2: Listed are the averaged values of the dynamical parameters along with their coherence conditions. It appears for $\Delta = -60.2$ GHz, lattice spacing $R = 690, 715$ nm are most suitable because it has high hopping rate along and well satisfy the coherence condition.

In [2] it was shown that quantum spin networks described by Hamiltonian with a harmonic spectrum (such as given below) follows perfect state transport (without loss).

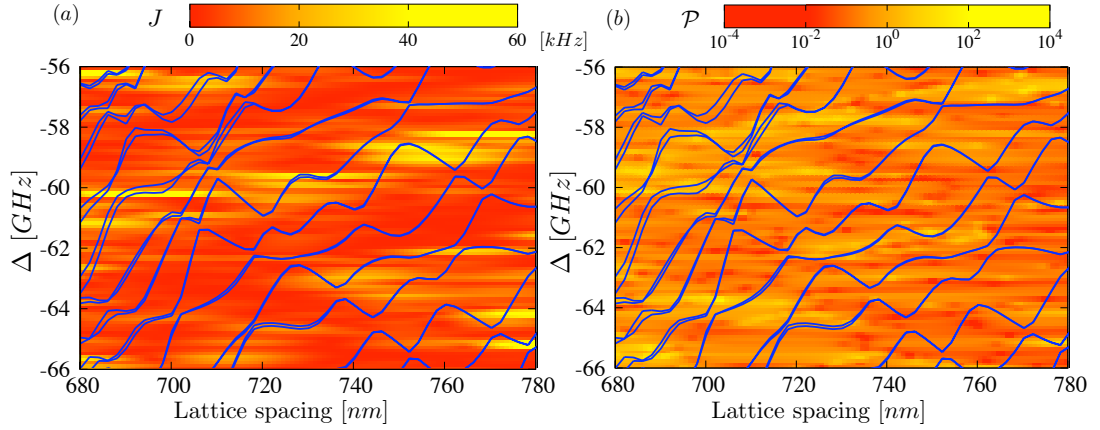


Figure 6.21: Left panel corresponds to the density plot of the tunneling $\langle 00|J|00\rangle$ while on the right panel its the density plot of the ratio $\mathcal{P} = \frac{\langle 00|J|00\rangle}{\langle 00|U|00\rangle}$ as a function of the detuning and lattice spacing.

$$H_{spin-network}(R) \simeq \hbar \begin{pmatrix} 0 & A_1 & 0 & \dots & 0 \\ A_1 & 0 & A_2 & \dots & 0 \\ 0 & A_2 & 0 & \dots & 0 \\ \vdots & \vdots & \vdots & \ddots & A_{N-1} \\ 0 & 0 & 0 & A_{N-1} & 0 \end{pmatrix}. \quad (6.86)$$

where the coupling term is given as $A_k = \sqrt{(N-k)k}$ and N is the number of spins in a 1D chain. Inspired from this model, we implement a similar perfect transport process in our 1D model for the ion by enforcing the following criteria on our Rabi frequency,

$$\Omega_k = \sqrt{(N-k-1)(k+1)} \Omega. \quad (6.87)$$

Thus for k to take values from 0 to 18, we have N=19. It has to be noted that our diagonal elements are non-zero and is also dependent on the intensity field. Therefore we not going to have perfect quantum transport with 100 % fidelity like in the spin chain [2]. Nevertheless if we can look for regions where $\langle 00|J|00\rangle \gg \langle 00|U|00\rangle$ (see Fig.6.21), then hopefully the transport process shows minimal dephasing. For a given detuning and distance, one can calculate the variation of U_k and $J_{k,k+1}$ at every site. We simulate the transport of the charge over a chain of 19 atoms by solving the discretized time dependent Schrödinger equation in (6.83) for a detuning as -60.2 GHz at lattice spacing 715 nm as shown in Fig.6.23. In Fig.6.23(a), we find that with time, the many-body wave function $|I^{(k)}\rangle$ is spreading coherently over few micrometers creating a Schrödinger kitten like state. While Fig.6.23(b), we achieve almost perfect quantum transport but the non-zero onsite energies U is responsible for the inertia in the transport process due to which the we see diffusion at later times.

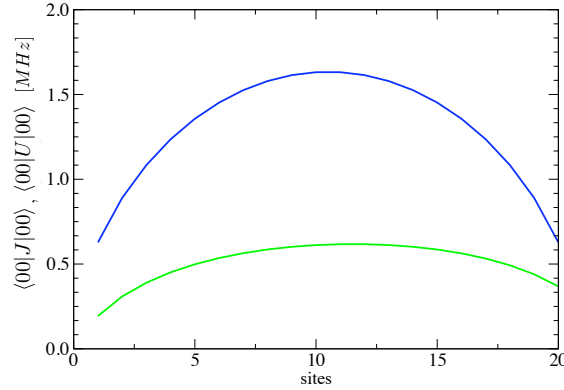


Figure 6.22: Both the figures are the plot the averaged values of U (green) and J (blue) with Rabi frequency from Eq.(6.87) into Eq.(6.84) at $\Delta = -60.2$ GHz, lattice spacing 715 nm.

6.7 Summary

We study ion transport in a gas of atoms by dressing the ion with neighbouring Rydberg atoms. Owing to the large size of the Rydberg electron, it tunnels across the ionic potential barrier and is captured by the ion. The physics of the hopping process is understood by studying a simpler model of ion-atom pair. We calculate the molecular spectrum of the Sr_2^+ Rydberg molecular ion in the (un)gerade basis. The potential curves come with a rich structure and contain the information of the polarizability and hopping rate of the Rydberg electron. The optical coupling of the electronic ground states to Rydberg molecular ion states is assumed to be adiabatic leading to dressed ground states. The dynamical equations are expressed in terms of the dressed ground states and determined by two parameters that are defined by the dressed ground state energies. Numerical results confirm that the Rydberg state closest to the laser frequency dominates the dynamics. This fact is exploited to derive analytical results for the dynamical parameters using different approximations. For spatially varying laser field, the derivation is more involved but with additional approximations, we reduce our Hamiltonian to a solvable lambda system similar to an EIT case. The dynamical parameters are spatially dependent and hence any motion of the ion or atom will result in variation of these parameters. In order to achieve coherent dynamics, we trap the particles in a double well. Conditions are derived for maintaining not only dressed ground states but also motional ground states during dynamical process. Density plots for these conditions over the parameter space of detuning and lattice spacing show that the possibility to have coherent charge transport is quite general. The model is then generalized to many sites and a spatially varying laser field is used to implement directionality in the transport process. A numerical simulation performed shows that the transport of the ion over 18 sites using the calculated dynamical parameters.

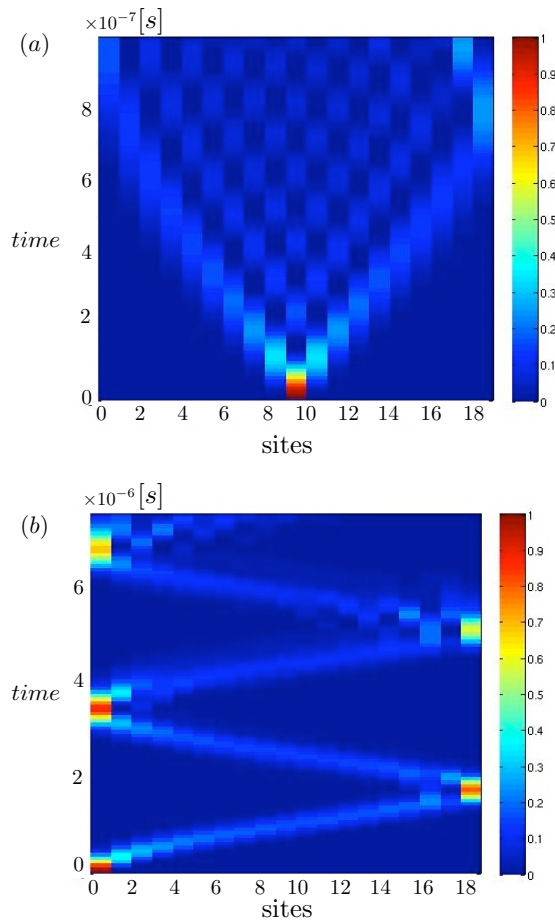


Figure 6.23: The figures show the dynamics of the ion by solving the discretized Eq.(6.83) for a lattice of 19 sites with lattice spacing 715 nm and detuning -60.2 GHz for a spatially varying field using dynamical parameters from Fig.6.22 (a) The ion initially located at site 9 and propagates in both directions. (b) The ion initially located at site 1 propagates coherently in one direction and then on reflection at the edge, propagates backwards and re-emerges at site 1.

Conclusion and Outlook

The field of ultra-cold atoms and Rydberg physics is mainly driven using alkali atoms. The reason for this is that experiments involving alkali atoms are easily turned into gases and their spectral transitions correspond to wavelengths that are accessible by the available lasers [125, 3, 129]. Recently there is a growing interest in alkaline-earth metals (Ca, Mg, Sr, Ba, Ra) for laser cooling [31, 15, 130] and realization of quantum devices [79, 80, 45]. The presence of two valence electrons in alkaline-earth atoms provide that additional degree of freedom for manipulation which is absent in alkali atoms. Although much of the interest so far has been in *alkaline-earth ground state* atoms, the use of *alkaline-earth Rydberg* atoms in ultra-cold systems are yet to be explored. With this motivation, the research presented in this thesis studies alkaline-earth Rydberg atoms in optical lattices and explores the possible applications to many-body physics.

In chapter 3 we lay down the ground work for the study of alkaline-earth Rydberg atoms by calculating the singly excited Rydberg states specifically for strontium (Sr) using an effective mean field theory approach. Using the active single electron approximation described in section 2.1, we reduced the problem of solving the multi-electron atom to an effective two electron atom. Strontium Rydberg energies obtained agreed very well with known experimental data as shown in section 3.3.1. Interaction between strontium Rydberg atoms were calculated using the energies and wave functions obtained in section 3.3.1 for ns singlet states and were found to be attractive (see section 3.3.2).

The Rydberg atoms are often sources of strong interactions to simulate quantum systems [206, 107, 124, 119, 156]. However strongly interacting atoms have significant motion which lead to de-coherence effects and is unfavourable for most many-body applications [26]. One approach is to trap the atoms in an optical lattice [86, 98, 122]. It is a challenge to trap a Rydberg atom along with a ground state atom in the same optical lattice while coupling the two internal states. In this context, in chapter 4 we show that alkaline-earth atoms offer a promising solution which was otherwise not possible with alkali atoms. In section 4.2, we calculate the core polarizability along with the Rydberg polarizability for a Rydberg atom and compare it with that of the ground state atom. Wavelengths (referred as magic wavelengths) of the trapping laser were identified that ensures identical trapping potential for both the internal states (ground and Rydberg). A broad range of experimentally relevant magic wavelengths were found around 323 nm and at 418 nm (see section 4.3). Both of these correspond to a blue detuned trapping laser which has the added benefit that it minimizes any intensity dependent decay process such as autoionization and photoionization. In order to balance

the strong Rydberg-Rydberg interactions among atoms in the optical lattice, one needs to have large lattice spacings of a few μm and rather large trapping frequencies of a few 100 kHz. This requires large peak intensities of $2 \times 10^5 \text{W}/\text{cm}^2$ at the maxima of the periodic intensity pattern. In this regard, the suppression of intensity dependent decay rates is an essential advantage. The over-all lifetime of the system was shown in section 4.4 to follow the natural lifetime of the Rydberg state for reasonable range of trapping laser intensities.

Using the magic lattice for strontium Rydberg atoms, we explored two specific examples of many-body physics.

Multiparticle entanglement

In chapter 5, we present a scheme for the production of multi-particle GHZ (Greenberger-Horne-Zeilinger) state. Generation and manipulation of entangled states is an active area of research because of its fundamental importance in quantum mechanics and its potential for quantum information applications [20, 96]. One of the challenges in this area is to have a scalable multi-particle entanglement. In general to have a large scale entanglement, one requires strong interactions between the particles. This was provided by the optical excitation of strontium atoms confined in a magic lattice to strongly interacting atomic states. This yields an effective Ising model with controllable parameters. The attractive Rydberg interactions in the system features a quantum phase transition between para- and ferromagnetic states. The effects of the spatial variation of the Rabi profile and the strong interactions on the motional states are described in section 5.2 with the conclusion that for large enough lattice spacing (few μm) and strong confinements (trapping frequencies with few hundred kHz), the atoms maintain their motional ground state. Lattice spacings larger than half the magic wavelength can be obtained for our optical lattice using a technique of tilted laser beams described in section 4.1.1. Previous works with ions/photons have had some success [169, 57, 216] with the current record of 14 particles being entangled experimentally [144]. Using suitable field ramps across the transition, we created a GHZ state for 15 atoms with a 0.997 fidelity for a pulse width of 1.2 μs .

Coherent ion transport in a lattice

In [41], the following question was asked, "What happens to a mixture of positive ions and neutral atoms at ultra low temperatures?". In the same article, charge hopping was considered by placing a Na^+ in a gas of Na atoms at μK temperature. A dilute gas was considered at very low temperatures such that the de Broglie wavelength of the electron was large enough to have a certain amount of overlap with the neighbouring ion. It is not obvious that this hopping would be coherent. Over time, as the hopping process continues, the motion of the atoms will heat the gas and lower the hopping probability. The effect of the motion of particles were not considered in [41] and the over all cross-section of the hopping process was quite low.

In [120], it was suggested to use a Rydberg state for enhancing charge transport. The

model consisted of two ions confined in a Penning trap with one common electron to share, similar to a H_2^+ model. With the help of an excitation laser, the electron would be excited to a Rydberg state and the de-localized wave function of the Rydberg electron would easily cross the ionic potential barrier onto the neighbouring ion. This system indeed had higher hopping rates compared to [41] but the details of the Rydberg states were not studied. An ion placed in the same trap to a Rydberg atom will cause significant mixing of the levels of the bare atomic states. Although limited to two particles, it is not clear if the system allows multiple charge exchange or in other words, if the lifetime of the system is significantly larger than the dynamical timescale so that charge exchange occurs more than once.

In chapter 6, we look into a particular charge transport process by placing an ion in a gas of ground state strontium atoms, both of which are confined in an optical lattice. The atoms are weakly dressed to Rydberg states and not excited as in the case of [120]. We show that by weakly mixing the Rydberg states to the ground state atoms, we already obtain very high hopping rates along with extended lifetime. The large lifetime will permit multiple hopping over many atoms like an electric current passing through an ensemble of atoms at low temperature as originally envisaged in [41]. The advantage of trapping the ion and the Rydberg dressed atoms in an optical lattice was to control the motion of the atoms in a systematic manner. In section 6.4, we determined analytical conditions for not populating the excited electronic states and excited motional states which depends on the trapping frequency and the particular Rydberg state to which it is coupled. Thus it is important to know the details of the excited states for a Rydberg molecular ion because accordingly a certain Rydberg state can be chosen which has higher hopping rate and satisfies the coherence condition. Sr_2^+ molecular ion Rydberg states were calculated in section 6.2. At small distances (little more than half a μm), the perturbative treatment fails and exact diagonalization was used to obtain the molecular ion potential curves. The Rydberg molecular potential curves have a ‘spaghetti like’ spectrum as a result of the multiple avoided crossings as shown in section 6.2.2. The corresponding wave functions reflect the fact that all the different bare Rydberg states (with different l) are strongly mixed. Numerical studies showed that not all the Rydberg states play an equal role in the charge transfer process but only the pair closest to the laser frequency. This simplified the study to a great extent allowing us to derive analytical expressions for the dynamical parameters given in section 6.5. For our trapping frequency $\omega_{\text{trap}} = 1$ MHz, we showed that the coherence condition is easily satisfied for a wide range of detunings and lattice spacings (650-750 nm). However, we can’t have too large lattice spacing since the hopping rate drops to low values. But for our chosen, value of $\Delta = -60.2$ GHz and lattice spacing of 715 nm, the hopping rate was sufficient to travel over a chain of 19 atoms well within the life time. In conclusion, coherent and controlled charge transport is achievable with the excitation laser and the trapping laser as our controlling knobs.

Future perspectives

The scenario of an ion immersed in an optical lattice at otherwise unity atomic filling with laser excitation to Rydberg states permits electron tunneling over large distances of several 100 nm to a nearby ion. The described scheme opens up several possibilities for simulation of quantum phenomena.

Simulation of Hubbard-Holstein model

The one dimensional Holstein model involves only the electron-phonon coupling and can be solved analytically [91]. The two dimensional Holstein model has been studied using quantum Monte Carlo (QMC) and density matrix renormalization group (DMRG) simulations based on Migdal-Eliashberg theory [135]. By including the repulsive Coulomb interaction of the electrons, the Holstein model is generalized to an effective Hubbard-Holstein model for which exact results are not available. QMC and simulations were done for small systems [177]. The study of the phase diagram for the Hubbard-Holstein model is crucial for understanding strongly correlated phenomena such as charge density wave and superconductivity in certain compounds [90]. It essentially consists of four terms in the Hamiltonian, the nearest neighbour hopping of the electron determined by coupling t , the on-site energy determined by the coupling U , the kinetic energy of the Einstein phonons with frequency ω_0 and the electron-phonon coupling term determined by g .

In [127], the ground state phase diagram of the one dimensional Hubbard-Holstein model was studied using a non-perturbative approach. However, the theory used was valid for very limited regions. Firstly, it assumed that the onsite energy was much larger than the hopping term, so that the model could be mapped to an effective Hubbard model. Also it was assumed that the phononic energy has to be much larger than the hopping term and thus the phase diagram was obtained in the limit where $t/\omega_0 \ll 1$ or so called the non-adiabatic limit. Apparently most of the literature obtained phase diagrams mainly within this regime [193, 37, 65].

Our model in section 6.4, particularly the Eq.(6.45), can be used to simulate the Hubbard-Holstein model for a more general parameter regime than [127]. The J and U in Eq.(6.45) are respectively the hopping and onsite coupling terms for the electron. The trapping frequency ω_{tr} corresponds to the phononic energy and the non-adiabatic coupling term which couples a particular state $|i\tilde{g}\rangle|n_1n_2\rangle$ to another another motional state $|i\tilde{g}\rangle|n'_1n'_2\rangle$ represents the electron-phonon coupling term. For the charge transport process, we wanted to suppress the higher motional states. However by playing with the trapping frequency, we can selectively allow the population of certain motional states, thereby controlling the electron-phonon coupling.

Study of many-body quantum pheonomena: Schrödinger kitten state, quantum walk and spin squeezing

While simulating the transport of the ion over 19 sites in section 6.6.2, we showed that the many-body wave function coherently de-localizes over distances of several tens of

micrometers creating an ionic Schrödinger kitten. The system can also be used to generate a quantum walk [1]. In a quantum random walk, due to the quantum interference of different paths, the spatial distribution goes as $\langle \hat{x}^2 \rangle \propto N^2$ as compared to the Binomial distribution of a classical walk $\langle \hat{x}^2 \rangle \propto N$, where N is the number of steps. To perform any quantum walk, we require two unitary operations. One is a flip operator that flips the state of the system and the other is the shift operator that translates the states. The hopping parameter takes part (or whole) of the ionic wave function and transports it across the sites which is similar to the shift operator. On reaching the edges, the ion starts to travel backwards. This is the flip operator where the right moving wave function becomes left moving and vice-versa. Thus after many such operations, the coherent many-body wave function will interfere multiple times to give the required distribution. An important feature of a quantum walk is its reversibility. Of course in our model, perfect reversibility would not be possible if the onsite energy U is large. But one may optimize the transport process by trying to obtain a perfect harmonic spectrum using a suitable laser profile for the spatially dependent U and J . Quantum walks have importance in finding quantum search algorithms that are faster than their classical counterpart [34]. Quantum walks have been realized previously using ions [213, 179], where they also showed the significance of the motional states entangling with the internal states leading to decoherence in the walk.

One can similarly use a lattice clock and dressed Rydberg states to achieve spin squeezing. An optical lattice clock consists of trapped strontium atoms using a laser with frequency corresponding to the intercombination transition from the singlet ground state 1S_0 to a meta-stable triplet state 3P_0 . Using another laser, the intermediate meta-stable state is weakly coupled to a Rydberg state which introduces the required long range interaction for multi-particle squeezing. Using the long range interacting Ising model described in section 5.6, the transverse and longitudinal fields can be manipulated in a systematic manner similar to a spin echo type protocol as is explored in [76].

There are experimental groups working with strontium atoms such as Thomas Killian's group at Rice university and particularly our experimental collaborators in Matthew Jones's group in Durham university, where they are actively pursuing to trap strontium Rydberg atoms in an optical lattice in the coming future.

Properties of spherical harmonics

As mentioned in chapter 2, the angular part of the Rydberg wave function is given by generalized spherical harmonics. For a specific orbital angular momentum l and magnetic number m , it is given as

$$\mathcal{Y}_{lm} = (-1)^m \sqrt{\frac{(2l+1)(l-m)!}{2(l+m)!}} \mathcal{P}_l^m(\cos \vartheta) e^{im\varphi}. \quad (\text{A.1})$$

where \mathcal{P}_l^m are the associated Legendre polynomials [32]. To derive expressions for the mean field potentials and energy correction, we will use some of the properties of spherical harmonics. Thus we briefly outline the properties that will be need for our derivations.

1. $\mathcal{Y}_{l,m}^*(\cos \vartheta, \varphi) = (-1)^{-m} \mathcal{Y}_{l,-m}(\cos \vartheta, \varphi)$.
2. $\frac{1}{|\mathbf{r}_{12}|} = \sum_{l'=0}^{\infty} \sum_{m'=-l'}^{l'} \frac{4\pi}{2l'+1} \frac{r_{<}^{l'}}{r_{>}^{l'+1}} \mathcal{Y}_{l',m'}^*(\cos \vartheta_1, \varphi_1) \mathcal{Y}_{l',m'}(\cos \vartheta_2, \varphi_2)$.
3. $\int \mathcal{Y}_{l_1,m_1}(\vartheta, \varphi) \mathcal{Y}_{l_2,m_2}(\cos \vartheta, \varphi) \mathcal{Y}_{l_3,m_3}(\cos \vartheta, \varphi) d\Omega$
 $= (-1)^{m_3} \sqrt{\frac{(2l_1+1)(1l_2+1)}{(2l_3+1)4\pi}} \langle l_1 l_2 0 0 | l_3 0 \rangle \langle l_1 l_2 m_1 m_2 | l_3 -m_3 \rangle$.

The big angular brackets are the Clebsch-Gordan coefficients [32]. These coefficients determine the contribution from each angular momentum state, when two states $|j_1 m_1\rangle$ and $|j_2 m_2\rangle$ are added to give a resultant state $|j_1, j_2; j m\rangle$ in the following manner,

$$|j_1, j_2; j m\rangle = \sum_{m_1, m_2} \langle j_1 j_2 m_1 m_2 | j_3 m_3 \rangle |j_1 m_1\rangle |j_2 m_2\rangle . \quad (\text{A.2})$$

The Clebsch-Gordan coefficients are non zero for $|j_1 - j_2| \leq j \leq j_1 + j_2$ and $m = m_1 + m_2$. One can analytically solve the angular part for the mean field potentials and energy corrections for the two electron Rydberg atom in order to obtain simplified expressions.

van der Waals coefficient for ns states

As discussed in section 2.2.5 of chapter 2, the van der Waals interaction between two Rydberg atoms, each in state $|ns\rangle$ is given by

$$V_{vdW} = \sum_{n'l'm', n''l''m''} \frac{|\langle n'l'm', n''l''m'' | V_{int}(\mathbf{R}) | ns, ns \rangle|^2}{\Delta E}, \quad (\text{B.1})$$

where $\Delta E = 2E_{ns} - (E_{n'l'm'} + E_{n''l''m''})$ and $V_{int}(\mathbf{R})$ is approximated using multipole expansion (refer to Eq.(2.16)) and is given as

$$V_{int}(\mathbf{R}) = \frac{1}{(4\pi\epsilon_0)} \left[\frac{\boldsymbol{\mu}_1 \cdot \boldsymbol{\mu}_2}{R^3} - \frac{3(\mathbf{R} \cdot \boldsymbol{\mu}_1)(\mathbf{R} \cdot \boldsymbol{\mu}_2)}{R^5} \right]. \quad (\text{B.2})$$

In order to obtain an expression for C_6 for ns states one evaluates $\langle n'p_0, n''p_0 | V_{int}(\mathbf{R}) | ns_0, ns \rangle$ for nearest dipole allowed Rydberg states ($n', n'' = n \pm 1$) including all the m_l states. Defining the radial components as $r_{i=1,2} = (x_i, y_i, z_i)$, $R = (R_x, R_y, R_z)$ and expressing the atomic state in terms of spherical polar co-ordinates we have

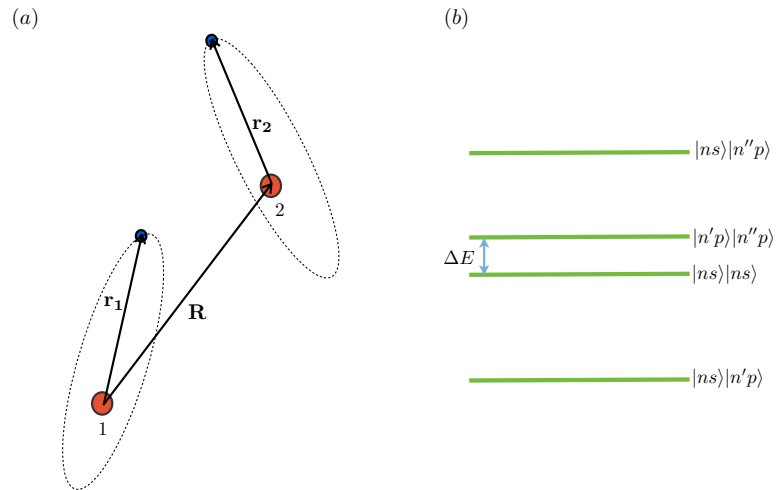


Figure B.1: (a) Schematic diagram of two neighbouring Rydberg atoms (b) Pair of Rydberg atoms interacts and couples to energetically close Rydberg states.

$$|ns0\rangle = \mathcal{Y}_{00}(\vartheta, \varphi) \mathcal{R}_{ns}(r_i) = \frac{\mathcal{R}_{ns}(r_i)}{\sqrt{4\pi}}, \quad (\text{B.3})$$

$$|np1\rangle = \mathcal{Y}_{11}(\vartheta, \varphi) \mathcal{R}_{np}(r_i) = -\exp(i\varphi) \sin \vartheta \sqrt{\frac{3}{8\pi}} \mathcal{R}_{np}(r_i), \quad (\text{B.4})$$

$$|np0\rangle = \mathcal{Y}_{10}(\vartheta, \varphi) \mathcal{R}_{np}(r_i) = \cos \vartheta \sqrt{\frac{3}{4\pi}} \mathcal{R}_{np}(r_i), \quad (\text{B.5})$$

$$|np-1\rangle = \mathcal{Y}_{1-1}(\vartheta, \varphi) \mathcal{R}_{np}(r_i) = \exp(-i\varphi) \sin \vartheta \sqrt{\frac{3}{8\pi}} \mathcal{R}_{np}(r_i). \quad (\text{B.6})$$

We use a short-hand notation for the different m states as $|l_{0,\pm}\rangle \equiv |lm_l = 0, \pm 1\rangle$. Thus the non-zero transition dipole moment for a single atom with an initial state $|ns\rangle$ can be shown to be

$$\langle ns|z_i|n'p_0\rangle = \frac{\mu_{ns,n'p}}{\sqrt{3}}, \quad (\text{B.7})$$

$$\langle ns|x_i|n'p_+\rangle = -\langle ns|x_i|n'p_-\rangle = -\frac{\mu_{ns,n'p}}{\sqrt{6}}, \quad (\text{B.8})$$

$$\langle ns|y_i|n'p_+\rangle = \langle ns|y_i|n'p_-\rangle = -i\frac{\mu_{ns,n'p}}{\sqrt{6}}. \quad (\text{B.9})$$

Using the above equations into Eq.(2.21), one obtains the following van-der Waals terms in the two atom basis,

$$\langle n'p_{\pm}, n''p_{\pm}|V_{int}(\mathbf{R})|ns_0, ns_0\rangle = \frac{\mu_{ns,n'p}^2 \mu_{ns,n''p}^2}{4} [(R_x^2 - R_y^2)^2 + 4R_x^2 R_y^2], \quad (\text{B.10})$$

$$\langle n'p_{\pm}, n''p_0|V_{int}(\mathbf{R})|ns_0, ns_0\rangle = \frac{\mu_{ns,n'p}^2 \mu_{ns,n''p}^2}{2} R_z^2 [R_x^2 + R_y^2], \quad (\text{B.11})$$

$$\langle n'p_{\pm}, n''p_{\mp}|V_{int}(\mathbf{R})|ns_0, ns_0\rangle = \mu_{ns,n'p}^2 \mu_{ns,n''p}^2 \left[\frac{R^4}{9} + \frac{(R_x^2 + R_y^2)^2}{4} - \frac{(R_x^2 + R_y^2)R^2}{3} \right], \quad (\text{B.12})$$

$$\langle n'p_0, n''p_0|V_{int}(\mathbf{R})|ns_0, ns_0\rangle = \frac{\mu_{ns,n'p}^2 \mu_{ns,n''p}^2}{9} R_z^2 [(R^2 - 3R_z^2)^2]. \quad (\text{B.13})$$

Multiplying by 2 with each of the above term to get the $\langle ns_0, ns_0|V_{int}(\mathbf{R})|n'p_{\pm,0}, n''p_{\pm,0}\rangle$ terms and then summing them all to get the total energy correction gives

$$V_{vdW} = \frac{4\mu_{ns,n'p}^2 \mu_{ns,n''p}^2}{3\Delta ER^6} = -\frac{C_6}{R^6} \quad (\text{B.14})$$

Mean field potentials and energy corrections

Here we calculate the Coulomb potentials and the exchange potentials used in the Hartree-Fock equations for the effective two electron atoms.

Mean field direct Coulomb potentials

The Coulomb potential due to the ground state electron is taken from Chapter 3 and $\frac{1}{r_{12}}$ is expanded in terms in terms of spherical harmonics as defined in property 2 in Appendix A. Thus,

$$\begin{aligned}
V_{5s} &= \int_0^\infty \frac{1}{r_{12}} \phi_{5s}^*(\mathbf{r}_1) \phi_{5s}(\mathbf{r}_1) d\mathbf{r}_1 \\
&= \left[\sum_{l'=0}^\infty \sum_{m'=-l'}^{l'} \frac{4\pi}{2l'+1} \frac{r_{<}^{l'}}{r_{>}^{l'+1}} \left(\int_0^\infty |\phi_{5s}(r_1)|^2 r_1^2 dr_1 \right) \times \right. \\
&\quad \left. \mathcal{Y}_{l',m'}^*(\vartheta_2, \varphi_2) \int \mathcal{Y}_{0,0}^*(\vartheta_1, \varphi_1) \mathcal{Y}_{l',m'}(\vartheta_1, \varphi_1) \mathcal{Y}_{0,0}(\vartheta_1, \varphi_1) d\Omega_1 \right] \\
&= \left[\sum_{l'=0}^\infty \sum_{m'=-l'}^{l'} \frac{4\pi}{2l'+1} \frac{r_{<}^{l'}}{r_{>}^{l'+1}} \left(\int_0^\infty |\phi_{5s}(r_1)|^2 r_1^2 dr_1 \right) \right. \\
&\quad \left. \mathcal{Y}_{l',m'}^*(\vartheta_2, \varphi_2) \sqrt{\frac{(2l'+1)}{4\pi}} \langle 0l'00 | 00 \rangle \langle 0l'0m' | 00 \rangle \right] \\
&= 4\pi \int_0^\infty |\phi_{5s}(r_1)|^2 \frac{r_1^2 dr_1}{r_{>}} \sqrt{\frac{1}{4\pi}} \sqrt{\frac{1}{4\pi}} = \int_0^\infty |\phi_{5s}(r_1)|^2 \frac{r_1^2 dr_1}{r_{>}}. \quad (C.1)
\end{aligned}$$

The above Clebsch-Gordan coefficients are non-zero provided $l', m' = 0$ (see Appendix A). Similarly for the Coulomb potential due to the Rydberg state electron,

$$\begin{aligned}
V_{nl} &= \int_0^\infty \frac{1}{\mathbf{r}_{12}} \phi_{nl}^*(\mathbf{r}_2) \phi_{nl}(\mathbf{r}_2) d\mathbf{r}_2 \\
&= \left[\sum_{l'=0}^\infty \sum_{m'=-l'}^{l'} \frac{4\pi}{2l'+1} \frac{r_{<}^{l'}}{r_{>}^{l'+1}} \left(\int_0^\infty |\phi_{nl}(r_2)|^2 r_2^2 dr_2 \right) \times \right. \\
&\quad \left. \mathcal{Y}_{l',m'}^*(\vartheta_2, \varphi_2) \int \mathcal{Y}_{l,m}^*(\vartheta_1, \varphi_1) \mathcal{Y}_{l',m'}(\vartheta_1, \varphi_1) \mathcal{Y}_{l,m}(\vartheta_1, \varphi_1) d\Omega_1 \right] \\
&= \left[\sum_{l'=0}^\infty \sum_{m'=-l'}^{l'} \frac{4\pi}{2l'+1} \frac{r_{<}^{l'}}{r_{>}^{l'+1}} \left(\int_0^\infty |\phi_{nl}(r_2)|^2 r_2^2 dr_2 \right) \right. \\
&\quad \left. (-1)^{-m} \mathcal{Y}_{l',m'}^*(\vartheta_2, \varphi_2) \sqrt{\frac{(2l+1)(2l'+1)}{4\pi(2l+1)}} \langle ll'00 | l0 \rangle \langle ll' - mm' | l - m \rangle \right]. \quad (\text{C.2})
\end{aligned}$$

The number of terms within the sum are determined by the rules of Clebsch-Gordan coefficients given in Appendix A. The above expression has only one term For $|ns\rangle$ states while it has three terms for $|np\rangle$ states. The higher the l , the more terms and hence more time consuming. Next, we use these Coulomb potentials to evaluate the first order energy corrections using perturbation theory. Due to the large asymmetry in the sizes of the Rydberg and ground wave function, we can treat the exchange energy and the Rydberg potential for the ground electron to be small.

First order energy corrections

The first order energy corrections are for the Rydberg potential and the exchange potential which are

$$E_D^{(1)} = \langle \phi_{nl}^{(0)}(\mathbf{r}_2) | V_{5s} | \phi_{nl}^{(0)}(\mathbf{r}_2) \rangle, \quad (\text{C.3})$$

$$E_{Ex}^{(1)} = \langle \phi_{nl}^{(0)}(\mathbf{r}_2) | V_{nl,5s}(r_2) | \phi_{5s}^{(0)}(\mathbf{r}_1) \rangle = \langle \phi_{5s}^{(0)}(\mathbf{r}_1) | V_{5s,nl}(r_1) | \phi_{nl}^{(0)}(\mathbf{r}_1) \rangle. \quad (\text{C.4})$$

The first order energy correction due to the Rydberg potential

$$\begin{aligned}
E_D^{(1)} &= \left[\sum_{l'=0}^{\infty} \sum_{m'=-l'}^{l'} \frac{4\pi}{2l'+1} \frac{r_{<}^{l'}}{r_{>}^{l'+1}} \left(\int_0^{\infty} |\phi_{5s}^{(0)}(r_1)|^2 |\phi_{nl}^{(0)}(r_2)|^2 r_1^2 r_2^2 dr_1 dr_2 \right) \right. \\
&\quad \int \mathcal{Y}_{0,0}^*(\vartheta_1, \varphi_1) \mathcal{Y}_{l',m'}^*(\vartheta_1, \varphi_1) \mathcal{Y}_{0,0}(\vartheta_1, \varphi_1) d\Omega_1 \\
&\quad \left. \times \int \mathcal{Y}_{l,m}^*(\vartheta_2, \varphi_2) \mathcal{Y}_{l',m'}(\vartheta_2, \varphi_2) \mathcal{Y}_{l,m}(\vartheta_2, \varphi_2) d\Omega_2 \right] \\
&= \left[\sum_{l'=0}^{\infty} \sum_{m'=-l'}^{l'} \frac{4\pi}{2l'+1} \frac{r_{<}^{l'}}{r_{>}^{l'+1}} \left(\int_0^{\infty} |\phi_{5s}^{(0)}(r_1)|^2 |\phi_{nl}^{(0)}(r_2)|^2 r_1^2 r_2^2 dr_1 dr_2 \right) \right. \\
&\quad \left((-1)^{-m'} \sqrt{\frac{2l'+1}{4\pi}} \langle 0l'00|00 \rangle \langle 0l'0m'|00 \rangle \right) \\
&\quad \left((-1)^{-m} \sqrt{\frac{(2l+1)(2l'+1)}{4\pi(2l+1)}} \langle ll'00|l0 \rangle \langle ll'-mm'|l-m \rangle \right) \left. \right] \\
&= \int_0^{\infty} |\phi_{5s}^{(0)}(r_1)|^2 |\phi_{nl}^{(0)}(r_2)|^2 \frac{1}{r_{>}} r_1^2 r_2^2 dr_1 dr_2 . \tag{C.5}
\end{aligned}$$

The above Clebsch-Gordan coefficients are non-zero provided $l', m' = 0$. Similarly the first order energy correction due to exchange potential is

$$\begin{aligned}
E_{Ex}^{(1)} &= \left[\sum_{l'=0}^{\infty} \sum_{m'=-l'}^{l'} \frac{4\pi}{2l'+1} \frac{r_{<}^{l'}}{r_{>}^{l'+1}} \left(\int_0^{\infty} \phi_{5s}^{(0)}(r_1) \phi_{nl}^{(0)}(r_2) \phi_{5s}^{(0)}(r_2) \phi_{nl}^{(0)}(r_1) d\mathbf{r}_2 d\mathbf{r}_1 \right) \right. \\
&\quad \int \mathcal{Y}_{0,0}^*(\vartheta_1, \varphi_1) \mathcal{Y}_{l',m'}^*(\vartheta_1, \varphi_1) \mathcal{Y}_{l,m}(\vartheta_1, \varphi_1) d\Omega_1 \\
&\quad \left. \times \int \mathcal{Y}_{l,m}^*(\vartheta_2, \varphi_2) \mathcal{Y}_{l',m'}(\vartheta_2, \varphi_2) \mathcal{Y}_{0,0}(\vartheta_2, \varphi_2) d\Omega_2 \right] \\
&= \left[\sum_{l'=0}^{\infty} \sum_{m'=-l'}^{l'} \frac{4\pi}{2l'+1} \frac{r_{<}^{l'}}{r_{>}^{l'+1}} \left(\int_0^{\infty} \phi_{5s}^{(0)}(r_1) \phi_{nl}^{(0)}(r_2) \phi_{5s}^{(0)}(r_2) \phi_{nl}^{(0)}(r_1) d\mathbf{r}_2 d\mathbf{r}_1 \right) \right. \\
&\quad \left((-1)^{-2m} \sqrt{\frac{2l'+1}{4\pi(2l+1)}} \langle 0l'00|l0 \rangle \langle 0l'0m'|lm \rangle \right) \\
&\quad \left((-1)^{-m} \sqrt{\frac{(2l+1)(2l'+1)}{4\pi}} \langle ll'00|00 \rangle \langle ll'-mm'|00 \rangle \right) \left. \right] \\
&= \frac{1}{2l+1} \int_0^{\infty} \phi_{5s}^{(0)}(r_1) \phi_{5s}^{(0)}(r_2) \phi_{nl}^{(0)}(r_1) \phi_{nl}^{(0)}(r_2) \frac{r_{<}^l}{r_{>}^{l+1}} r_1^2 r_2^2 dr_1 dr_2 . \tag{C.6}
\end{aligned}$$

The above Clebsch-Gordan coefficients are non-zero provided $l' = l$ and $m' = m = 0$.

Non-adiabatic couplings

The Born-Oppenheimer approximation separates the motional dynamics (dynamics of the trapped nuclei) from the electronic dynamics. If this approximation is not valid then there can be significant coupling between the dressed electronic states due to the motion of the trapped nuclei. This means that though we initially start with the dressed ground state, during the dynamics we may end up in a excited dressed state. Loss of population from the dressed ground state to the excited dressed states via the non-adiabatic couplings can cause serious limitations to the lifetime of the system. Hence here we estimate the strength of the non-adiabatic couplings. The time dependent Schrödinger equation,

$$i\hbar \frac{d|\Psi\rangle}{dt} = (\hat{H}_{\text{opt}}^+ + \hat{H}_{\text{opt}}^- + \hat{H}_{CoM})|\Psi\rangle, \quad (\text{D.1})$$

where \hat{H}_{opt}^\pm and \hat{H}_{CoM} are taken from Eq.(6.27) and Eq.(6.42) of chapter 6. The corresponding wave function is

$$|\Psi\rangle = \sum_{n_1, n_2} \sum_{\beta} \left[c_{n_1 n_2}^{\beta,+}(t) |\xi^{\beta,+}(r, R)\rangle + c_{n_1 n_2}^{\beta,-}(t) |\xi^{\beta,-}(r, R)\rangle \right] |n_1 n_2\rangle. \quad (\text{D.2})$$

Multiplying by $\langle n_1 n_2 | \langle \tilde{g}^\pm |$ throughout the time dependent Schrödinger equation gives,

$$\begin{aligned} i\dot{c}_{n_1 n_2}^{\tilde{g},\pm}(t) &= \left(\langle n_1 n_2 | \omega_{\text{opt}}^{\tilde{g},\pm}(R) | n_1 n_2 \rangle + \omega_{n_1 n_2} \right) c_{n_1 n_2}^{\tilde{g},\pm}(t) \\ &+ \sum_{n'_1, n'_2 \neq n_1 n_2} \langle n_1 n_2 | \omega_{\text{opt}}^{\tilde{g},\pm}(R) | n'_1 n'_2 \rangle c_{n'_1 n'_2}^{\tilde{g},\pm}(t) \\ &- \sum_{i=1,2} \sum_{\beta \neq 0} \sum_{n'_1, n'_2 \neq n_1 n_2} \left[\langle n_1 n_2 | \langle \tilde{g}^\pm | \frac{\hbar^2 \nabla_{Z_i}^2}{2M} \xi^{\beta,\pm} | n'_1 n'_2 \rangle \right. \\ &\left. + \frac{\hbar^2}{M} \langle n_1 n_2 | \langle \tilde{g}^\pm | \nabla_{Z_i} \xi^{\beta,\pm} | \nabla_{Z_i} (n'_1 n'_2) \rangle \right] c_{n'_1 n'_2}^{\beta,\pm}(t). \end{aligned} \quad (\text{D.3})$$

where $Z_{i=1,2}$ is the relative motion of the nucleus at site 1 or site 2 with respect to the center of every site. In general there are two types of non-adiabatic matrix elements. One is the second term in the first line where higher motional states are coupled. The other type is in the second and third lines which involves the derivatives of the dressed electronic eigenstates. The first one is tackled in the main chapter 6 in section 6.4. Evaluating the double derivative for the specific motional states $|00\rangle$,

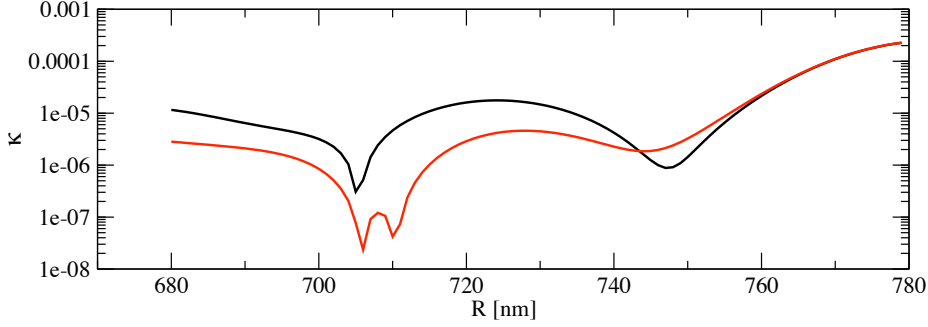


Figure D.1: Plotting κ defined in Eq.(D.7) for the gerade (black) and ungerade (red) states.

$$\langle 00 | \langle \tilde{g}^\pm | \frac{\hbar^2 \nabla_{Z_i}^2}{2M} \xi^{\tilde{g}, \pm}(r, R) | 00 \rangle = \frac{m}{M} \langle 00 | \langle \tilde{g}^\pm | \frac{\hbar^2 \nabla_{Z_i}^2}{2m} \xi^{\beta, \pm}(r, R) | 00 \rangle, \quad (\text{D.4})$$

while the first derivative is written as

$$\begin{aligned} & \frac{\hbar^2}{M} \langle 00 | \langle \tilde{g}^\pm | \nabla_{Z_i} \xi^{\beta, \pm} | \nabla_{Z_i} (00) \rangle \\ &= \frac{\hbar^2}{M} \langle 00 | \langle \tilde{g}^\pm | \nabla_{Z_i} \xi^{\beta, \pm} | \frac{\hat{p}_i}{-i\hbar} (00) \rangle \\ &= \frac{\hbar^2}{M} \langle 00 | \langle \tilde{g}^\pm | \nabla_{Z_i} \xi^{\beta, \pm} | \sqrt{\frac{M\omega_{\text{tr}}}{2\hbar}} (\hat{a}_i - \hat{a}_i^\dagger) (00) \rangle \\ &= \frac{\hbar^2}{\sqrt{2}M\sigma_0} \left(\langle 00 | \langle \tilde{g}^\pm | \nabla_{Z_i} \xi^{\beta, \pm} | 00 \rangle - 2\sqrt{2} \langle 00 | \langle \tilde{g}^\pm | \nabla_{Z_i} \xi^{\beta, \pm} | 01 \rangle \right). \end{aligned} \quad (\text{D.5})$$

where $\sigma_0 = \sqrt{\hbar/M\omega_{\text{tr}}}$. The conditions that ensure that excited dressed states are not populated due to the non-adiabatic terms are

$$\begin{aligned} & \frac{m^2}{M^2} \frac{(\langle 00 | \langle \tilde{g}^\pm | \frac{\hbar^2 \nabla_{Z_i}^2}{2m} \xi^{\beta=1, \pm}(r, R) | 00 \rangle)^2}{\langle 00 | \omega_{\text{opt}}^{\beta=1, \pm}(R) | 00 \rangle - \langle 00 | \omega_{\text{opt}}^{\tilde{g}^\pm}(R) | 00 \rangle} \ll 1 \\ & \frac{\hbar^2}{\sqrt{2}M\sigma_0} \frac{(\langle 00 | \langle \xi^{\tilde{g}, \pm} | \nabla_{Z_i} \xi^{\beta=1, \pm} | 00 \rangle)^2}{\langle 00 | \omega_{\text{opt}}^{\beta=1, \pm}(R) | 00 \rangle - \langle 00 | \omega_{\text{opt}}^{\tilde{g}^\pm}(R) | 00 \rangle} \ll 1 \\ & \frac{2\hbar^2}{M\sigma_0} \frac{(\langle 00 | \langle \xi^{\tilde{g}, \pm} | \nabla_{Z_i} \xi^{\beta=1, \pm} | 01 \rangle)^2}{\langle 01 | \omega_{\text{opt}}^{\beta=1, \pm}(R) | 01 \rangle - \langle 00 | \omega_{\text{opt}}^{\tilde{g}^\pm}(R) | 00 \rangle} \ll 1 \end{aligned} \quad (\text{D.6})$$

The first condition is easily satisfied even when the Rabi frequencies are comparable to the difference in the dressed energy state due to the ratio $\frac{m}{M}$. While for the second condition, one has to evaluate the the variation of the dressed eigenfunction with the parameter Z_i . Defining the following quantity,

$$\kappa = \frac{\hbar^2}{\sqrt{2}M\sigma_0} \frac{(\langle 00 | \langle \xi^{\tilde{g}, \pm} | \nabla_{Z_i} \xi^{\beta=1, \pm} | 00 \rangle)^2}{\langle 00 | \omega_{\text{opt}}^{\beta=1, \pm}(R) | 00 \rangle - \langle 00 | \omega_{\text{opt}}^{\tilde{g}^\pm}(R) | 00 \rangle}, \quad (\text{D.7})$$

we show in Fig.D.1, that the non-adiabatic couplings are indeed small for the dressed ground states.

Spatially varying laser field for N sites

We extend the derivation of dynamical equations for a spatially varying field given in section 6.5.2 to N sites. Using the many-body Hamiltonian in Eq.(6.77) and the many-body reduced basis Eq.(6.76) defined in chapter 6 , we re-write the dynamical equations for the ground state,

$$i\partial_t C_k^I = \frac{\Omega_{k-1}}{2\sqrt{2}} (C_{k-1}^{E,+} - C_{k-1}^{E,-}) + \frac{\Omega_{k+1}}{2\sqrt{2}} (C_k^{E,+} + C_k^{E,-}) , \quad (\text{E.1})$$

$$i\partial_t C_{k-1}^I = \frac{\Omega_{k-2}}{2\sqrt{2}} (C_{k-2}^{E,+} - C_{k-2}^{E,-}) + \frac{\Omega_k}{2\sqrt{2}} (C_{k-1}^{E,+} + C_{k-1}^{E,-}) , \quad (\text{E.2})$$

$$i\partial_t C_{k+1}^I = \frac{\Omega_k}{2\sqrt{2}} (C_k^{E,+} - C_k^{E,-}) + \frac{\Omega_{k+2}}{2\sqrt{2}} (C_{k+1}^{E,+} + C_{k+1}^{E,-}) . \quad (\text{E.3})$$

where we expressed the excited states in the (un)gerade basis using the definition in Eq.(6.81), which we re-write here

$$C_k^{E,\pm} = \frac{1}{\sqrt{2}} (C_k^R \pm C_{k+1}^L) . \quad (\text{E.4})$$

The dynamical equations for the excited states correspondingly are

$$i\partial_t C_k^{E,+} = -\Delta^+ C_k^{E,+} + \frac{\Omega_{k+1}}{2\sqrt{2}} C_k^I + \frac{\Omega_k}{2\sqrt{2}} C_{k+1}^I , \quad (\text{E.5a})$$

$$i\partial_t C_k^{E,-} = -\Delta^- C_k^{E,-} + \frac{\Omega_{k+1}}{2\sqrt{2}} C_k^I - \frac{\Omega_k}{2\sqrt{2}} C_{k+1}^I . \quad (\text{E.5b})$$

$$i\partial_t C_{k-1}^{E,+} = -\Delta^+ C_{k-1}^{E,+} + \frac{\Omega_k}{2\sqrt{2}} C_{k-1}^I + \frac{\Omega_{k-1}}{2\sqrt{2}} C_k^I , \quad (\text{E.5c})$$

$$i\partial_t C_{k-1}^{E,-} = -\Delta^- C_{k-1}^{E,-} + \frac{\Omega_k}{2\sqrt{2}} C_{k-1}^I - \frac{\Omega_{k-1}}{2\sqrt{2}} C_k^I . \quad (\text{E.5d})$$

Similar to the analysis in section 6.5.2, we assume that the Rydberg state of either symmetry can be adiabatically eliminated. Assuming that $\Delta^+ \gg \Omega_{k+1}, \Omega_k$ implying that the gerade excited states $|E^{+,(k)}\rangle$ and $|E^{+,(k-1)}\rangle$ can be adiabatically eliminated. Thus terms like $\frac{\Omega_{k+1}\Omega_k}{8\Delta^+}$ and $\frac{\Omega_k^2}{8\Delta^+}$ are considered to be negligible compared to Δ^- and

Ω_k . We thus end up with two sets of lambda systems that are coupled to a common many-body ground states.

$$i\partial_t \begin{pmatrix} C_k^I \\ C_{k-1}^I \\ C_{k-1}^{E,-} \end{pmatrix} = \begin{pmatrix} 0 & 0 & \frac{\Omega_k}{2\sqrt{2}} \\ 0 & 0 & -\frac{\Omega_{k-1}}{2\sqrt{2}} \\ \frac{\Omega_k}{2\sqrt{2}} & -\frac{\Omega_{k-1}}{2\sqrt{2}} & -\Delta^- \end{pmatrix} \begin{pmatrix} C_k^I \\ C_{k-1}^I \\ C_{k-1}^{E,-} \end{pmatrix}. \quad (\text{E.6})$$

and

$$i\partial_t \begin{pmatrix} C_k^I \\ C_{k+1}^I \\ C_k^{E,-} \end{pmatrix} = \begin{pmatrix} 0 & 0 & \frac{\Omega_{k+1}}{2\sqrt{2}} \\ 0 & 0 & -\frac{\Omega_k}{2\sqrt{2}} \\ \frac{\Omega_{k+1}}{2\sqrt{2}} & -\frac{\Omega_k}{2\sqrt{2}} & -\Delta^- \end{pmatrix} \begin{pmatrix} C_k^I \\ C_{k+1}^I \\ C_k^{E,-} \end{pmatrix}. \quad (\text{E.7})$$

By writing the above reduced equations, we have made another approximation for the many-sites that did not exist for the two sites. The ground states $|I^{(k-1)}\rangle$ and $|I^{(k+1)}\rangle$ also couple to the excited states $|E^{\pm,(k-2)}\rangle$ and $|E^{\pm,(k+1)}\rangle$ respectively. However we start with the initial condition that the ion is at site k and thus as we argued in the beginning of section 6.6 that the probability to have double excitation is very low. Hence $|C_{k-1}^{E,\pm}|^2, |C_k^{E,\pm}|^2 \gg |C_{k-2}^{E,\pm}|^2, |C_{k+1}^{E,\pm}|^2$. Thus following the same procedure as in section 6.5.2, we have the following dynamical equation,

$$i\partial_t C_k^I = (U_{k-1} + U_k) C_k^I + J_{k,k-1} C_{k-1}^I + J_{k,k+1} C_{k+1}^I. \quad (\text{E.8})$$

where

$$U_k = \begin{cases} \frac{-\Delta^- + \sqrt{(\Delta^-)^2 + (\Omega_{k+1}^2 + \Omega_k^2)/2}}{2} (\sin^2 \sigma) & \text{if } \Delta^- > 0, \\ \frac{-\Delta^- - \sqrt{(\Delta^-)^2 + (\Omega_{k+1}^2 + \Omega_k^2)/2}}{2} (\sin^2 \sigma) & \text{if } \Delta^- < 0, \end{cases} \quad (\text{E.9})$$

$$J_{k+1,k} = \begin{cases} \frac{\Delta^- - \sqrt{(\Delta^-)^2 + (\Omega_{k+1}^2 + \Omega_k^2)/2}}{2} \left(\frac{\sin 2\sigma}{2}\right) & \text{if } \Delta^- > 0, \\ \frac{\Delta^- + \sqrt{(\Delta^-)^2 + (\Omega_{k+1}^2 + \Omega_k^2)/2}}{2} \left(\frac{\sin 2\sigma}{2}\right) & \text{if } \Delta^- < 0, \end{cases} \quad (\text{E.10})$$

where $\tan \sigma = \frac{\Omega_{k+1}}{\Omega_k}$ and $\tan 2\rho = \frac{\sqrt{(\Omega_{k+1}^2 + \Omega_k^2)/2}}{\Delta^-}$.

Spin degree of Freedom

We may encounter a problem regarding the electron tunneling if the spin degree of the additional core electrons is taken into account. The scheme is based on optical dressing of the singlet ground state to a highly excited singlet Rydberg state. However, since the singlet and triplet Rydberg states are nearly degenerate the excited singlet state is equally coupled to a triplet state of an adjacent particle. The trouble is, that this state is not coupled to the original ground state, resulting in an open channel for the hopping process, or in other words, a possible source for loss of population into undesired many-body states.

Considering many particle basis and assuming that we have initially one singlet, ground state atom and one ion, there two possible (uncoupled) configuration corresponding to a total spin of the three electrons of $M = 1/2$ and $M = -1/2$, respectively. We re-write the Hamiltonian (ignoring the detuning for now) and the wave function we are considering.

$$\begin{aligned} \hat{H}_{\text{Many sites}} = & \sum_{k=1}^{N-1} \left[-\hbar\Delta |R^{(k)}\rangle\langle R^{(k)}| + \frac{\hbar\Omega_{k+1}}{2} \left(|R^{(k)}\rangle\langle I^{(k)}| + \text{h.c.} \right) \right] \\ & + \sum_{k=2}^N \left[-\hbar\Delta |L^{(k)}\rangle\langle L^{(k)}| + \frac{\hbar\Omega_{k-1}}{2} \left(|L^{(k)}\rangle\langle I^{(k)}| + \text{h.c.} \right) \right] \\ & + \sum_{k=1}^{N-1} \frac{T}{2} \left[|R^{(k)}\rangle\langle L^{(k+1)}| + \text{h.c.} \right] . \end{aligned} \quad (\text{F.1})$$

$$\Psi = \sum_k \left(C_k^I |I^{(k)}\rangle + C_k^R |R^{(k)}\rangle + C_k^L |L^{(k)}\rangle \right) \quad (\text{F.2})$$

The equation of motion in terms of the amplitude are

$$\begin{aligned} i\partial_t C_k^I &= \frac{\Omega_{k-1}}{2} C_k^L + \frac{\Omega_{k+1}}{2} C_k^R \\ i\partial_t C_{(\uparrow g_{k-1} \downarrow g_{k-1})(\uparrow g_k)(\uparrow g_{k+1} \downarrow g_{k+1})} & \\ &= \frac{\Omega_{k-1}}{2} \left[C_{(\uparrow e_{k-1} \downarrow g_{k-1})(\uparrow g_k)(\uparrow g_{k+1} \downarrow g_{k+1})} + C_{(\uparrow g_{k-1} \downarrow e_{k-1})(\uparrow g_k)(\uparrow g_{k+1} \downarrow g_{k+1})} \right] \\ &+ \frac{\Omega_{k+1}}{2} \left[C_{(\uparrow g_{k-1} \downarrow g_{k-1})(\uparrow g_k)(\uparrow e_{k+1} \downarrow g_{k+1})} + C_{(\uparrow g_{k-1} \downarrow g_{k-1})(\uparrow g_k)(\uparrow g_{k+1} \downarrow e_{k+1})} \right] \end{aligned} \quad (\text{F.3})$$

The dynamical equation for the excited atom on the right of the ion is

$$i\partial_t C_{(\uparrow g_{k-1} \downarrow g_{k-1})(\uparrow g_k)(\uparrow g_{k+1} \downarrow e_{k+1})} = -\Delta C_{(\uparrow g_{k-1} \downarrow g_{k-1})(\uparrow g_k)(\uparrow g_{k+1} \downarrow e_{k+1})} + \frac{\Omega_{k+1}}{2} C_{a_{k-1} i_k a_{k+1}} \\ + \frac{T}{\hbar} C_{(\uparrow g_{k-1} \downarrow g_{k-1})(\uparrow g_k \uparrow e_k)(\downarrow g_{k+1})} \quad (\text{F.4})$$

$$i\partial_t C_{(\uparrow g_{k-1} \downarrow g_{k-1})(\uparrow g_k)(\uparrow g_{k+1} \downarrow e_{k+1})} = -\Delta C_{(\uparrow g_{k-1} \downarrow g_{k-1})(\uparrow g_k)(\uparrow g_{k+1} \downarrow e_{k+1})} + \frac{\Omega_{k+1}}{2} C_{a_{k-1} i_k a_{k+1}} \\ + \frac{T}{\hbar} C_{(\uparrow g_{k-1} \downarrow g_{k-1})(\uparrow g_k \downarrow e_k)(\uparrow g_{k+1})} \quad (\text{F.5})$$

Similarly the dynamical equation for the excited atom on the left atom of the ion is

$$i\partial_t C_{(\uparrow e_{k-1} \downarrow g_{k-1})(\uparrow g_k)(\uparrow g_{k+1} \downarrow g_{k+1})} = -\Delta C_{(\uparrow e_{k-1} \downarrow g_{k-1})(\uparrow g_k)(\uparrow g_{k+1} \downarrow g_{k+1})} + \frac{\Omega_{k-1}}{2} C_{a_{k-1} i_k a_{k+1}} \\ + \frac{T}{\hbar} C_{(\downarrow g_{k-1})(\uparrow e_k \uparrow g_k)(\uparrow g_{k+1} \downarrow g_{k+1})} \quad (\text{F.6})$$

$$i\partial_t C_{(\uparrow g_{k-1} \downarrow e_{k-1})(\uparrow g_k)(\uparrow g_{k+1} \downarrow g_{k+1})} = -\Delta C_{(\uparrow g_{k-1} \downarrow e_{k-1})(\uparrow g_k)(\uparrow g_{k+1} \downarrow g_{k+1})} + \frac{\Omega_{k-1}}{2} C_{a_{k-1} i_k a_{k+1}} \\ + \frac{T}{\hbar} C_{(\uparrow g_{k-1})(\downarrow e_k \uparrow g_k)(\uparrow g_{k+1} \downarrow g_{k+1})} \quad (\text{F.7})$$

The states that are not stable due to Pauli principle and so will tunnel through to give the following two equations,

$$C_{(\downarrow g_{k-1})(\uparrow e_k \uparrow g_k)(\uparrow g_{k+1} \downarrow g_{k+1})} = \frac{T}{\hbar \Delta} C_{(\uparrow e_{k-1} \downarrow g_{k-1})(\uparrow g_k)(\uparrow g_{k+1} \downarrow g_{k+1})} \quad (\text{F.8})$$

$$C_{(\uparrow g_{k-1} \downarrow g_{k-1})(\uparrow g_k \uparrow e_k)(\downarrow g_{k+1})} = \frac{T}{\hbar \Delta} C_{(\uparrow g_{k-1} \downarrow g_{k-1})(\uparrow g_k)(\uparrow e_{k+1} \downarrow g_{k+1})} \quad (\text{F.9})$$

Thus in Eqs.(F.4) and (F.6), we get

$$i\partial_t C_{(\uparrow g_{k-1} \downarrow g_{k-1})(\uparrow g_k)(\uparrow g_{k+1} \downarrow e_{k+1})} = -\Delta C_{(\uparrow g_{k-1} \downarrow g_{k-1})(\uparrow g_k)(\uparrow g_{k+1} \downarrow e_{k+1})} + \frac{\Omega_{k+1}}{2} C_{a_{k-1} i_k a_{k+1}} \\ + \frac{T^2}{\hbar^2 \Delta} C_{(\uparrow g_{k-1} \downarrow g_{k-1})(\uparrow g_k)(\uparrow e_k \downarrow g_{k+1})} \quad (\text{F.10})$$

$$i\partial_t C_{(\uparrow e_{k-1} \downarrow g_{k-1})(\uparrow g_k)(\uparrow g_{k+1} \downarrow g_{k+1})} = -\Delta C_{(\uparrow e_{k-1} \downarrow g_{k-1})(\uparrow g_k)(\uparrow g_{k+1} \downarrow g_{k+1})} + \frac{\Omega_{k-1}}{2} C_{a_{k-1} i_k a_{k+1}} \\ + \frac{T^2}{\hbar^2 \Delta} C_{(\downarrow g_{k-1} \uparrow e_k)(\uparrow g_k)(\uparrow g_{k+1} \downarrow g_{k+1})} \quad (\text{F.11})$$

This implies that the states that violate Pauli exclusion principle are simply adiabatically eliminated and returns to the Pauli obeying Rydberg states at the rate of $(T/\hbar\Delta)T$.

Bibliography

- [1] Y. Aharonov, L. Davidovich, and N. Zagury. Quantum random walks. *Phys. Rev. A* **48**, 1687–1690, 1993.
- [2] A. Ajoy and P. Cappellaro. Quantum Simulation via Filtered Hamiltonian Engineering: Application to Perfect Quantum Transport in Spin Networks. *Phys. Rev. Lett.* **110**, 220503, 2013.
- [3] G. Alber, T. Haslwanter, and P. Zoller. One-photon resonant two-photon excitation of Rydberg series close to threshold. *J. Opt. Soc. Am. B* **5**, (12) 2439–2445, 1988.
- [4] L. Allen and J. H. Eberly. *Optical Resonance and Two-Level Atoms*. Courier Dover Publications, New York, 1987.
- [5] M. H. Anderson, J. R. Ensher, M. R. Matthews, C. E. Wieman, and E. A. Cornell. Observation of Bose-Einstein Condensation in a Dilute Atomic Vapor. *Science* **269**, (5221) 198–201, 1995.
- [6] S. E. Anderson and G. Raithel. Dependence of Rydberg-Atom Optical Lattices on the Angular Wave Function. *Phys. Rev. Lett.* **109**, 023001, 2012.
- [7] S. E. Anderson, K. C. Younge, and G. Raithel. Trapping Rydberg Atoms in an Optical Lattice. *Phys. Rev. Lett.* **107**, 263001, 2011.
- [8] W. R. Anderson, J. R. Veale, and T. F. Gallagher. Resonant Dipole-Dipole Energy Transfer in a Nearly Frozen Rydberg Gas. *Phys. Rev. Lett.* **80**, 249–252, 1998.
- [9] A. Ashkin. Acceleration and Trapping of Particles by Radiation Pressure. *Phys. Rev. Lett.* **24**, 156–159, 1970.
- [10] M. Aymar, P. Camus, M. Dieulin, and C. Morillon. Two-photon spectroscopy of neutral barium: Observations of the highly excited even levels and theoretical analysis of the $J = 0$ spectrum. *Phys. Rev. A* **18**, 2173–2183, 1978.
- [11] M. Aymar, A. Debarre, and O. Robaux. Highly excited levels of neutral ytterbium. II. Multichannel quantum defect analysis of odd- and even-parity spectra. *Journal of Physics B: Atomic and Molecular Physics* **13**, (6) 1089, 1980.
- [12] M. Aymar, C. H. Greene, and E. Luc-Koenig. Multichannel Rydberg spectroscopy of complex atoms. *Rev. Mod. Phys.* **68**, 1015–1123, 1996.
- [13] J. Balmer. Note on the Spectral Lines of Hydrogen (translated). *Annalen der Physik und Chemie* **25**, 80–85, 1885.
- [14] G. Bannasch and T. Pohl. Rydberg-atom formation in strongly correlated ultracold plasmas. *Phys. Rev. A* **84**, 052710, 2011.

- [15] Z. W. Barber, C. W. Hoyt, C. W. Oates, L. Hollberg, A. V. Taichenachev, and V. I. Yudin. Direct Excitation of the Forbidden Clock Transition in Neutral ^{174}Yb Atoms Confined to an Optical Lattice. *Phys. Rev. Lett.* **96**, 083002, 2006.
- [16] D. R. Bates and A. Damgaard. The Calculation of the Absolute Strengths of Spectral Lines. *Philosophical Transactions of the Royal Society of London. Series A, Mathematical and Physical Sciences* **242**, (842) 101–122, 1949.
- [17] L. Béguin, A. Vernier, R. Chicireanu, T. Lahaye, and A. Browaeys. Direct Measurement of the van der Waals Interaction between Two Rydberg Atoms. *Phys. Rev. Lett.* **110**, 263201, 2013.
- [18] R. Beigang, K. Lücke, A. Timmermann, P. West, and D. Frölich. Determination of absolute level energies of $5sns1S0$ and $5snd1D2$ Rydberg series of Sr. *Optics Communications* **42**, (1) 19–24, 1982.
- [19] J. Bell. On the Problem of Hidden Variables in Quantum Mechanics. *Rev. Mod. Phys.* **38**, 447–452, 1966.
- [20] C. H. Bennett and D. P. DiVincenzo. Quantum information and computation. *Nature* **404**, 247–255, 2000.
- [21] K. Bergmann, H. Theuer, and B. W. Shore. Coherent population transfer among quantum states of atoms and molecules. *Rev. Mod. Phys.* **70**, 1003–1025, 1998.
- [22] M. V. Berry and M. Tabor. Calculating the bound spectrum by path summation in action-angle variables. *Journal of Physics A: Mathematical and General* **10**, (3) 371, 1977.
- [23] I. Beterov, I. Ryabtsev, D. Tretyakov, and V. Entin. Quasiclassical calculations of blackbody-radiation-induced depopulation rates and effective lifetimes of Rydberg nS , nP , and nD alkali-metal atoms with $n \leq 80$. *Phys. Rev. A* **79**, (5), 2009.
- [24] H. A. Bethe and E. E. Salpeter. *Quantum mechanics of One and Two electron atoms*. Berlin : Springer ; New York : Academic Press, January 1, 1957.
- [25] S. A. Bhatti, C. L. Cromer, and W. E. Cooke. Analysis of the Rydberg character of the $5d7d^1D_2$ state of barium. *Phys. Rev. A* **24**, 161–165, 1981.
- [26] I. Bloch. Ultracold quantum gases in optical lattices. *Nat Phys* **1**, (1) 23–30, 2005.
- [27] I. Bloch, J. Dalibard, and W. Zwerger. Many-body physics with ultracold gases. *Rev. Mod. Phys.* **80**, 885–964, 2008.
- [28] N. Bohr. I. On the constitution of atoms and molecules. *Philosophical Magazine Series 6* **26**, (151) 1–25, 1913.
- [29] I. Bouchoule and K. Mølmer. Spin squeezing of atoms by the dipole interaction in virtually excited Rydberg states. *Phys. Rev. A* **65**, 041803, 2002.

- [30] D. Bouwmeester, J.-W. Pan, M. Daniell, H. Weinfurter, and A. Zeilinger. Observation of Three-Photon Greenberger-Horne-Zeilinger Entanglement. *Phys. Rev. Lett.* **82**, 1345–1349, 1999.
- [31] M. M. Boyd, T. Zelevinsky, A. D. Ludlow, S. Blatt, T. Zanon-Willette, S. M. Foreman, and J. Ye. Nuclear spin effects in optical lattice clocks. *Phys. Rev. A* **76**, 022510, 2007.
- [32] B. Bransden and C. Joachain. *Physics of Atoms and Molecules*. Addison Wesley Longman, 2 edition, June 23, 2003.
- [33] C. H. Cheng, C. Y. Lee, and T. F. Gallagher. Production of Circular Rydberg States with Circularly Polarized Microwave Fields. *Phys. Rev. Lett.* **73**, 3078–3081, 1994.
- [34] A. M. Childs. Universal Computation by Quantum Walk. *Phys. Rev. Lett.* **102**, 180501, 2009.
- [35] S. Chu. Nobel Lecture: The manipulation of neutral particles. *Rev. Mod. Phys.* **70**, 685–706, 1998.
- [36] S. Chu, J. E. Bjorkholm, A. Ashkin, and A. Cable. Experimental Observation of Optically Trapped Atoms. *Phys. Rev. Lett.* **57**, 314–317, 1986.
- [37] R. T. Clay and R. P. Hardikar. Intermediate Phase of the One Dimensional Half-Filled Hubbard-Holstein Model. *Phys. Rev. Lett.* **95**, 096401, 2005.
- [38] C. N. Cohen-Tannoudji. Nobel Lecture: Manipulating atoms with photons. *Rev. Mod. Phys.* **70**, 707–719, 1998.
- [39] W. E. Cooke, T. F. Gallagher, R. M. Hill, and S. A. Edelstein. Resonance measurements of $d - f$ and $d - g$ intervals in lithium Rydberg states. *Phys. Rev. A* **16**, 1141–1145, 1977.
- [40] S. L. Cornish, N. R. Claussen, J. L. Roberts, E. A. Cornell, and C. E. Wieman. Stable ^{85}Rb Bose-Einstein Condensates with Widely Tunable Interactions. *Phys. Rev. Lett.* **85**, 1795–1798, 2000.
- [41] R. Côté. From Classical Mobility to Hopping Conductivity: Charge Hopping in an Ultracold Gas. *Phys. Rev. Lett.* **85**, 5316–5319, 2000.
- [42] R. Côté, V. Kharchenko, and M. D. Lukin. Mesoscopic Molecular Ions in Bose-Einstein Condensates. *Phys. Rev. Lett.* **89**, 093001, 2002.
- [43] C. Dai and X. Zhao. Study of Sr 5snns Rydberg series. *J. Quant. Spectrosc. Radiat. Transfer* **54**, (1019) 8, 1995.
- [44] A. Daley, M. Boyd, J. Ye, and P. Zoller. Quantum Computing with Alkaline-Earth-Metal Atoms. *Physical Review Letters* **101**, (17), 2008.

- [45] A. J. Daley, M. M. Boyd, J. Ye, and P. Zoller. Quantum Computing with Alkaline-Earth-Metal Atoms. *Phys. Rev. Lett.* **101**, 170504, 2008.
- [46] J. Dalibard and C. Cohen-Tannoudji. Atomic motion in laser light: connection between semiclassical and quantum descriptions. *Journal of Physics B: Atomic and Molecular Physics* **18**, (8) 1661, 1985.
- [47] J. Dalibard, F. Gerbier, G. Juzeliūnas, and P. Öhberg. *Colloquium* : Artificial gauge potentials for neutral atoms. *Rev. Mod. Phys.* **83**, 1523–1543, 2011.
- [48] B. Damski, H.-U. Everts, A. Honecker, H. Fehrmann, L. Santos, and M. Lewenstein. Atomic Fermi Gas in the Trimerized Kagomé Lattice at 2/3 Filling. *Phys. Rev. Lett.* **95**, 060403, 2005.
- [49] N. Davidson, H. Jin Lee, C. S. Adams, M. Kasevich, and S. Chu. Long Atomic Coherence Times in an Optical Dipole Trap. *Phys. Rev. Lett.* **74**, 1311–1314, 1995.
- [50] Y. de Escobar, P. Mickelson, M. Yan, B. DeSalvo, S. Nagel, and T. Killian. Bose-Einstein Condensation of Sr84. *Physical Review Letters* **103**, (20), 2009.
- [51] Y. N. M. de Escobar, P. G. Mickelson, M. Yan, B. J. DeSalvo, S. B. Nagel, and T. C. Killian. Bose-Einstein Condensation of ^{84}Sr . *Phys. Rev. Lett.* **103**, 200402, 2009.
- [52] A. L. de Oliveira, M. W. Mancini, V. S. Bagnato, and L. G. Marcassa. Rydberg Cold Collisions Dominated by Ultralong Range Potential. *Phys. Rev. Lett.* **90**, 143002, 2003.
- [53] E. Demler and F. Zhou. Spinor Bosonic Atoms in Optical Lattices: Symmetry Breaking and Fractionalization. *Phys. Rev. Lett.* **88**, 163001, 2002.
- [54] A. Derevianko, S. G. Porsev, S. Kotochigova, E. Tiesinga, and P. S. Julienne. Ultracold Collision Properties of Metastable Alkaline-Earth Atoms. *Phys. Rev. Lett.* **90**, 063002, 2003.
- [55] J. P. Dowling and J. Gea-Banacloche. Schrödinger modal structure of cubical, pyramidal, and conical, evanescent light-wave gravitational atom traps. *Phys. Rev. A* **52**, 3997–4003, 1995.
- [56] L.-M. Duan, E. Demler, and M. D. Lukin. Controlling Spin Exchange Interactions of Ultracold Atoms in Optical Lattices. *Phys. Rev. Lett.* **91**, 090402, 2003.
- [57] W. Dur, G. Vidal, and J. I. Cirac. Three qubits can be entangled in two inequivalent ways. *Phys. Rev. A* **62**, 062314, 2000.
- [58] S. Dutta, J. Guest, D. Feldbaum, A. Walz-Flannigan, and G. Raithel. Ponderomotive Optical Lattice for Rydberg Atoms. *Physical Review Letters* **85**, (26) 5551–5554, 2000.

- [59] L. G. D'yachkov and P. M. Pankratov. On the use of the semiclassical approximation for the calculation of oscillator strengths and photoionization cross sections. *Journal of Physics B: Atomic, Molecular and Optical Physics* **27**, (3) 461–472, 1994.
- [60] P. Esherick. Bound, even-parity $J=0$ and $J=2$ spectra of Sr. *Phys. Rev. A* **15**, (5) 1920–1936, 1977.
- [61] C. Fabre, S. Haroche, and P. Goy. Addendum to "Millimeter spectroscopy in sodium Rydberg states". *Phys. Rev. A* **22**, 778–781, 1980.
- [62] U. Fano. Effects of Configuration Interaction on Intensities and Phase Shifts. *Phys. Rev.* **124**, 1866–1878, 1961.
- [63] U. Fano. Quantum Defect Theory of l Uncoupling in H_2 as an Example of Channel-Interaction Treatment. *Phys. Rev. A* **2**, 353–365, 1970.
- [64] S. M. Farooqi, D. Tong, S. Krishnan, J. Stanojevic, Y. P. Zhang, J. R. Ensher, A. S. Estrin, C. Boisseau, R. Côté, E. E. Eyler, and P. L. Gould. Long-Range Molecular Resonances in a Cold Rydberg Gas. *Phys. Rev. Lett.* **91**, 183002, 2003.
- [65] H. Fehske, G. Wellein, G. Hager, A. Weiße, and A. R. Bishop. Quantum lattice dynamical effects on single-particle excitations in one-dimensional Mott and Peierls insulators. *Phys. Rev. B* **69**, 165115, 2004.
- [66] G. Ferrari, P. Cancio, R. Drullinger, G. Giusfredi, N. Poli, M. Prevedelli, C. Toninelli, and G. M. Tino. Precision Frequency Measurement of Visible Intercombination Lines of Strontium. *Phys. Rev. Lett.* **91**, 243002, 2003.
- [67] R. P. Feynman. Forces in Molecules. *Phys. Rev.* **56**, 340–343, 1939.
- [68] M. Fleischhauer, A. Imamoglu, and J. P. Marangos. Electromagnetically induced transparency: Optics in coherent media. *Rev. Mod. Phys.* **77**, 633–673, 2005.
- [69] R. R. Freeman and D. Kleppner. Core polarization and quantum defects in high-angular-momentum states of alkali atoms. *Phys. Rev. A* **14**, 1614–1619, 1976.
- [70] S. Friedrich. *Theoretical Atomic Physics*. Berlin: Springer, 3 edition, November 9, 2010.
- [71] J. R. Fuhr and W. L. Wiese. *NIST Atomic Transition Probabilities CRC Handbook of Chemistry and Physics*. CRC Press, Boca Raton, Florida, 92 edition, 2005.
- [72] T. Fukuhara, S. Sugawa, M. Sugimoto, S. Taie, and Y. Takahashi. Mott insulator of ultracold alkaline-earth-metal-like atoms. *Phys. Rev. A* **79**, 041604, 2009.
- [73] A. Gaëtan, Y. Miroshnychenko, T. Wilk, A. Chotia, M. Viteau, D. Comparat, P. Pillet, A. Browaeys, and P. Grangier. Observation of collective excitation of two individual atoms in the Rydberg blockade regime. *Nature Physics* **5**, (2) 115–118, 2009.

- [74] T. F. Gallagher. *Rydberg Atoms*. Cambridge University Press, Cambridge, 1994.
- [75] T. F. Gallagher, S. A. Edelstein, and R. M. Hill. Collisional Angular Momentum Mixing in Rydberg States of Sodium. *Phys. Rev. Lett.* **35**, 644–647, 1975.
- [76] L. I. R. Gil, R. Mukherjee, E. M. Bridge, M. P. A. Jones, and T. Pohl. *Spin squeezing in a Rydberg lattice clock*. arXiv: 1306.6240, 2013.
- [77] Y. Gnedin, A. Mihajlov, L. Ignjatovic, N. Sakan, V. Sreckovic, M. Zakharov, N. Bezuglov, and A. Klycharev. Rydberg atoms in astrophysics. *New Astronomy Reviews* **53**, (7) 259 – 265, 2009.
- [78] W. Gornik. Lifetime measurements of highly excited levels of sr I using stepwise excitation by two pulsed dye lasers. *Zeitschrift für Physik A* **283**, (3) 231–234, 1977.
- [79] A. Gorshkov, A. Rey, A. Daley, M. Boyd, J. Ye, P. Zoller, and M. Lukin. Alkaline-Earth-Metal Atoms as Few-Qubit Quantum Registers. *Physical Review Letters* **102**, (11), 2009.
- [80] A. V. Gorshkov, M. Hermele, V. Gurarie, C. Xu, P. S. Julienne, J. Ye, P. Zoller, E. Demler, M. D. Lukin, and A. M. Rey. Two-orbital SU(N) magnetism with ultracold alkaline-earth atoms. *Nature Physics* **6**, (4) 289–295, 2010.
- [81] A. V. Gorshkov, J. Otterbach, M. Fleischhauer, T. Pohl, and M. D. Lukin. Photon-Photon Interactions via Rydberg Blockade. *Phys. Rev. Lett.* **107**, 133602, 2011.
- [82] F. Gounand, P. R. Fournier, and J. Berlande. Collisional depopulation of Rydberg P states of rubidium at thermal energies. *Phys. Rev. A* **15**, 2212–2220, 1977.
- [83] S. Goutis, M. Aymar, M. Kompitsas, and P. Camus. The perturbed even-parity $J = 1\ e\ ,\ 2\ e$ autoionizing spectra of strontium below the $4d\ 5/2$ threshold: observation and theoretical analysis. *Journal of Physics B: Atomic, Molecular and Optical Physics* **25**, (16) 3433, 1992.
- [84] P. Grafström, J. Zhan-Kui, G. Jönsson, C. Levinson, H. Lundberg, and S. Svanberg. Natural radiative lifetimes in the interacting $5snd\ 1,3D_2$ sequences in Sr. *Phys. Rev. A* **27**, (2) 947–949, 1983.
- [85] C. H. Greene and M. Aymar. Spin-orbit effects in the heavy alkaline-earth atoms. *Phys. Rev. A* **44**, 1773–1790, 1991.
- [86] M. Greiner, O. Mandel, T. Esslinger, T. W. Hansch, and I. Bloch. Quantum phase transition from a superfluid to a Mott insulator in a gas of ultracold atoms. *Nature* **415**, (6867) 39–44, 2002.
- [87] M. Greiner, C. A. Regal, and D. S. Jin. Emergence of a molecular Bose-Einstein condensate from a Fermi gas. *Nature* **426**, (6966) 537–540, 2003.

- [88] R. Grimm. Low-temperature physics: A quantum revolution. *Nature* **435**, (7045) 1035–1036, 2005.
- [89] C. Guet and W. R. Johnson. Relativistic many-body calculations of transition rates for Ca^+ , Sr^+ , and Ba^+ . *Phys. Rev. A* **44**, 1531–1535, 1991.
- [90] O. Gunnarsson. Superconductivity in fullerides. *Rev. Mod. Phys.* **69**, 575–606, 1997.
- [91] O. Gunnarsson, V. Meden, and K. Schönhammer. Corrections to Migdal’s theorem for spectral functions: A cumulant treatment of the time-dependent Green’s function. *Phys. Rev. B* **50**, 10462–10473, 1994.
- [92] M. C. Gutzwiller. Periodic Orbits and Classical Quantization Conditions. *Journal of Mathematical Physics* **12**, (3) 343–358, 1971.
- [93] Z. Hadzibabic, P. Kruger, M. Cheneau, B. Battelier, and J. Dalibard. Berezinskii-Kosterlitz-Thouless crossover in a trapped atomic gas. *Nature* **441**, (7097) 1118–1121, 2006.
- [94] J. Han, Y. Jamil, D. V. L. Norum, P. J. Tanner, and T. F. Gallagher. Rb nf quantum defects from millimeter-wave spectroscopy of cold ^{85}Rb Rydberg atoms. *Phys. Rev. A* **74**, 054502, 2006.
- [95] L. Holmlid. Optical stimulated emission transitions in Rydberg matter observed in the range 800–14000 nm. *Journal of Physics B: Atomic, Molecular and Optical Physics* **37**, (2) 357, 2004.
- [96] R. Horodecki, P. Horodecki, M. Horodecki, and K. Horodecki. Quantum entanglement. *Rev. Mod. Phys.* **81**, 865–942, 2009.
- [97] R. G. Hulet and D. Kleppner. Rydberg Atoms in "Circular" States. *Phys. Rev. Lett.* **51**, 1430–1433, 1983.
- [98] D. Jaksch, C. Bruder, J. I. Cirac, C. W. Gardiner, and P. Zoller. Cold Bosonic Atoms in Optical Lattices. *Phys. Rev. Lett.* **81**, 3108–3111, 1998.
- [99] D. Jaksch, J. I. Cirac, P. Zoller, S. L. Rolston, R. Côté, and M. D. Lukin. Fast Quantum Gates for Neutral Atoms. *Phys. Rev. Lett.* **85**, 2208–2211, 2000.
- [100] T. H. Jeys, M. C. Copel, G. B. McMillian, F. B. Dunning, and R. F. Stebbings. Sodium d-state fine structure in an electric field. *Journal of Physics B: Atomic and Molecular Physics* **16**, (20) 3747, 1983.
- [101] D. Jiang, B. Arora, M. S. Safronova, and C. W. Clark. Blackbody-radiation shift in a 88Sr^+ ion optical frequency standard. *Journal of Physics B: Atomic, Molecular and Optical Physics* **42**, (15) 154020, 2009.

- [102] M. Johanning, A. Braun, N. Timoney, V. Elman, W. Neuhauser, and C. Wunderlich. Individual Addressing of Trapped Ions and Coupling of Motional and Spin States Using rf Radiation. *Phys. Rev. Lett.* **102**, 073004, 2009.
- [103] U. Kaldor and S. Wilson. *Theoretical Chemistry and Physics of Heavy and Super-heavy Elements*. Springer Netherlands, November 30, 2003.
- [104] H. Katori, K. Hashiguchi, E. Y. Il'inova, and V. D. Ovsianikov. Magic Wavelength to Make Optical Lattice Clocks Insensitive to Atomic Motion. *Phys. Rev. Lett.* **103**, 153004, 2009.
- [105] H. Katori, T. Ido, Y. Isoya, and M. Kuwata-Gonokami. Magneto-Optical Trapping and Cooling of Strontium Atoms down to the Photon Recoil Temperature. *Phys. Rev. Lett.* **82**, 1116–1119, 1999.
- [106] D. E. Kelleher and E. B. Saloman. Rydberg states with anisotropic ion cores: Stark effect. *Phys. Rev. A* **35**, 3327–3338, 1987.
- [107] M. Kiffner, W. Li, and D. Jaksch. Magnetic Monopoles and Synthetic Spin-Orbit Coupling in Rydberg Macrodimers. *Phys. Rev. Lett.* **110**, 170402, 2013.
- [108] B. Knuffman and G. Raithel. Multipole transitions of Rydberg atoms in modulated ponderomotive potentials. *Physical Review A* **75**, (5), 2007.
- [109] T. Koga. Hylleraas wave functions revisited. *The Journal of Chemical Physics* **96**, (2) 1276–1279, 1992.
- [110] S. Korenblit, D. Kafri, W. C. Campbell, R. Islam, E. E. Edwards, Z.-X. Gong, G.-D. Lin, L.-M. Duan, J. Kim, K. Kim, and C. Monroe. Quantum simulation of spin models on an arbitrary lattice with trapped ions. *New Journal of Physics* **14**, (9) 095024, 2012.
- [111] V. A. Kostelecký and M. M. Nieto. Analytical wave functions for atomic quantum-defect theory. *Phys. Rev. A* **32**, 3243–3246, 1985.
- [112] J. Kuang and C. D. Lin. Molecular integrals over spherical Gaussian-type orbitals: I. *Journal of Physics B: Atomic, Molecular and Optical Physics* **30**, (11) 2529, 1997.
- [113] T. Kuga, Y. Torii, N. Shiokawa, T. Hirano, Y. Shimizu, and H. Sasada. Novel Optical Trap of Atoms with a Doughnut Beam. *Phys. Rev. Lett.* **78**, 4713–4716, 1997.
- [114] S. Kunze, R. Hohmann, H.-J. Kluge, J. Lantzsch, L. Monz, J. Stenner, K. Stratmann, K. Wendt, and K. Zimmer. Lifetime measurements of highly excited Rydberg states of strontium I. *Zeitschrift für Physik D Atoms, Molecules and Clusters* **27**, (2) 111–114, 1993.

- [115] J. Lahiri and A. Mukherji. Electrostatic Polarizability and Shielding Factors for Ions of Neon Configuration. *Phys. Rev.* **153**, 386–387, 1967.
- [116] V. Lange, M. Khan, U. Eichmann, and W. Sandner. Rydberg states of the strontium ion. *Zeitschrift für Physik D Atoms, Molecules and Clusters* **18**, (4) 319–324, 1991.
- [117] D. Leibfried, R. Blatt, C. Monroe, and D. Wineland. Quantum dynamics of single trapped ions. *Rev. Mod. Phys.* **75**, 281–324, 2003.
- [118] J. G. Leopold and I. C. Percival. The semiclassical two-electron atom and the old quantum theory. *Journal of Physics B: Atomic and Molecular Physics* **13**, (6) 1037, 1980.
- [119] I. Lesanovsky and H. Katsura. Interacting Fibonacci anyons in a Rydberg gas. *Phys. Rev. A* **86**, 041601, 2012.
- [120] I. Lesanovsky, M. Müller, and P. Zoller. Trap-assisted creation of giant molecules and Rydberg-mediated coherent charge transfer in a Penning trap. *Phys. Rev. A* **79**, 010701, 2009.
- [121] V. Letokhov and B. Pavlik. Spectral line narrowing in a gas by atoms trapped in a standing light wave. *Applied physics* **9**, (3) 229–237, 1976.
- [122] M. Lewenstein, A. Sanpera, V. Ahufinger, B. Damski, A. Sen(De), and U. Sen. Ultracold atomic gases in optical lattices: mimicking condensed matter physics and beyond. *Advances in Physics* **56**, 243–379, 2007.
- [123] T. C. Li, H. Kelkar, D. Medellin, and M. G. Raizen. Real-time control of the periodicity of a standing wave: an optical accordion. *Opt. Express* **16**, (8) 5465–5470, 2008.
- [124] W. Li, A. W. Glaetzle, R. Nath, and I. Lesanovsky. Parallel execution of quantum gates in a long linear ion chain via Rydberg mode shaping. *Phys. Rev. A* **87**, 052304, 2013.
- [125] W. Li, I. Mourachko, M. W. Noel, and T. F. Gallagher. Millimeter-wave spectroscopy of cold Rb Rydberg atoms in a magneto-optical trap: Quantum defects of the ns , np , and nd series. *Phys. Rev. A* **67**, 052502, 2003.
- [126] W. Li, P. J. Tanner, and T. F. Gallagher. Dipole-Dipole Excitation and Ionization in an Ultracold Gas of Rydberg Atoms. *Phys. Rev. Lett.* **94**, 173001, 2005.
- [127] W. Linden, E. Berger, and P. Valasek. The Hubbard-Holstein model. *Journal of Low Temperature Physics* **99**, (3-4) 517–525, 1995.
- [128] I. Lontos, S. Cohen, and A. Bolovinos. Single and double ionization of strontium in the vicinity of four-photon excitation of the $5p\ 2\ 1\ S\ 0$ doubly excited state. *Journal of Physics B: Atomic, Molecular and Optical Physics* **41**, (4) 045601, 2008.

- [129] R. Löw, H. Weimer, J. Nipper, J. B. Balewski, B. Butscher, H. P. Büchler, and T. Pfau. An experimental and theoretical guide to strongly interacting Rydberg gases. *Journal of Physics B: Atomic, Molecular and Optical Physics* **45**, (11) 113001, 2012.
- [130] A. D. Ludlow, T. Zelevinsky, G. K. Campbell, S. Blatt, M. M. Boyd, M. H. G. de Miranda, M. J. Martin, J. W. Thomsen, S. M. Foreman, J. Ye, T. M. Fortier, J. E. Stalnaker, S. A. Diddams, Y. Le Coq, Z. W. Barber, N. Poli, N. D. Lemke, K. M. Beck, and C. W. Oates. Sr Lattice Clock at 1×10^{16} Fractional Uncertainty by Remote Optical Evaluation with a Ca Clock. *Science* **319**, (5871) 1805–1808, 2008.
- [131] M. D. Lukin, M. Fleischhauer, R. Cote, L. M. Duan, D. Jaksch, J. I. Cirac, and P. Zoller. Dipole Blockade and Quantum Information Processing in Mesoscopic Atomic Ensembles. *Phys. Rev. Lett.* **87**, 037901, 2001.
- [132] R. P. Madden and K. Codling. New Autoionizing Atomic Energy Levels in He, Ne, and Ar. *Phys. Rev. Lett.* **10**, 516–518, 1963.
- [133] M. Marinescu, H. R. Sadeghpour, and A. Dalgarno. Dispersion coefficients for alkali-metal dimers. *Phys. Rev. A* **49**, 982–988, 1994.
- [134] F. Markert, P. Würtz, A. Koglbauer, T. Gericke, A. Vogler, and H. Ott. ac-Stark shift and photoionization of Rydberg atoms in an optical dipole trap. *New Journal of Physics* **12**, (11) 113003, 2010.
- [135] F. Marsiglio. Pairing and charge-density-wave correlations in the Holstein model at half-filling. *Phys. Rev. B* **42**, 2416–2424, 1990.
- [136] F. Maucher, N. Henkel, M. Saffman, W. Królikowski, S. Skupin, and T. Pohl. Rydberg-Induced Solitons: Three-Dimensional Self-Trapping of Matter Waves. *Phys. Rev. Lett.* **106**, 170401, 2011.
- [137] J. E. Mayer and M. G. Mayer. The Polarizabilities of Ions from Spectra. *Phys. Rev.* **43**, 605–611, 1933.
- [138] H. J. Metcalf and P. van der Straten. Laser cooling and trapping of atoms. *J. Opt. Soc. Am. B* **20**, (5) 887–908, 2003.
- [139] Z. Miao-chan, D. Chang-jian, and L. Shi-ben. Stark structure of the Rydberg states of alkaline-earth atoms. *Chinese Physics* **10**, (10) 929, 2001.
- [140] J. Millen, G. Lochead, G. R. Corbett, R. M. Potvliege, and M. P. A. Jones. Spectroscopy of a cold strontium Rydberg gas. *Journal of Physics B: Atomic, Molecular and Optical Physics* **44**, (18) 184001, 2011.
- [141] J. Millen, G. Lochead, and M. Jones. Two-Electron Excitation of an Interacting Cold Rydberg Gas. *Physical Review Letters* **105**, (21), 2010.

- [142] J. Mitroy and M. W. J. Bromley. Semiempirical calculation of van der Waals coefficients for alkali-metal and alkaline-earth-metal atoms. *Phys. Rev. A* **68**, 052714, 2003.
- [143] R. W. Molof, H. L. Schwartz, T. M. Miller, and B. Bederson. Measurements of electric dipole polarizabilities of the alkali-metal atoms and the metastable noble-gas atoms. *Phys. Rev. A* **10**, 1131–1140, 1974.
- [144] T. Monz, P. Schindler, J. T. Barreiro, M. Chwalla, D. Nigg, W. A. Coish, M. Harlander, W. Hänsel, M. Hennrich, and R. Blatt. 14-Qubit Entanglement: Creation and Coherence. *Phys. Rev. Lett.* **106**, 130506, 2011.
- [145] C. E. Moore. *Atomic Energy Levels, Natl. Stand. Ref. Data Ser. 35*. U.S. GPO, Washington, D.C., 1971.
- [146] I. Mourachko, D. Comparat, F. de Tomasi, A. Fioretti, P. Nosbaum, V. M. Akulin, and P. Pillet. Many-Body Effects in a Frozen Rydberg Gas. *Phys. Rev. Lett.* **80**, 253–256, 1998.
- [147] R. Mukherjee, I. Lesanovsky, and T. Pohl. *Coherent control of ion-transport via Rydberg dressing of an atomic optical lattice*. (In preparation).
- [148] R. Mukherjee, J. Millen, R. Nath, M. P. A. Jones, and T. Pohl. Many-body physics with alkaline-earth Rydberg lattices. *Journal of Physics B: Atomic, Molecular and Optical Physics* **44**, (18) 184010, 2011.
- [149] M. Müller, L. Liang, I. Lesanovsky, and P. Zoller. Trapped Rydberg ions: from spin chains to fast quantum gates. *New Journal of Physics* **10**, (9) 093009, 2008.
- [150] J. Murray-Krezan and R. R. Jones. Measurement of the electronic momentum distributions of Rydberg Stark states. *Phys. Rev. A* **75**, 063411, 2007.
- [151] K. D. Nelson, X. Li, and D. S. Weiss. Imaging single atoms in a three-dimensional array. *Nat Phys* **3**, (8) 556–560, 2007.
- [152] P. M. Oppeneer and W. Hierse. Two-center overlap integrals over Slater-type orbitals constrained to a spherical integration volume: Analytical expressions. *Phys. Rev. A* **50**, 2232–2238, 1994.
- [153] K. Osterloh, M. Baig, L. Santos, P. Zoller, and M. Lewenstein. Cold Atoms in Non-Abelian Gauge Potentials: From the Hofstadter "Moth" to Lattice Gauge Theory. *Phys. Rev. Lett.* **95**, 010403, 2005.
- [154] A. Osterwalder and F. Merkt. Using High Rydberg States as Electric Field Sensors. *Phys. Rev. Lett.* **82**, 1831–1834, 1999.
- [155] S. H. Paul W. Ein neues Massenspektrometer ohne Magnetfeld. *Zeitschrift für Naturforschung A* **8**, 448–450, 1953.

- [156] D. Petrosyan, M. Höning, and M. Fleischhauer. Spatial correlations of Rydberg excitations in optically driven atomic ensembles. *Phys. Rev. A* **87**, 053414, 2013.
- [157] T. Peyronel, O. Firstenberg, Q.-Y. Liang, S. Hofferberth, A. V. Gorshkov, T. Pohl, M. D. Lukin, and V. Vuletic. Quantum nonlinear optics with single photons enabled by strongly interacting atoms. *Nature* **488**, (7409) 57–60, 2012.
- [158] G. Philip and J.-P. Connerade. The controlled excitation of forbidden transitions in the two photon spectrum of strontium by sing collisond and electric fields. *Optics Communications* **279**, (141) 8, 2007.
- [159] W. D. Phillips. Nobel Lecture: Laser cooling and trapping of neutral atoms. *Rev. Mod. Phys.* **70**, 721–741, 1998.
- [160] T. Pohl, E. Demler, and M. D. Lukin. Dynamical Crystallization in the Dipole Blockade of Ultracold Atoms. *Phys. Rev. Lett.* **104**, 043002, 2010.
- [161] T. Pohl, D. Vrinceanu, and H. R. Sadeghpour. Rydberg Atom Formation in Ultracold Plasmas: Small Energy Transfer with Large Consequences. *Phys. Rev. Lett.* **100**, 223201, 2008.
- [162] M. Poirier. Autoionization of Rydberg states with large angular momentum: Application to alkaline-earth atoms. *Phys. Rev. A* **38**, 3484–3497, 1988.
- [163] R. M. Potvliege and C. S. Adams. Photo-ionization in far-off-resonance optical lattices. *New Journal of Physics* **8**, (8) 163–163, 2006.
- [164] J. D. Pritchard, A. Gauguet, K. J. Weatherill, and C. S. Adams. Optical non-linearity in a dynamical Rydberg gas. *Journal of Physics B: Atomic, Molecular and Optical Physics* **44**, (18) 184019, 2011.
- [165] E. L. Raab, M. Prentiss, A. Cable, S. Chu, and D. E. Pritchard. Trapping of Neutral Sodium Atoms with Radiation Pressure. *Phys. Rev. Lett.* **59**, 2631–2634, 1987.
- [166] J. M. Raimond, G. Vitrant, and S. Haroche. Spectral line broadening due to the interaction between very excited atoms: 'the dense Rydberg gas'. *Journal of Physics B: Atomic and Molecular Physics* **14**, (21) L655, 1981.
- [167] K. Rudenberg. A Study of Two-Center Integrals Useful in Calculations on Molecular Structure. II. The Two-Center Exchange Integrals. *The Journal of Chemical Physics* **19**, (12) 1459–1477, 1951.
- [168] S. Sachdev. *Quantum phase transitions*. Cambridge University Press, 2 edition, May 9, 2011.
- [169] C. A. Sackett, D. Kielpinski, B. E. King, C. Langer, V. Meyer, C. J. Myatt, M. Rowe, Q. A. Turchette, W. M. Itano, D. J. Wineland, and C. Monroe. Experimental entanglement of four particles. *Nature* **404**, (6775) 256–259, 2000.

- [170] M. Saffman and T. G. Walker. Creating single-atom and single-photon sources from entangled atomic ensembles. *Phys. Rev. A* **66**, 065403, 2002.
- [171] M. Saffman and T. G. Walker. Analysis of a quantum logic device based on dipole-dipole interactions of optically trapped Rydberg atoms. *Phys. Rev. A* **72**, 022347, 2005.
- [172] M. Saffman, T. G. Walker, and K. Mølmer. Quantum information with Rydberg atoms. *Rev. Mod. Phys.* **82**, 2313–2363, 2010.
- [173] H. P. Saha and N. C. Sil. Evaluation of exchange matrix elements with momentum transfer for ion-atom collisions. *Journal of Physics B: Atomic and Molecular Physics* **12**, (4) 585, 1979.
- [174] K. Sakimoto. Multichannel quantum-defect theory of the Stark effect. *Journal of Physics B: Atomic and Molecular Physics* **19**, (19) 3011, 1986.
- [175] C. Salomon, J. Dalibard, A. Aspect, H. Metcalf, and C. Cohen-Tannoudji. Channeling atoms in a laser standing wave. *Phys. Rev. Lett.* **59**, 1659–1662, 1987.
- [176] R. Santra, K. V. Christ, and C. H. Greene. Properties of metastable alkaline-earth-metal atoms calculated using an accurate effective core potential. *Phys. Rev. A* **69**, 042510, 2004.
- [177] R. T. Scalettar, N. E. Bickers, and D. J. Scalapino. Competition of pairing and Peierls – charge-density-wave correlations in a two-dimensional electron-phonon model. *Phys. Rev. B* **40**, 197–200, 1989.
- [178] S. Schmid, A. Härter, and J. H. Denschlag. Dynamics of a Cold Trapped Ion in a Bose-Einstein Condensate. *Phys. Rev. Lett.* **105**, 133202, 2010.
- [179] H. Schmitz, R. Matjeschk, C. Schneider, J. Glueckert, M. Enderlein, T. Huber, and T. Schaetz. Quantum Walk of a Trapped Ion in Phase Space. *Phys. Rev. Lett.* **103**, 090504, 2009.
- [180] C. Schneider, D. Porras, and T. Schaetz. Experimental quantum simulations of many-body physics with trapped ions. *Reports on Progress in Physics* **75**, (2) 024401, 2012.
- [181] T. Schulte, S. Drenkelforth, J. Kruse, W. Ertmer, J. Arlt, K. Sacha, J. Zakrzewski, and M. Lewenstein. Routes Towards Anderson-Like Localization of Bose-Einstein Condensates in Disordered Optical Lattices. *Phys. Rev. Lett.* **95**, 170411, 2005.
- [182] A. Schwarzkopf, R. E. Sapiro, and G. Raithel. Imaging Spatial Correlations of Rydberg Excitations in Cold Atom Clouds. *Phys. Rev. Lett.* **107**, 103001, 2011.
- [183] M. J. Seaton. Quantum defect theory. *Rep.Prog.Phys.* **46**, (167), 1983.
- [184] S. Sevinçli, N. Henkel, C. Ates, and T. Pohl. Nonlocal Nonlinear Optics in Cold Rydberg Gases. *Phys. Rev. Lett.* **107**, 153001, 2011.

- [185] C. E. Simien, Y. C. Chen, P. Gupta, S. Laha, Y. N. Martinez, P. G. Mickelson, S. B. Nagel, and T. C. Killian. Using Absorption Imaging to Study Ion Dynamics in an Ultracold Neutral Plasma. *Phys. Rev. Lett.* **92**, 143001, 2004.
- [186] K. Singer, M. Reetz-Lamour, T. Amthor, L. G. Marcassa, and M. Weidemüller. Suppression of Excitation and Spectral Broadening Induced by Interactions in a Cold Gas of Rydberg Atoms. *Phys. Rev. Lett.* **93**, 163001.
- [187] K. Singer, J. Stanojevic, M. Weidemüller, and R. Côté. Long-range interactions between alkali Rydberg atom pairs correlated to the ns-n s, np-np and nd-nd asymptotes. *Journal of Physics B: Atomic, Molecular and Optical Physics* **38**, (2) S295, 2005.
- [188] E. A. Solov'ev. Quasiclassical perturbation theory for the helium atom and the heliumlike ion. *Sov. Phys. JETP* **62**, (1148), 1985.
- [189] S. Stellmer, R. Grimm, and F. Schreck. Production of quantum-degenerate strontium gases. *Phys. Rev. A* **87**, 013611, 2013.
- [190] S. Stellmer, M. Tey, B. Huang, R. Grimm, and F. Schreck. Bose-Einstein Condensation of Strontium. *Physical Review Letters* **103**, (20), 2009.
- [191] M. Takamoto and H. Katori. Spectroscopy of the 1S_0 - 3P_0 Clock Transition of ^{87}Sr in an Optical Lattice. *Phys. Rev. Lett.* **91**, 223001, 2003.
- [192] J. Tallant, D. Booth, and J. Shaffer. Photoionization rates of Cs Rydberg atoms in a 1064-nm far-off-resonance trap. *Physical Review A* **82**, (6), 2010.
- [193] M. Tezuka, R. Arita, and H. Aoki. Phase diagram for the one-dimensional Hubbard-Holstein model: A density-matrix renormalization group study. *Phys. Rev. B* **76**, 155114, 2007.
- [194] G. M. Tino, N. Poli, R. Drullinger, G. Ferrari, and F. Sorrentino. Laser cooling and trapping of atomic strontium for ultracold atoms physics, high-precision spectroscopy and quantum sensors. *Modern Physics Letters B* **20**, (21) 1287–1320, 2006.
- [195] D. Tong, S. M. Farooqi, J. Stanojevic, S. Krishnan, Y. P. Zhang, R. Côté, E. E. Eyler, and P. L. Gould. Local Blockade of Rydberg Excitation in an Ultracold Gas. *Phys. Rev. Lett.* **93**, 063001, 2004.
- [196] E. Urban, T. A. Johnson, T. Henage, L. Isenhower, D. D. Yavuz, T. G. Walker, and M. Saffman. Observation of Rydberg blockade between two atoms. *Nat Phys* **5**, (2) 110–114, 2009.
- [197] N. Vaeck, M. Godefroid, and J. E. Hansen. Multiconfiguration Hartree-Fock calculations for singlet terms in neutral strontium. *Phys. Rev. A* **38**, 2830–2845, 1988.

- [198] C. L. Vaillant, M. P. A. Jones, and R. M. Potvliege. Long-range Rydberg-Rydberg interactions in calcium, strontium and ytterbium. *Journal of Physics B: Atomic, Molecular and Optical Physics* **45**, (13) 135004, 2012.
- [199] K. A. H. van Leeuwen, W. Hogervorst, and B. H. Post. Stark effect in barium $6snd$ 1D_2 Rydberg states; evidence of strong perturbations in the 1F_3 series. *Phys. Rev. A* **28**, 1901–1907, 1983.
- [200] F. Verstraete, J. Dehaene, and B. De Moor. Normal forms and entanglement measures for multipartite quantum states. *Phys. Rev. A* **68**, 012103, 2003.
- [201] G. Vitrant, J. M. Raimond, M. Gross, and S. Haroche. Rydberg to plasma evolution in a dense gas of very excited atoms. *Journal of Physics B: Atomic and Molecular Physics* **15**, (2) L49, 1982.
- [202] T. Vogt, M. Viteau, A. Chotia, J. Zhao, D. Comparat, and P. Pillet. Electric-Field Induced Dipole Blockade with Rydberg Atoms. *Phys. Rev. Lett.* **99**, 073002, 2007.
- [203] T. Vogt, M. Viteau, J. Zhao, A. Chotia, D. Comparat, and P. Pillet. Dipole Blockade at Förster Resonances in High Resolution Laser Excitation of Rydberg States of Cesium Atoms. *Phys. Rev. Lett.* **97**, 083003, 2006.
- [204] T. Walker and M. Saffman. Consequences of Zeeman degeneracy for the van der Waals blockade between Rydberg atoms. *Physical Review A* **77**, (3), 2008.
- [205] H. Weimer, R. Löw, T. Pfau, and H. P. Büchler. Quantum Critical Behavior in Strongly Interacting Rydberg Gases. *Phys. Rev. Lett.* **101**, 250601, 2008.
- [206] H. Weimer, M. Müller, I. Lesanovsky, P. Zoller, and H. P. Büchler. A Rydberg quantum simulator. *Nature Physics* **6**, (5) 382–388, 2010.
- [207] T. Wilk, A. Gaëtan, C. Evellin, J. Wolters, Y. Miroshnychenko, P. Grangier, and A. Browaeys. Entanglement of Two Individual Neutral Atoms Using Rydberg Blockade. *Physical Review Letters* **104**, (1), 2010.
- [208] D. J. Wineland and W. M. Itano. Laser cooling of atoms. *Phys. Rev. A* **20**, 1521–1540, 1979.
- [209] D. J. Wineland, C. Monroe, W. M. Itano, D. Leibfried, B. E. King, and D. M. Meekhof. *Experimental issues in coherent quantum-state manipulation of trapped atomic ions*. arXiv:quant-ph/9710025, 1997.
- [210] E. Y. Xu, Y. Zhu, O. C. Mullins, and T. F. Gallagher. Sr $5pnd$ $J=3$ autoionizing series and interference of excitation due to bound-state perturbation. *Phys. Rev. A* **35**, 1138–1148, 1987.
- [211] K. C. Younge, S. E. Anderson, and G. Raithel. Adiabatic potentials for Rydberg atoms in a ponderomotive optical lattice. *New Journal of Physics* **12**, (2) 023031, 2010.

-
- [212] K. C. Younge, B. Knuffman, S. E. Anderson, and G. Raithel. State-Dependent Energy Shifts of Rydberg Atoms in a Ponderomotive Optical Lattice. *Physical Review Letters* **104**, (17), 2010.
- [213] F. Zähringer, G. Kirchmair, R. Gerritsma, E. Solano, R. Blatt, and C. F. Roos. Realization of a Quantum Walk with One and Two Trapped Ions. *Phys. Rev. Lett.* **104**, 100503, 2010.
- [214] A. Zeilinger, M. A. Horne, and D. M. Greenberger. Higher-order quantum entanglement. *NASA Conf. Publ.* **3135**, 73–81, 1992.
- [215] C. Zener. Non-Adiabatic Crossing of Energy Levels. *Proceedings of the Royal Society of London. Series A* **137**, (833) 696–702, 1932.
- [216] Z. Zhao. Experimental demonstration of five-photon entanglement and open-destination teleportation. *Nature* **430**, 54–58, 2004.
- [217] M. L. Zimmerman, T. W. Ducas, M. G. Littman, and D. Kleppner. Stark structure of barium Rydberg states. *Journal of Physics B: Atomic and Molecular Physics* **11**, (1) L11, 1978.
- [218] M. L. Zimmerman, M. G. Littman, M. M. Kash, and D. Kleppner. Stark structure of the Rydberg states of alkali-metal atoms. *Phys. Rev. A* **20**, 2251–2275, 1979.

Acknowledgements

I would like to begin by thanking Prof Jan Michael Rost for giving me this opportunity to do my doctoral studies here at the MPI-PKS and in this culturally beautiful city of Germany, Dresden. I truly benefited from the well equipped infrastructure of the institute and felt very much at home in Dresden throughout my studies. I would like to express my deepest gratitude to my supervisor, Dr Thomas Pohl for his ceaseless input not only on the subject matter but also in general for research skills. I am indebted to the many passionate and instructive discussions I have had with him over the many years. He taught me to be always critical of ones results and introduced me to the “devil that lies in the details”. I very much thank him for the delicious original Thüringer Roster (or so he claims) at many of his barbeque parties and buying me countless free beer to improve my stamina on beer drinking.

I would like to also acknowledge many of the group members with whom I have had the good fortune of discussing physics among other things. I would start by thanking Alexey Mikaberidze and Andrey Lyubon’ko for their friendship and support. I miss our philosophical group, Bubhutsa. I also thank my colleagues and friends; Jovica Stanojevic, Weibin Li, Rejish Nath, Cenap Ates, Christian Gnodtke, Alexander Croy, Mickael Grech, Georg Bannasch, Nils Henkel, Michael Genkin, Sebastian Wüster, Alexander Eisfeld, Fabio Cinti, Tommaso Macri and Laura Gil. I would like to express my sincerest gratitude to Michael Genkin and Sebastian Wüster for proof reading my thesis countless times. I would also thank my office-mates for tolerating me particularly, Martin Zumsande and Gesa Böhme. Special thanks to the coffee masters of the Institute.

Many thanks to the entire IT department for their patience and constant support. Special thanks to the Guest program of the MPI-PKS and all the staff members who make life at the institute seemingly effortless. I guess thanks to all who contributed to the funds for the table tennis and kicker table since I have most definitely enjoyed both. Lastly I would like to thank my parents for their love, understanding and faith in me.

Versicherung

Hiermit versichere ich, dass ich die vorliegende Arbeit ohne unzulässige Hilfe Dritter und ohne Benutzung anderer als der angegebenen Hilfsmittel angefertigt habe; die aus fremden Quellen direkt oder indirekt übernommenen Gedanken sind als solche kenntlich gemacht. Die Arbeit wurde bisher weder im Inland noch im Ausland in gleicher oder ähnlicher Form einer anderen Prüfungsbehörde vorgelegt.

Die Arbeit wurde am Max-Planck-Institut für Physik komplexer Systeme in der Abteilung Endliche Systeme angefertigt und von Prof. Dr. Jan-Michael Rost betreut. Ich erkenne die Promotionsordnung der Fakultät Mathematik und Naturwissenschaften der Technischen Universität Dresden vom 23.02.2011 an.

Rick MUKHERJEE